UNIVERSITY OF SOUTHAMPTON

Laser Direct Write Techniques for the Fabrication of Paper-Based Diagnostic Devices

by

Ioannis N. Katis

Thesis submitted for the degree of Doctor of Philosophy

in the
Faculty of Physical Sciences and Engineering
Optoelectronics Research Centre

December 2015

Declaration of Authorship

I, Ioannis N. Katis, declare that this thesis titled, ‘Laser Direct Write Techniques for the Fabrication of Paper-Based Diagnostic Devices’ and the work presented in it are my own. I confirm that:

- This work was done wholly or mainly while in candidature for a research degree at this University.
- Where any part of this thesis has previously been submitted for a degree or any other qualification at this University or any other institution, this has been clearly stated.
- Where I have consulted the published work of others, this is always clearly attributed.
- Where I have quoted from the work of others, the source is always given. With the exception of such quotations, this thesis is entirely my own work.
- I have acknowledged all main sources of help.
- Where the thesis is based on work done by myself jointly with others, I have made clear exactly what was done by others and what I have contributed myself.
- Parts of this work have been published as shown in Appendix C.

Signed:

Date:

UNIVERSITY OF SOUTHAMPTON

Abstract

Faculty of Physical Sciences and Engineering
Optoelectronics Research Centre

Doctor of Philosophy

by Ioannis N. Katis

We report on the use of laser direct-write techniques for the fabrication of point-of-care paper-based diagnostic sensors. These include laser-based deposition, laser ablation and laser-induced photo-polymerisation.

Firstly, Laser Induced Forward Transfer (LIFT) was employed to deposit biomolecules from a donor film onto paper receivers. Paper was chosen as the ideal receiver because of its inherent properties which make it an efficient and suitable platform for point-of-care diagnostic sensors. Both enzyme-tagged and untagged antibodies were LIFT-printed and their viability was confirmed via a colorimetric enzyme-linked immunosorbent assay (ELISA).

Secondly, we report on the laser-based structuring of paper-based fluidic devices. Laser-scanning the paper defines the areas that will be polymerised, thus creating barriers that keep the liquid solutions contained. Complicated devices are easy to fabricate and the flexibility of this technique allows for unique patterns, making it appropriate for rapid prototyping but also for large-scale production. Furthermore, the laser patterning technique allows control of the depth or degree of polymerisation, thereby allowing the liquid to wick through but also imposition of flow delays.

Finally, the use of lasers for the fabrication of a 'master' which can be used for casting a PDMS mould for applications in micro-contact printing.

The combination of the above mentioned techniques represent the platform technology for the rapid, precise and versatile laser-based fabrication of diagnostic point-of-care sensors.

Acknowledgements

First of all, I would like to thank Collin and Rob for their continuous support and guidance that made the course of this PhD as smooth as possible. You are both the best supervisors a student can ask for! A great thanks to Peijun who helped move the project forward with his input and hard work. Thanks also to all members of the LIFT group for the scientific discussions and common work, especially Matthias Feinaeugle who guided me through my first steps in this project.

The work in this thesis has been kindly supported by the British Engineering and Physical Sciences Research Council (EPSRC) through the grant EP/K023454/1, "Laser-printable point-of-care sensors for low-cost medical diagnosis and disease monitoring".

I would also like to acknowledge the scientific input and practical help from all the people in the Faculty of Medicine, the Institute for Life Sciences and the Southampton General Hospital. Special thanks to Dr. Judith Holloway as well as Dr. Jens Madsen, Dr. Spiros Garbis and Prof. Peter Smith for their help in understanding and implementing the biological experiments. Thanks also to Dr. Susan Pang from LGC for providing samples and reagents and also helping and providing advice. I thank for the technical support from Neil Sessions, Chris Nash and the rest of the technical team. Thanks also to the fellows in PKF for making the Portakabin the best office around the university.

Finally, a big thanks to my family and friends, here and back home, without whom I would not be where I am now. I am glad that you are too many to acknowledge all of you, but thank you all for making me who I am. Finally, my greatest thank you goes to Dora for her love and partnership through life.

Contents

List of Figures

List of Tables

Abbreviations

LIFT	Laser Induced Forward Transfer
ELISA	Enzyme Linked Immunosorbent Assay
POC	Point Of Care
LOC	Lab On Chip
DRL	Dynamic Release Layer
DRL-LIFT	Dynamic Release Layer Laser Induced Forward Transfer
BA-LIFT	Blister-Actuated Laser Induced Forward Transfer
MAPLE-DW	Matrix-Assisted Pulsed Laser Evaporation Direct-Write
LDT	Laser Decal Transfer
LIBT	Laser Induced Backward Transfer
MPA	Multi-Photon Absorption
IgG	Immunoglobulin G
HRP	Horseradish Peroxidase
ALP	Alkaline Phosphatase
FDA	Food and Drug Administration
TNFα	Tumor Necrosis Factor
TMB	3,3',5,5'-Tetramethylbenzidine
BSA	Bovine Serum Albumin
PBS	Phosphate Buffered Saline
KrF	Krypton Fluoride
QR	Quick Response
CRP	C-Reactive Protein
Nd:YVO$_4$	Neodymium-doped Yttrium Orthovanadate
CW	Continuous Wave
TBS	Tris Buffered Saline

LDW	Laser Direct-Write
μ**CP**	Micro Contact Printing
PDMS	Polydimethylsiloxane
TRITC	Tetramethylrhodamineisothiocyanate
RPM	Round Per Minute
μ**PAD**	Microfluidic Paper-based Analytical Devices
PS	Polystyrene
AKD	Alkyl Ketene Dimer
Il-6	Interleukin 6
DMD	Digital Micro-mirror Device
TBPB	Tert-Butyl Peroxybenzoate
PVDF	Polyvinylidene Fluoride

This is for my father.

Chapter 1

Introduction

In recent years, the requirements for simple, accurate and low-cost diagnostic solutions in both developing and developed countries have led to a rapid progress in the fabrication of point-of-care (POC) devices, and microfluidic engineering technology has been widely used for implementing lab-on-chip-type (LOC) type POC devices since its origins in the 1990s. The main drivers behind LOC POC devices are the possibility of reducing the quantity of valuable samples or reagents that would be needed, faster detection times which would result from the compact structure of such devices, and, perhaps most importantly, the reduced cost to the health system and ease of testing for the patient. For many global diseases, diagnostic platforms are required that are self-contained, stable in environmental extremes, do not need electricity and can be operated with minimal training. However, although this technology is promising and there have been a large number of achievements in this field, there are few clear front runners in the development of commercialised products, particularly in the context of paper-based tests, and we see this as the ideal opportunity for our technology to make a very positive contribution.

When compared with other silicon, silica or polymer-based LOC-type microfluidic devices, porous paper-based structures offer considerable advantages as they do not require any additional pumps because of the inherent ability of paper to wick fluids via capillary forces. This provides an enormous benefit in terms of both the cost and manufacturability of any such test, and this has led to the development of many paper-based devices for simple colorimetric bio-assays. In addition to paper, porous nitrocellulose membranes - since their first demonstration in the 1960s - have been widely used, due to some key features, such as their smooth surface, uniform pore size and high protein-binding capability. A large number of biological assays, namely blotting assays, flow-through assays and lateral flow tests, have been developed on these porous nitrocellulose membranes, and hence nitrocellulose-based microfluidic devices are currently regarded as the ideal choice for improving the performance of existing POC assays.

The basic question remaining is how to manufacture these tests on such porous platform media to a standard that will be acceptable to, and adoptable by, existing established manufacturers in the healthcare sector. Using this technology to bring to market a new range of diagnostic devices would represent a step change in advancement of world health. While several methods have been reported in the literature to date for the fabrication of fluidic patterns in such porous media, none of the current techniques, which include the use of photolithography, inkjet printing, printing of wax, and plasma oxidation, plotting, and shaping have as yet made the breakthrough towards fabrication protocols that would enable manufacturing at the world market level. What is needed is a simple, rapid, safe, cheap and versatile process that can be adopted immediately, and we believe, as a result of our LDW paper-patterning work under our existing feasibility grant, we have now defined and demonstrated the proof-of-principle for such a process. The next steps are to refine the technique, build and test prototypes, and in due course bring the technology to market with all the associated global benefits.

1.1 Motivation and main objectives

There is one main objective in this work, and this is to introduce novel laser-based techniques for the fabrication of medical diagnostic devices and to try and improve on their capabilities. The specific subgroup of medical diagnostic devices that was targeted through this work was paper-based point-of-care diagnostic devices. There are two prerequisites for the manufacture of such a device. The first is the deposition or printing of the biomolecules and reagents that will perform the biological or chemical assay on the paper device. The second is the creation of channels, test zones, and other required structures inside the paper device. These structures should be able to contain the reagents on specific areas of the device, as well as to control the direction and speed of their flow, according to the required steps of the biochemical assay that the device will perform.

Regarding the deposition of the reagents on the devices, Laser Induced Forward Transfer (LIFT) was considered an ideal candidate to explore. LIFT allows the precise deposition of a wide range of materials on a similarly wide range of receiver substrates, making it a very flexible technique. The objective was to explore different materials which could contain and protect the reagents and that could be LIFT-printed. The reagents had to be usable and accessible after LIFT-printing, for the biochemical assay to proceed.

Also, LIFT-printing had to be performed on paper substrates, as this was the material of interest in this case.

Concerning the structuring of the paper devices, it was realised that laser-based photo-polymerisation can provide the flexibility and simplicity required during the manufacturing process, even for complex designs and functions. The target was to investigate whether this novel technique is capable of producing high quality paper-based diagnostic devices in a cost-effective, scalable and rapid manner. In order to achieve this, various materials had to be tested such as polymers and membranes.

A similar, laser direct-write approach was considered as the solution to the problem of creating micron-scale features on materials that could be used to cast a mould for micro-contact printing of biomolecules.

All these different objectives and their suggested solutions had the same goal that was to merge two different fields, laser physics and biology, into this highly multi-disciplinary work and produce an outcome that, it is hoped, will move the field of point-of-care diagnostics forward.

1.2 Outline of this thesis

In chapter 2, a general description of the laser direct-write techniques will be presented. Additive and subtractive laser-based techniques will be discussed, with more focus given on Laser Induced Forward Transfer, photo-polymerisation and ablation. Additionally, point-of-care diagnostic sensors will be introduced, and a more in-depth analysis of paper-based sensors will be given. Finally, Enzyme Linked Immunosorbent Assays will be presented, as they are the main type of assay used in this work.

Chapter 3 is focused on Laser Induced Forward Transfer, and more specifically on its applications for laser-printing of biomolecules on paper-based diagnostic devices. Trials of LIFT of several different materials containing antibodies will be discussed, and the main results of glycerol-based donors will be presented.

Chapter 4 will introduce a novel laser-based manufacturing technique for the fabrication of structures in porous media such as cellulose paper and nitrocellulose membrane. This technique is based on photo-polymerisation and allows the creation of fluidic channels and barriers inside the volume of the substrate, thus providing additional functionalities and properties on paper-based devices. More specifically, it can lead to miniaturisation and multiplexing of these devices, allowing for cheaper manufacturing and more complex designs and testing. Furthermore, several different diagnostic assays will be presented, both on cellulose and nitrocellulose, and for detection in water as well as in human bodily fluids.

In chapter 5, the paper patterning technique of the previous chapter is utilised to give additional properties to paper-based devices. More specifically, photo-polymerised barriers fabricated inside the volume of the paper are used to impose delays on the fluidic flows. Here, two different types of barriers will be presented, made with pulsed and c.w. lasers accordingly. A semi-automated paper-based test for the detection of CRP that requires minimal input from the user is also presented in this chapter.

Chapter 6 describes a novel technique for the fabrication of micro-contact printing devices. This technique uses a digital multi-mirror device to create arbitrarily shaped structures via either ablation or photo-polymerisation in a substrate. This substrate, the master, is then used to cast the complementary pattern in PDMS. The PDMS mould is then used as a stamp for micro-contact printing of ink and proteins.

Finally, in chapter 7 the main conclusions and contributions of this work to the field are outlined. The thoughts and ideas for future work and the future prospects of this project are presented.

Chapter 2

Background

2.1 Laser Direct-Write Techniques

Laser direct-write (LDW) is a sub-class of a wide group of processes called direct writing. Direct writing includes any technique or process capable of depositing, removing or processing different types of materials over various surfaces following a preset pattern [1]. They are typically processes that employ computer-controlled translation stages that move a pattern-generating device such as laser writing optics or ink deposition nozzles [2]. Direct writing is distinct from conventional rapid prototyping in terms of the track width ranging from sub-microns to millimetres, and the range of materials that can be deposited include metals, ceramics, polymers, electronically and optically functional materials, as well as biological materials [3].

Laser direct-write allows for the deposition, removal, or modification of material through the interaction with a laser beam. LDW is highly versatile and several processes have been developed for each type of application and precursor, i.e. solid, liquid, gas.

2.1.1 Laser Direct-Write Subtraction

Laser Direct-Write Subtraction (LDW-) includes techniques and processes that result in photochemical, photothermal, or photophysical ablation on a substrate, directly creating the features of interest. Common processes that fit this description are laser scribing, cutting, drilling, or etching. All of them are able to produce surface relief structures or holes in a material. The fundamental interactions that lead to material removal can be either thermal or athermal, depending primarily on the material and environment characteristics as well as the pulse duration of the laser. The nature of these interactions has a direct effect on the quality of the produced features. For example, when the material is thermally removed, there is a tendency for a heat-affected zone to occur near the vicinity of the removed material. This zone has structures and properties that can differ from the bulk material and can exhibit additional surface relief. On the other hand, athermal absorption caused by ultrafast lasers can reduce the formation of a heat-affected zone, thus enabling features smaller than the diffraction limit [4, 5].

2.1.1.1 Laser ablation

Laser ablation is the process in which a laser beam is focused on a surface to remove material from the irradiated area. Laser ablation is usually driven by absorption and heat transfer with subsequent melting and evaporation of the illuminated material. The ability of the material to absorb laser energy limits the depth to which that energy can perform useful ablation. Ablation depth is determined by the absorption depth and the thermal diffusion length of the material. The depth is also a function of beam energy density, the laser pulse duration, and the laser wavelength.

Lasers used for micromachining are normally pulsed lasers which have a relatively low duty cycle, or less commonly they may be a continuous wave laser (c.w.). That is, the pulse width (time) is very short compared to the time between pulses. Therefore, even though excimer lasers have a low average power compared to other larger lasers, their peak power can be quite large. The peak intensity and fluence of the laser is given by

$$\text{Peak intensity (Watts/cm}^2) = \frac{\text{Peak power (W)}}{\text{Focal spot area (cm}^2)} \tag{2.1}$$

$$\text{Fluence (Joules/cm}^2) = \frac{\text{Laser pulse energy (J)}}{\text{Focal spot area (cm}^2)} \tag{2.2}$$

while the peak power is

$$\text{Peak power (W)} = \frac{\text{Laser pulse energy (J)}}{\text{Pulse duration (sec)}} \tag{2.3}$$

There are several key parameters to consider for laser ablation. The first is selection of a wavelength with a minimum absorption depth. This will help ensure a high energy deposition in a small volume for rapid and complete ablation. The second parameter is a short pulse duration to maximize peak power and to minimize thermal conduction to the surrounding work material. The third parameter is the pulse repetition rate. If the rate is too low, all of the energy which was not used for ablation will leave the ablation zone allowing cooling. If the residual heat can be retained, thus limiting the time for conduction, by a rapid pulse repetition rate, the ablation will be more efficient. More of the incident energy will go toward ablation and less will be lost to the surrounding work material and the environment. The fourth parameter is the beam quality. Beam quality is measured by the brightness (energy), the focusability, and the homogeneity. The beam energy is of no use if it cannot be properly and efficiently delivered to the ablation region. Further, if the beam is not of a controlled size, the ablation region may be larger than desired with excessive slope in the sidewalls.

As described in chapter 6, laser ablation was utilised to create micron-sized features on Bi_2Te_3 films for micro-contact printing applications.

2.1.2 Laser Direct-Write Addition

2.1.2.1 Laser Induced Forward Transfer

LIFT is a laser-based direct-write additive technique used for depositing materials from a thin donor film onto a receiver substrate, as shown schematically in Fig. 2.1. The donor film is pre-deposited on a carrier that is transparent to the incident laser light, and photons from the laser source provide the driving force that transfers a small volume of the donor material onto the accepting receiver. The LIFT technique was first proposed by Bohandy et al. [6] for deposition of Cu films using an ArF excimer laser, but since then it has been employed for printing a wide range of materials including metals, oxides, polymers, ceramics, organics as well as biomaterials, for applications as diverse as embedded electronic circuits, integrated photonic devices and tissue engineering [7–13]. For printing of biological donor materials, the transfer of cells [14–19], fungi [20], proteins [21–24], antigens [25], bacteria [26] and DNA [27–30] has already been reported in the literature, where one of the most fundamental requirements is to demonstrate the printing of viable and undamaged samples. This laser-based approach to printing of biomaterials has several inherent advantages; operation in a standard ambient environment allows printing of a wide range of materials with the further possibility of transferring multi-layered (either vertical stacks, or horizontally patterned) structures composed of different materials. In addition, a further flexibility presents itself in the form of precise control of the size and shape of the printed pixels which is possible by controlling the parameters of the incident laser light such as wavelength, pulse duration, energy density and spatial beam profile.

During LIFT, a laser pulse is focused or imaged onto the interface between the donor and the carrier and it is absorbed within a small volume of the donor. This rapid absorption leads to an explosive phase transformation within the donor-carrier interface, which is

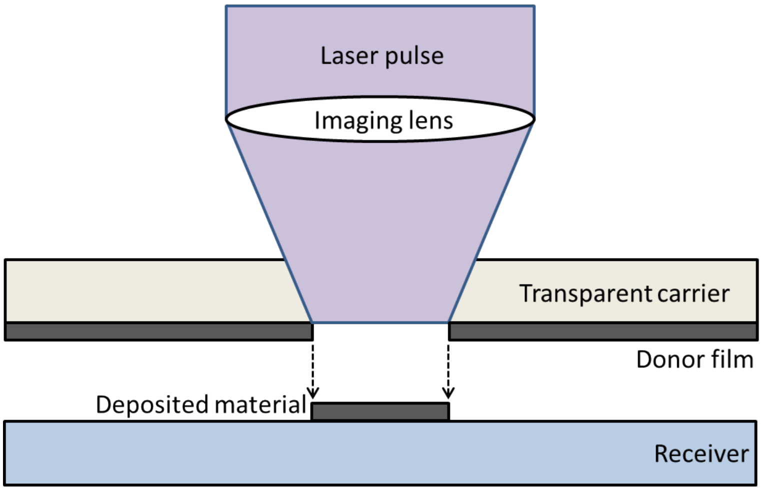

FIGURE 2.1: Schematic of the LIFT configuration.

followed by the expansion of the heated volume, which causes a small area of the donor to detach from the carrier and be transferred onto the receiver [31].

Usually, the receiver is in contact or separated some few microns from the donor via a spacer. The lateral dimensions of the transferred material are defined by the lateral dimensions of the incident laser pulse and by the phase of the donor material (liquid, solid, paste). The LIFT-printed spots are typically in the range of microns to millimeters. The LIFT-printed material is also termed the pad or the flyer.

2.1.2.2 LIFT with dynamic release layer

As described earlier, LIFT relies on the absorptivity of the incident laser light within a small volume of the donor [32] and some donor films cannot tolerate such direct illumination from the laser pulse. Therefore, when the donor material is transparent to the laser pulses or is very delicate, it is necessary to introduce a dynamic release layer (DRL) between the carrier and the donor as seen in Fig. 2.2. The added benefit of using such a DRL is that it can facilitate the propulsion of the flyer.

It is very important that during LIFT-printing, the biomaterial (antibodies) intended for transfer onto the paper receiver needs to be protected against direct exposure to any laser radiation since interaction with high energy laser pulses could lead to significant loss of biological or chemical properties of the material. We have therefore chosen for this work, this modified LIFT procedure referred to as Dynamic Release Layer (DRL-LIFT), which employs the use of a sacrificial layer that absorbs the energy of the incident laser pulses and transforms it into mechanical energy that propels the donor material to the receiver. The DRL prevents the laser light from damaging the donor and this is

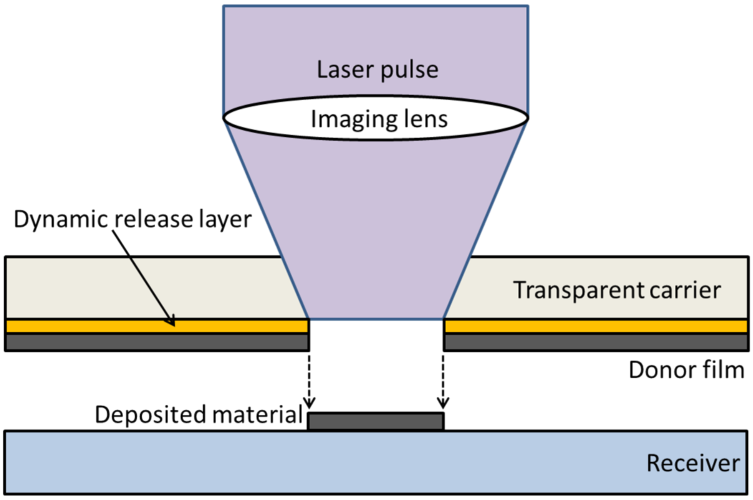

FIGURE 2.2: Schematic of the Dynamic Release Layer LIFT configuration.

especially important when LIFT-printing sensitive materials. The material chosen as a DRL therefore needs to have a low ablation threshold and a high absorption coefficient to minimize excessive heating of the donor, and thereby the possibility of any denaturing of the transferred antibodies. Materials commonly used as DRLs include gold [33], silver [20], titanium [26, 29, 34] and polymers such as triazene [15, 35–37].

There are cases where the DRL remains intact and the propulsion of the donor film is facilitated through the mechanical flexibility of the DRL. This technique is termed as blister-actuated LIFT (BA-LIFT), where a flexible DRL is deformed after the absorption of the laser pulse, and transfers the momentum of the deformation to an area of the donor film, which is subsequently ejected and transferred to the receiver [38–40].

As described in chapter 3, DRL-LIFT has been used to print biomolecules on paper substrates, as a paper-based diagnostics fabrication tool.

2.1.2.3 Matrix-assisted pulsed laser evaporation

Matrix-assisted pulsed laser evaporation direct-write (MAPLE-DW) is a laser-based process in which the donor is embedded within a matrix, or a solution, that acts as the DRL. The matrix evaporates during and/or after the transfer, and only the donor remains as a deposit on the receiver as seen in Fig. 2.3 [41]. The liquid donor can be frozen prior to LIFT-printing in order to suppress or reduce premature evaporation, but also to improve donor handling. Similarly to DRL-LIFT, the laser pulse causes the DRL to propel the donor towards the receiver. The transfer mechanism of MAPLE LIFT is identical; the heating induced by the laser pulse causes the DRL to evaporate and expand, therefore providing the mechanical thrust required for transfer. MAPLE DW has been used for the printing of viable biomaterials [41], metals [42], and entire sensors [43]. Another very similar technique, called Laser Decal Transfer (LDT), employs a solvent as the matrix and usually the deposits are cured post-transfer [44].

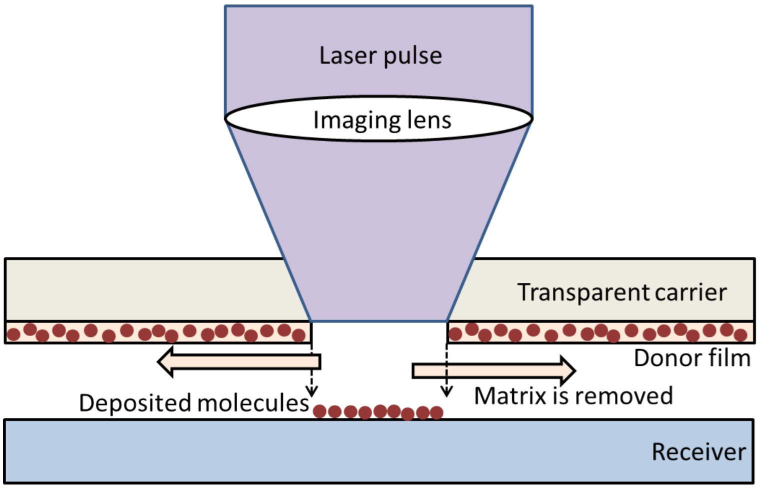

Figure 2.3: Schematic of the Matrix-Assisted Pulsed Laser Evaporation configuration.

2.1.2.4 Laser-induced backward transfer

Laser-induced backward transfer (LIBT) is based on similar mechanisms as LIFT, with the difference that the donor-carrier-receiver configuration is reversed. The receiver is placed in the beam path and the donor is facing the laser pulse as seen in Fig. 2.4. Obviously, the receiver needs to be transparent to the laser pulses, whereas the carrier is opaque. The laser pulse passes through the carrier and is absorbed by the donor, or in the case that the donor is also transparent, at the interface of the donor and opaque carrier. The pulse is absorbed, the donor material is heated and expanded and is propelled backward and towards the receiver. This technique was first demonstrated for the fabrication of nano-size metal particles [45] and it has also been applied to the transfer of liquids from a self-replenishing donor [46].

2.1.3 Laser Direct-Write Modification

2.1.3.1 Photo-induced polymerisation

Polymerisation is a process in which relatively small molecules, called monomers, combine chemically to produce very large chain or network molecules, called polymers [47]. Photo-induced polymerisation is a polymerisation reaction where initiation is triggered by radiation. A photoinitiator is usually added to the formulation, since most monomers

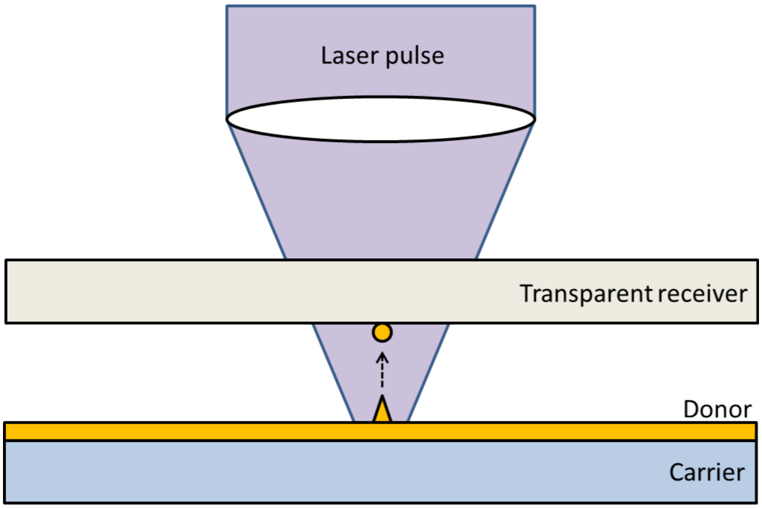

Figure 2.4: Schematic of the LIBT setup showing the reverse configuration.

do not produce sufficient initiating species under illumination from a light source. Photoinitiation usually requires UV light, although other radiation, including visible light, can be employed. The polymer formation is a fast transformation of the liquid monomer into a solid material. There are two major chemical schemes that are commonly used in photopolymerisation, each requiring a specialized photoinitiator. In free radical polymerization a complex ion (radical) is split off the initiator by the light radiation and that combines with a monomer molecule to start the reaction. In cationic polymerization, light causes a strong acid to be released by the initiator and that in turn starts the bonding process. Most photopolymers today are based on the free radical scheme, but more advanced materials use cationic polymerization which frequently offers better final solid material properties.

Once the polymerization process starts, it continues because it's a chain reaction. Each time monomer or binder molecules link to form a gelling solid, they liberate other radicals or acid molecules that in turn cause additional molecules to bond - and so on. In some cases the propagation can even proceed in the dark for a short time after the light source is removed. The chain reaction continues to propagate until radicals recombine to form non-reactive products, or the ingredients needed for the reaction are no longer available in the correct proportions, or finally by trapping reactive molecules in the hardening matrix where they can no longer move into position to combine.

One of the great advantages of laser-based polymerisation is the rapidity of the curing process, with extensive crosslinking usually being achieved within a single second. Lasers are very advantageous for polymerising applications as, not only they have great energy output, but they also emit light coherently. The spatial coherence of the laser emission allows the beam to be focused down to very small dimensions, and this enables the generation of high resolution patterns. Another advantage is that the light intensity does not change by varying the distance from the laser, and this enables uniform illumination of large and also non-planar objects. Additionally, one great advantage of using lasers as the light source, is that the decrease in curing rate, as chain propagation is increasingly hindered during solidification, can be compensated for by the higher rate of initiation occuring due to the intense laser irradiation. There are other characteristics and advantages of laser-induced photo-polymerisation and they are summarised in Fig. 2.5.

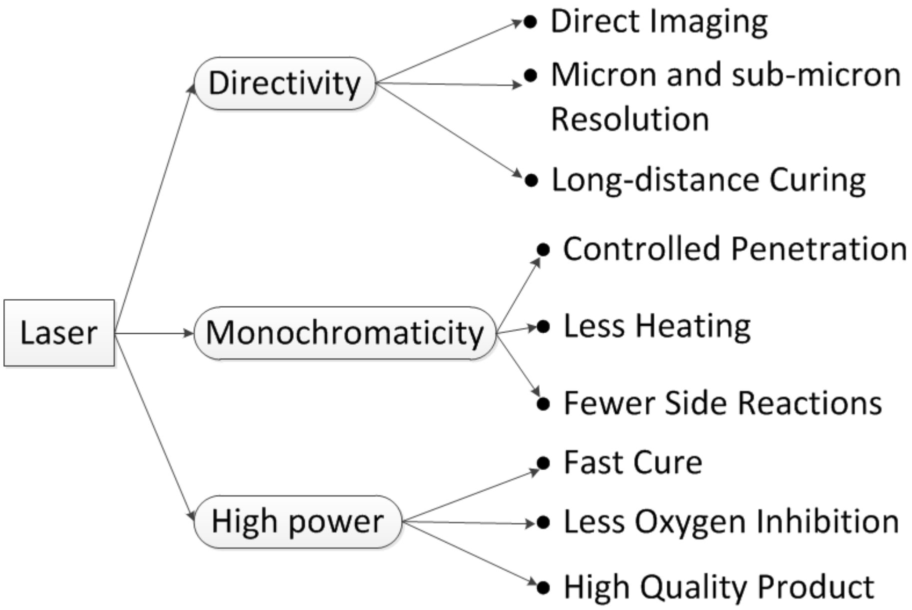

FIGURE 2.5: Performance characteristics of laser-induced photo-polymerisation [47].

Photopolymerisation guarantees spatial resolution, compared to thermal polymerisation, as the polymerisation occurs only in the illuminated areas. Applications of photopolymerisation range from manufacture of optical disks and microcircuits using photolithography [48, 49], to dental healthcare, display screens, optoelectronics [50, 51], energy storage and microfluidic devices [52].

As shown in chapters 4 and 5, photopolymerisation was used to fabricate structures within paper substrates, as a paper-based diagnostics manufacturing tool.

2.1.3.2 Multi-photon polymerisation

Complex topographical structures can be fabricated with sub-micron resolution, by tightly focusing a pulsed laser beam within a three-dimensionally defined focal volume of photo-sensitive polymers [53]. This is achieved through multi-photon absorption (MPA) by the material that causes solidification. This means that photochemical or photophysical transformations are restricted to occur within the focal volume of the laser beam and by moving the focal position, intricate three-dimensional microstructures can be created. In MPA, an electronic transition in a material is driven not by a single photon, but rather by two or more photons combined. The probability for MPA depends on the intensity of the light used to the power of the number of photons that must be absorbed to drive the transition, because multiple photons must be present simultaneously. By using femtosecond 3D laser scanning using micro-stages, plastic models of animals, buildings and micron-sized words can be produced [54–56]. This technique has also been used to direct-write 3D protein microstructures, opening opportunities for creating complex cellular interfaces for cell growth [57, 58].

As described in chapter 6, multi-photon polymerisation was used to generate micron-sized features on polymer, for micro-contact printing applications.

2.2 Medical and biochemical diagnostics

2.2.1 Immunoassays

Immunoassays are biochemical methods of antigen detection that are highly sensitive and specific, depending mostly on the binding specificity or affinity of an antibody to a macromolecule. Immunoassays have many different formats and variations, and are usually run in multiple steps with reagents being added and washed away at different steps of the assay. Immunoassays became considerably simpler to perform and more popular when techniques for chemically linking enzymes to antibodies were demonstrated in the 1960s [59].

In immunology, an antibody or an immunoglobulin, is a large, Y-shaped protein produced by plasma cells that is used by the immune system to identify and neutralise pathogens such as bacteria and viruses. The macromolecule bound by an antibody is called an antigen and the area of an antigen to which the antibody binds is referred to as an epitope. Antibodies do not recognise the whole antigen molecule, but they bind non-covalently to specific epitopes of these antigens. The non-covalent bonding includes electrostatic interactions (ionic bonding, hydrogen bonding, halogen bonding), Van der Waals forces, and hydrophobic interactions, which are reversible and determine the strength of interaction between antibodies and antigens. The antibodies we have chosen for our experiments are Immunoglobulin G (IgG), an antibody isotype composed of four peptide chains, two identical heavy chains and two identical light chains arranged in a Y-shape, and which thus provides two antigen binding sites as shown in Fig. 2.6.

They are the most abundant antibody isotype found in blood and major components of the immune system and are therefore extensively used as a diagnostic tool for many conditions.

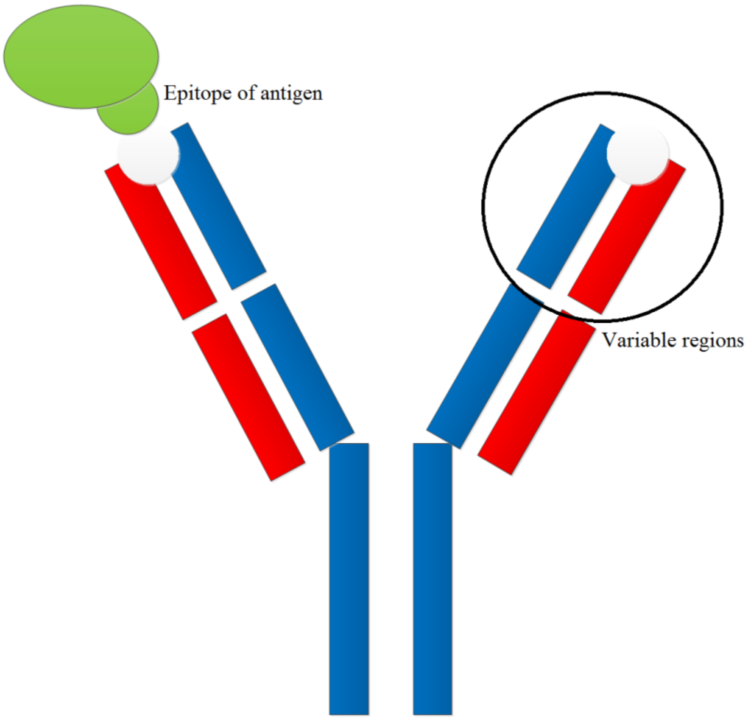

FIGURE 2.6: Schematic of the structure of an IgG antibody.

In addition to the binding of an antibody to its antigen, the other key aspect of all immunoassays is the means to produce a measurable signal in response to this binding. A large number of labels or tags exist in modern immunoassays, and they allow for detection through different means. These labels are detectable either because they produce a colour change in a solution, fluoresce under light, they emit radiation, or because they can be induced to emit light.

The antibodies that bind directly to the specific antigen are known as primary antibodies. The secondary antibodies are usually conjugated or labeled with enzymes or nanoparticles and are used as detection antibodies to determine the concentration of the antigen [60].

2.2.2 Enzyme Linked Immunosorbent Assay (ELISA)

ELISAs are a commonly used type of immunoassay that typically employs Immunoglobulin G (IgG) antibodies that are raised in animals and that are directed against a vast range of proteins for different conditions, diseases and allergens. These antibodies can be either monoclonal or polyclonal, which means that they bind to a very specific binding site or multiple binding sites of antigens respectively. The binding of the antigen and antibody is detected using an enzyme linked to a secondary antibody, which turns the antigen-antibody complex into a coloured product when chromogenic enzyme substrate is added. Enzymes are one of the most popular labels for immunoassays and they include horseradish peroxidase (HRP), alkaline phosphatase (ALP) or glucose oxidase. In some cases, these enzymes are exposed to reagents that cause them to produce light or chemiluminescence instead of a colouration of the solution. ELISAs are useful methods in not only detecting but also quantifying antigens in samples, and they provide relatively fast, highly specific, highly sensitive, and very robust detection through enzymatic signal amplification [61].

Typically, ELISAs have four main steps, consisting of coating, blocking, reacting of antigen and antibody, and developing colour, while there are intermittent washing steps. There are different formats of ELISAs, namely direct, indirect, competitive, and non-competitive (sandwich ELISA) [62]. The format that is used is determined by the purpose of the experiment and the types of antibodies and antigens used. Direct ELISAs, the simplest format, involves binding of the antigen directly to a microtiter multi-well plate and the subsequent introduction of an enzyme-labelled secondary antibody as shown in Fig. 2.7a. Similarly, in the case of indirect ELISAs, the antigen is first bound on the plate, but is instead followed by an unlabelled primary antibody. Subsequently, an enzyme-labelled secondary antibody is introduced, that binds specifically to the primary antibody, as seen in Fig. 2.7b. Non-competitive ELISAs first require the binding of the capture antibody to the microtiter plate and the subsequent binding of the antigen to the capture antibody. Following that, an enzyme-conjugated detection antibody, specific to the antigen, is added and bound to the antigen as seen in Fig. 2.7c. The last format of ELISA, which is competitive, involves the incubation in solution of a primary unlabeled antibody and the antigen. The antibody-antigen complexes are then added on the microtiter plate that is pre-coated with the same antigen. Any unbound antibody will be removed by washing the substrate, which means that the more antigen in the sample, the less antibody will be able to bind to the antigen in the substrate, hence the assay is competitive. Lastly, the secondary enzyme-linked antibody that is specific to the primary antibody is added, and the remaining enzyme produce a chromogenic or fluorescent signal (Fig. 2.7d). A competitive ELISA works in the inverse way of the other ELISAs, meaning that the higher the antigen concentration in the sample, the weaker the eventual signal. The major advantage of a competitive ELISA is the ability to use crude or impure samples and still selectively bind any antigen that may be present.

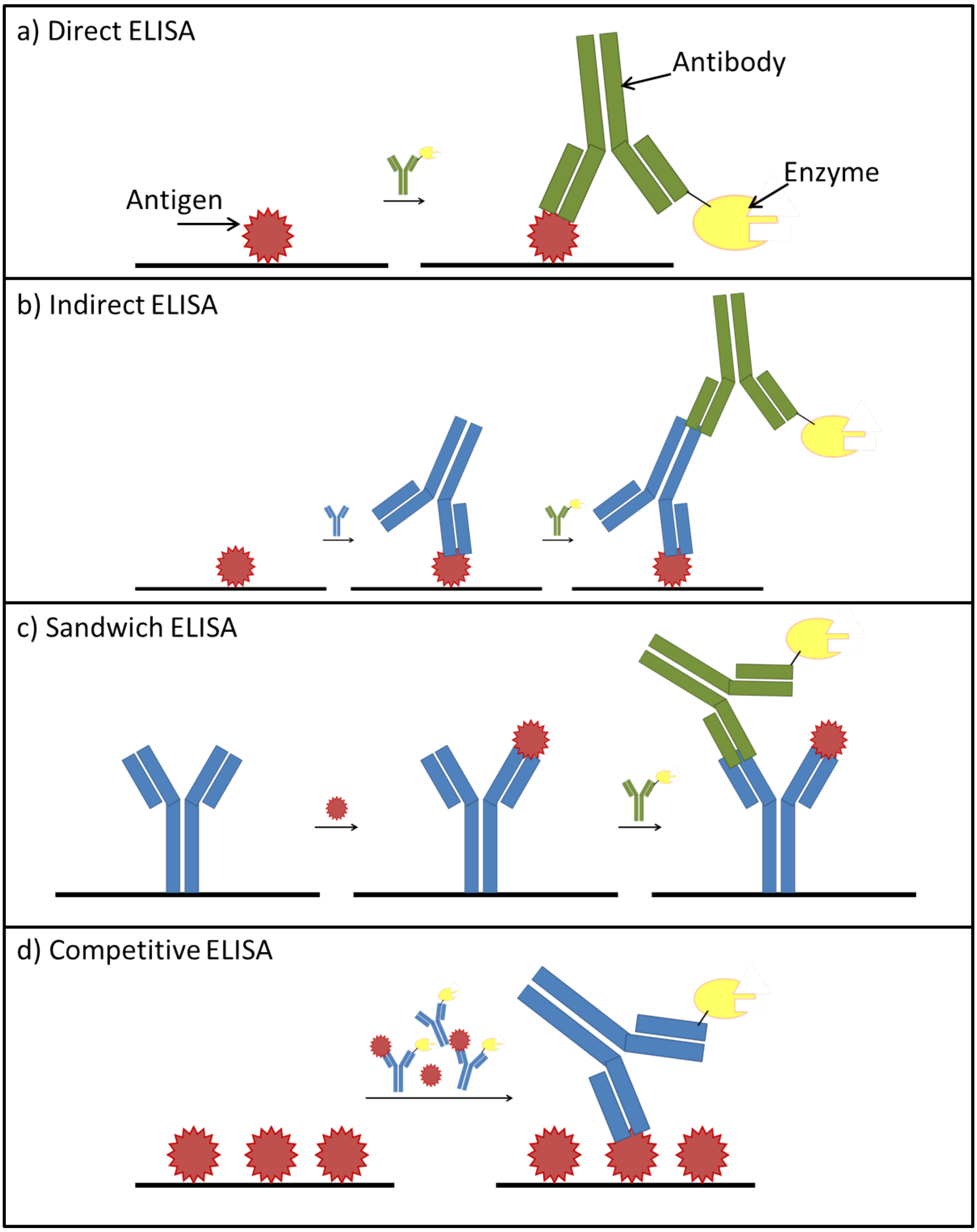

FIGURE 2.7: Schematic of the several ELISA formats, namely (a) direct, (b) indirect, (c) sandwich, and (d) competitive.

2.2.3 Point-of-care biosensors

Both in developed and developing countries, early and accurate diagnosis is important for the health of patients. It allows for prompt and proper treatment of patients, limits the spread of disease in the general public and minimises the waste of resources on ineffective treatment [63]. In the absence of diagnostic tests, disease in low-resource settings is often treated based on clinical symptoms and local prevalence of disease, and in that case, many patients stay untreated, or are treated for the wrong disease, or even remain completely untreated. It is therefore of utmost importance that diagnostics become widely available, especially in areas with low resources.

Point-of-care devices are diagnostics specifically designed to be used at the site where the patient is located, outside a diagnostic laboratory, by non-laboratory staff. In recent years, there has been much research in developing and fabricating paper-based point-of-care devices for biochemical analysis and medical diagnostics [64, 65]. This research has been driven by the need for reliable diagnostic tools in the developing world where there is little or no infrastructure, trained personnel and hence expensive technologies cannot be afforded [66]. POC diagnostic tests should be Affordable by those at risk of infection, Sensitive (few false positives), Specific (few false negatives), User-friendly (simple to perform and requiring minimal training), Rapid (to enable treatment at first visit) and Robust, Equipment-free and Deliverable to those who need it, following the ASSURED criteria set out by the World Health Organisation. A list of the attributes that a simple test should have, as set by the Food and Drug Administration (FDA) can be seen in Table 2.1.

Table 2.1: Attributes of a simple test as set by the FDA. [67]

Fully automated instrument or unitised, self-contained test
Uses direct unprocessed specimens
Needs only basic, non-technique-dependent specimen manipulation
Needs only basic, non-technique-dependent reagent manipulation
Needs no operator intervention during the analysis steps
Needs no technical or specialised training
Needs no electronic or mechanical maintenance
Produces results that require no operator calibration, interpretation, or calculations
Produces results that are clear to read, such as positive or negative, a direct read-out of numerical values, the clear presence or absense of a line, or obvious colour gradiations
Has test performance comparable to a traceable reference method, as demonstrated by studies in which intended operators perform the test
Contains a quick reference instruction sheet written at the educational level of the user

There are tests already available that target diseases such as HIV, malaria and tuberculosis, which are the major causes of infection that afflict mostly the developing world. These rapid POC tests are also far more cost-effective (0.25-30 USD per test) compared to typical laboratory tests.

2.2.4 Paper-based and lateral flow diagnostics

The concept and the first demonstration of paper-based diagnostic devices were given by the Whitesides group in Harvard University [68, 69]. There are several advantages in using paper as the platform for diagnostic technologies. Paper is widely manufactured from renewable resources and is inexpensive. Its porous structure allows wicking of liquids without the use of external pumps. It is suitable for biological applications since it is biocompatible while its properties can be easily altered to suit different applications. It can be easily stored and transported and it is also combustible and biodegradable.

Lateral flow biosensors are rapid, immunochromatographic test strips that are able to diagnose a wide range of analytes in a sample without the need for specialized and expensive equipment or human resources [70, 71]. They are typically used for medical diagnostics either for home testing, point of care testing or laboratory use, and are one of the most widely available and used application is the home pregnancy test.

These assays consist of several zones, typically made from different materials and each serves one or more different purposes (Fig. 2.8). The sample pad is the starting part of the test where the sample is added on the strip and, if required is treated to be compatible with the rest of the strip. The sample flows to the conjugate pad where a specific conjugate has been immobilised during the manufacture of the strip. This conjugate is usually colloidal gold, or coloured or fluorescent or magnetic latex microparticles, which are conjugated to biomolecules that bind to the target analyte of the test strip, and then migrate to the next section of the strip as a complex. This next section is the reaction pad on which are the test and control lines. These lines are composed typically of antibodies that bind to the target analyte and the conjugated biomolecule respectively. In this way, the complex analyte-conjugate will bind to the test line only if the analyte is present in the sample, but will bind to the control line regardless of the presence of the target analyte. A colorimetric change at the test and control lines indicates the presence of the analyte and the correct implementation of the assay as seen in Fig. 2.9. One of our main objectives is to develop a laser-printed prototype device that performs as a lateral flow sensor.

There are different reaction mechanisms of paper-based diagnostics, with the main categories being chemical, biological and electrochemical reactions [72]. Most chemical

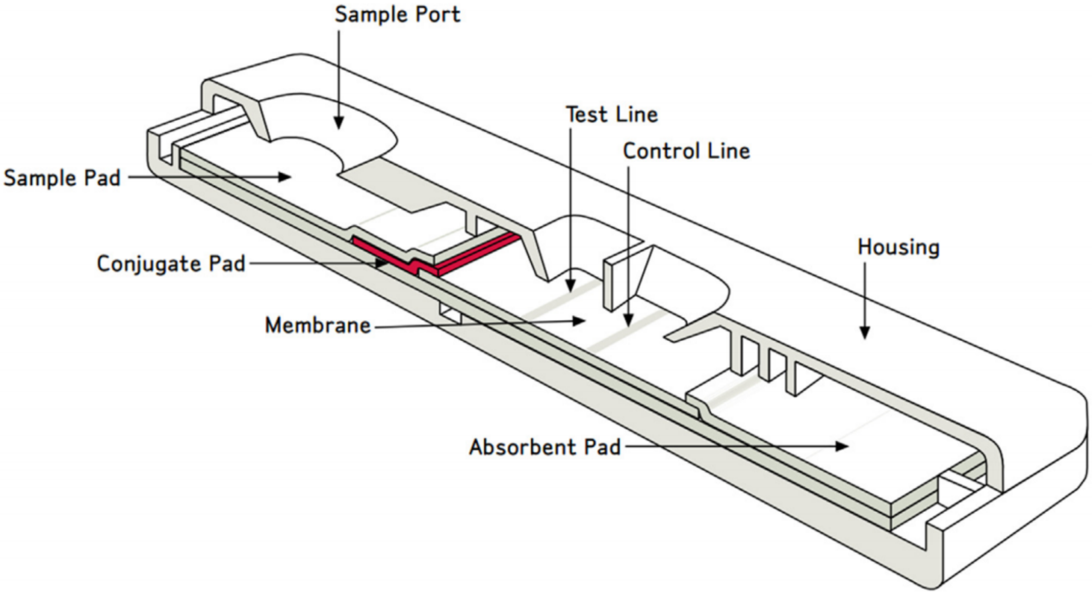

FIGURE 2.8: Schematic of a lateral flow biosensor. [72]

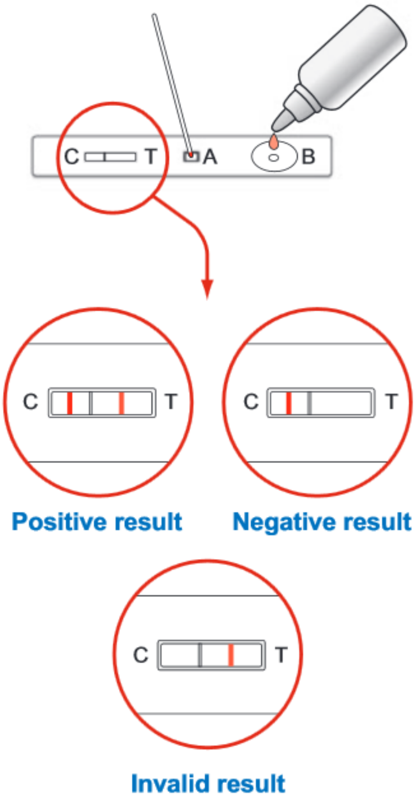

FIGURE 2.9: Typical steps in a lateral-flow test. A is the specimen inlet, B the buffer port, C the control window, and T the test result window. A test result is only valid if a line is observed in the C window. [67]

reactions produce a colour change, such as the redox reaction, the precipitation reaction and the enzymatic reaction. These reactions are usually one-step procedures, as for example the BSA, glucose and nitrite detection tests presented in this thesis. Biological reactions are either based on antigen-antibody binding (similar to immunoassays) or on nucleic acid hybridisation. During this work, only the former reactions were used for the detection of CRP, TNFα etc.

Paper-based ELISAs have been rapidly developed in recent years which allow minimal reagent volumes and simple equipment and materials, and facilitates cheap, quick and reliable diagnostics. They have several advantages compared to a conventional ELISA that is performed on a microtiter plate, while retaining a similar level of specificity and sensitivity. The antibodies and other reagents store well on the nitrocellulose materials used in paper-based tests, so room temperature storage for at least a year can be achieved. These paper based ELISA tests, in a lateral-flow form, require only a few minutes and little sophistication from the user, as they are often as simple as dipping the strip into a body fluid and waiting for the signal to develop. A major drawback of these tests is that they are rarely quantitative, which is inadequate in many cases. It is possible though, that by using a photometric reader or even a camera, some tests can become at least semi-quantitative. Throughout this thesis, we replaced the microtiter plate with laser-patterned paper-based microfluidic devices to implement multi-step ELISAs for detection of a range of analytes including CRP, IL-6 etc., and we have also demonstrated that these tests can be semi-quantitative by using a simple camera to read the results.

Chapter 3

Laser Induced Forward Transfer of antibodies on paper

3.1 Introduction

The development and applications of point-of-care diagnostic devices have been growing significantly over the last few years for use away from the medical and laboratory infrastructure present in a hospital or doctor's surgery [64, 66]. These tests require very small sample volumes (less than 1 ml) with little or no preparation, and provide the result much faster than routine lab tests (in minutes or tens of minutes), can be facilitated and interpreted without any special training or equipment, can be administered in the home environment, and most importantly are cheap to buy and transport. The deposition and subsequent immobilisation of biomolecules on the device during its fabrication has a critical role and is usually achieved by spotting, injection or photolithography. The ultimate goal of this study is the development of paper-based diagnostic devices using an alternative, laser-based, deposition procedure called Laser Induced Forward Transfer (LIFT), which enables printing of reagent volumes as low as a few nanolitres with high spatial printing flexibility. With the end-goal of developing low-cost colorimetric point-of-care diagnostic sensors on paper, in this chapter, we report our results on the LIFT-printing of antibodies, both untagged and conjugated with enzymes.

Use of cellulose paper as a platform to build low-cost sensing devices was proposed by Whitesides et al. in 2007, and since then its use for developing such sensing devices has been well-documented [73]. Paper is readily available in a range of different grades, thicknesses and forms, and has a wide variety of properties such as hydrophilicity, porosity, and capability to wick liquid solutions. Additional features that make paper very attractive for point-of-care sensors are that liquid flow can occur without the need for external pumps, and the properties of the paper can also be adjusted by suitable pre-treatment processes [74, 75]. Finally, it is easily and inexpensively stored and transported, is biocompatible and can be incinerated for easy and safe disposal after use. We have chosen paper as the receiver medium onto which the sensor would be fabricated, because of all these intrinsic benefits in addition to fulfilling the low-cost requirement. The present work demonstrates the use of one of the most routinely employed papers - cellulose-based filter paper - as the receiving substrate for our LIFT-printing studies.

It is very important that during LIFT-printing, the biomolecules (antibodies) intended for transfer onto the paper receiver need to be protected against direct exposure to any laser radiation, since interaction with high energy laser pulses could lead to significant loss of biological or chemical functionality. We have therefore chosen for this work a modified LIFT procedure, referred to as Dynamic Release Layer (DRL-LIFT) [76], which employs the use of a sacrificial layer that absorbs the energy of the incident laser pulses and transforms it into mechanical energy that propels the donor material to the receiver. The material chosen as a DRL therefore needs to have a low ablation threshold and a high absorption coefficient to minimize excessive heating of the donor, and thereby the possibility of any denaturing of the transferred antibodies. Materials commonly used as DRLs include gold [33], silver [20], titanium [26, 29], and polymers such as triazene [15, 35–37].

In this chapter, we present a DRL-LIFT-printing approach that uses an Au DRL to transfer a donor that contains either enzyme-tagged or untagged antibodies. The viability of the antibodies post-transfer was validated by an indirect colorimetric Enzyme Linked Immunosorbent Assay (ELISA) [73]. ELISA is a commonly used method for biochemical analysis that provides high sensitivity and selectivity through enzymatic signal amplification. Paper-based ELISA tests [77] allow for quick and reliable diagnostics with minimal reagent volumes and in conjunction with the patterning ability of LIFT should make possible the fabrication of personalised biosensors, and this concept is further described in a later section. Our results demonstrate the first steps towards our final goal of laser-printed point-of-care paper-based diagnostic sensors. Part of the work in this chapter has been published in [78] and [79].

3.2 Materials and methods

The untagged antibodies used in the present experiments were purified mouse IgG2a (BD Biosciences, UK, 557353). The enzyme-conjugated antibodies were goat anti-mouse IgG (H+L) (Life Technologies, UK, G21040) tagged with horseradish peroxidase (HRP), an enzyme which has the ability to catalyze the conversion of the chromogenic substrate, 3,3',5,5'-Tetramethylbenzidine (TMB) (Sigma-Aldrich, T0440). TMB acts as the hydrogen donor for the reduction of hydrogen peroxide to water by peroxidase enzymes, HRP in this case. This oxidation of 3,3',5,5'-Tetramethylbenzidine results in 3,3',5,5'-Tetramethylbenzidine diimine (Fig. 3.1) which imparts to the solution a characteristic colour change (to blue) that is easily detectable visually by the human eye or a camera. Although in our case the colour was detected using a camera, it is most common to use a spectrophotometer at a wavelength of 650 nm for these measurements. This reaction can also be halted by adding a stop reagent such as sulphuric acid that turns the TMB solution yellow and then the colour can be measured at 450 nm. The protein used in the blocking step was 98% lyophilised bovine serum albumin (BSA) (Sigma-Aldrich, A3059) in a 2% concentration of Phosphate Buffered Saline (PBS) (PAA Laboratories, UK, H15-001). The gelatine used was commercially available food grade gelatine, in the forms of sheets, cubes and powder. The agarose used was molecular biology grade (Sigma-Aldrich, A9539). The glycerol used for the donor film was 99% pure (Fisher Scientific, G/0600/08) and Tween20 (Sigma-Aldrich, P1379) was used as a surfactant in the washing and blocking steps.

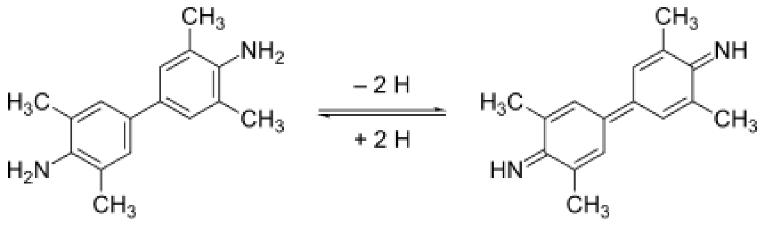

FIGURE 3.1: Oxidation of 3,3',5,5'-Tetramethylbenzidine that results in 3,3',5,5'-Tetramethylbenzidine diimine.

3.3 Experimental setup

The schematic in Fig. 3.2 shows the experimental setup used for these trial LIFT-printing experiments. The laser used for these experiments was a KrF excimer operating at 248 nm at a selected repetition rate of 1 Hz, pulse duration of ~10 ns, and delivering a maximum energy of ~400 mJ per pulse. An aperture was used to select a smaller central area of the beam which had an acceptable spatial uniformity, and this was subsequently imaged via a lens with a focal length of 30 cm onto the interface of the fused silica carrier and the donor providing a laser spot area that varied from ~200 μm x ~200 μm up to ~1000 μm x 1000 μm, large enough to produce a transfer-printed pixel that could be observed without the aid of an imaging device such as a camera. The energy density required for printing should exceed the LIFT threshold, which was experimentally determined to be ~200 mJ/cm^2. Glass slides were used as attenuators to decrease the energy of the incident laser pulses. Two standard manual xyz-axes translational stages were used for positioning the donor and the receiver, which were separately controllable, allowing for LIFT-printing from different areas of the donor onto selected areas of the receiver. The vertical axis of both translation stages was adjusted such that the plane of the donor was set at the image plane of the aperture and the receiver was set using spacers at a separation of ~100 μm from the donor surface.

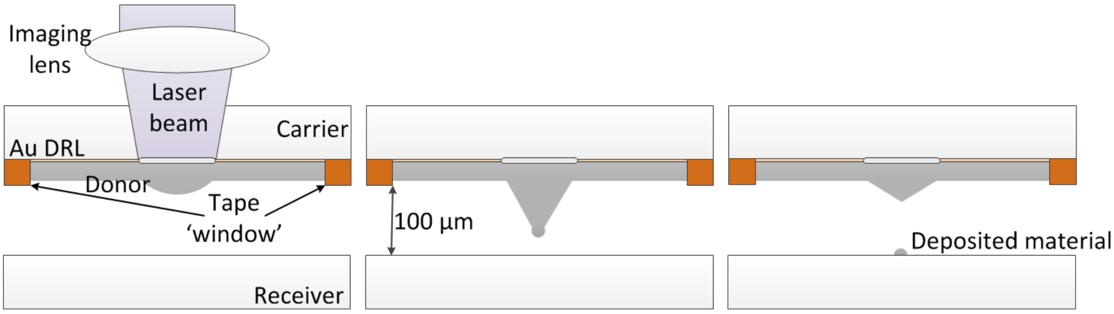

FIGURE 3.2: Schematic of LIFT-printing using a liquid donor.

3.4 Preparation of the donor films and experimental results

There were several materials that were considered as the donor matrix that could incorporate the biomolecules for LIFT-printing. In a liquid form, glycerol was chosen as the most effective one, as it had also been used in previous publications [23, 80, 81] and was known to have all the right attributes for this work. In a solid form, donors made from gelatine and Agar were considered and trialled.

3.4.1 Gelatine donor films

The first material that was trialled was food-grade gelatine because of its biocompatibility and the fact that a solid film can be produced from a liquid solution at a temperature that does not result in the denaturation of the antibodies in the solution. As seen in Fig. 3.3, gelatine has a melting point of less than 50 °C for concentrations of less than 50% (w/v) [82], whereas antibodies start denaturing at temperatures over 50 °C [83]. This is also regardless of the bloom value of the gelatin, which is a measure of the strength of a gel. Therefore, this method will allow the antibodies to retain their structural form and consequently their biological and immunological properties.

In order to produce a thin film on the quartz or fused silica carrier substrate, the gelatine was put in an oven at 120 °C for 10 minutes in order for it to melt and was then

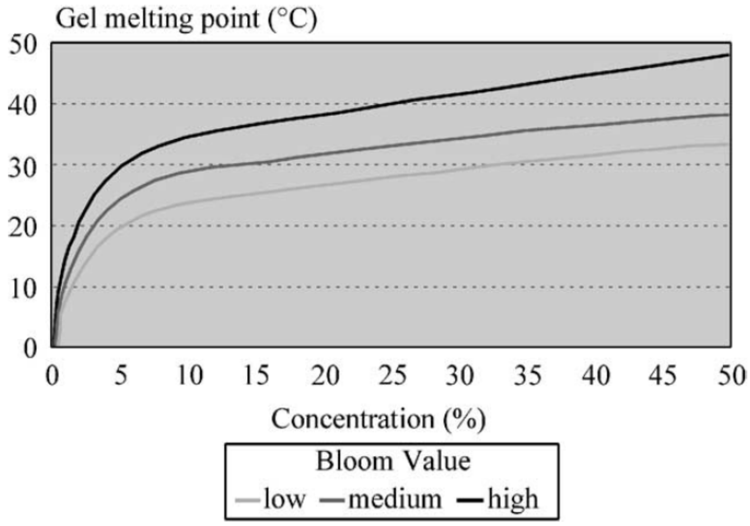

Figure 3.3: Melting points of gelatine [82]. Higher concentrations and bloom values require higher melting temperatures.

transferred on a hot plate at 45 °C. A solution of 15 ml of PBS that also contained the enzyme-tagged antibodies was then added to the beaker and the gelatine was dissolved in it. The solution was thoroughly mixed until it was uniform and a few drops were spin-coated on the quartz substrate, with the spin-coating speed determining the thickness of the film produced as seen in Fig. 3.4 [82]. Through trials of different speeds and measurement of the thickness of each film, the spin coater rotation speed was chosen to be 7,000 RPM. After spin-coating, the film was left to dry and cool at room temperature. Its thickness was then measured using an interferometric microscope and profilometer (ZeScope) with results seen in Fig. 3.5.

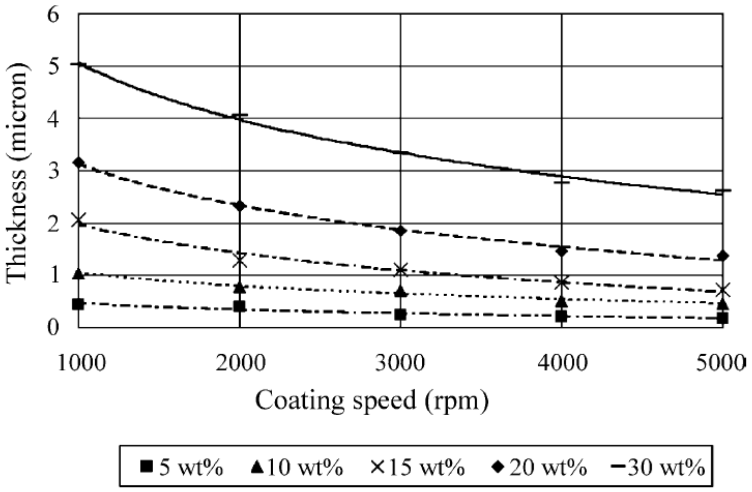

Figure 3.4: The thickness of gelatin film vs coating speed for different concentrations [82]. Higher coating speed produces thinner gelatin films.

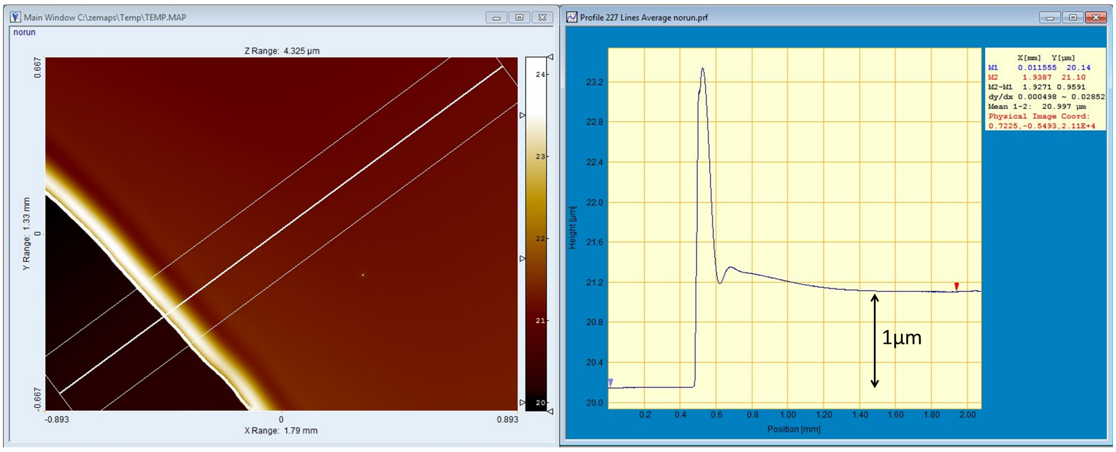

```
       X[mm]   Y[µm]
M1     0.011555  20.14
M2      1.9387  21.10
M2-M1  1.9271 0.9591
dy/dx 0.000498 ~ 0.02852
Mean 1-2:  20.997 µm
Physical Image Coord:
0.7225,-0.5493,2.11E+4
```

FIGURE 3.5: Profile of a gelatine film spin coated on a quartz slide at 7000 RPM. The thickness of the film is ∼1 μm.

In order to find the optimal parameters for LIFT using a gelatine donor, several lines of spots were LIFT-printed using different laser energies varying from ∼2 mJ/pulse to ∼7.3 mJ/pulse, corresponding to excimer voltages ranging from 19 kV to 30 kV. The separation between donor and receiver was kept at ∼100 μm and the spot size was 200 x 200 μm. Following the LIFT-printing experiments, the donors and the receivers were observed under an optical microscope. Figure 3.6 shows sets of areas on the donor film that have been LIFT printed from. It is apparent that LIFT was not possible, although there is a clear outline at the areas where the laser beam hit the donor. Even at the highest laser intensity, the material seems to have been partly modified or melted, but it has not been clearly removed from the carrier. Increasing the energy of the laser pulses resulted in more debris at the chosen deposition sites and at the surrounding areas, generated either by the donor or the paper receiver. These results are further confirmed through Fig. 3.7 that shows the profile of the LIFT-printed areas on the donor film, and clearly shows that the material has been removed only partially, to a depth of ∼0.2 μm of the 1 μm thick film.

The attempt of the LIFT-printed spots on the paper receiver did not lead to any quantifiable results. Although the spots were clearly visible with the naked eye as they were darker compared to the white background of the paper, they were not visible under the optical microscope, partly because of the complex fibrous nature of the paper that do not allow for adequate focusing, and partly because any transferred material would be transparent. The method of ensuring that the LIFT-printing was performed correctly was by incorporating the enzyme-tagged antibodies in the donor film, because the LIFT-printed pixels could subsequently be visualised via a colour change produced by adding the chromogenic substrate. As expected, the addition of TMB did not produce any

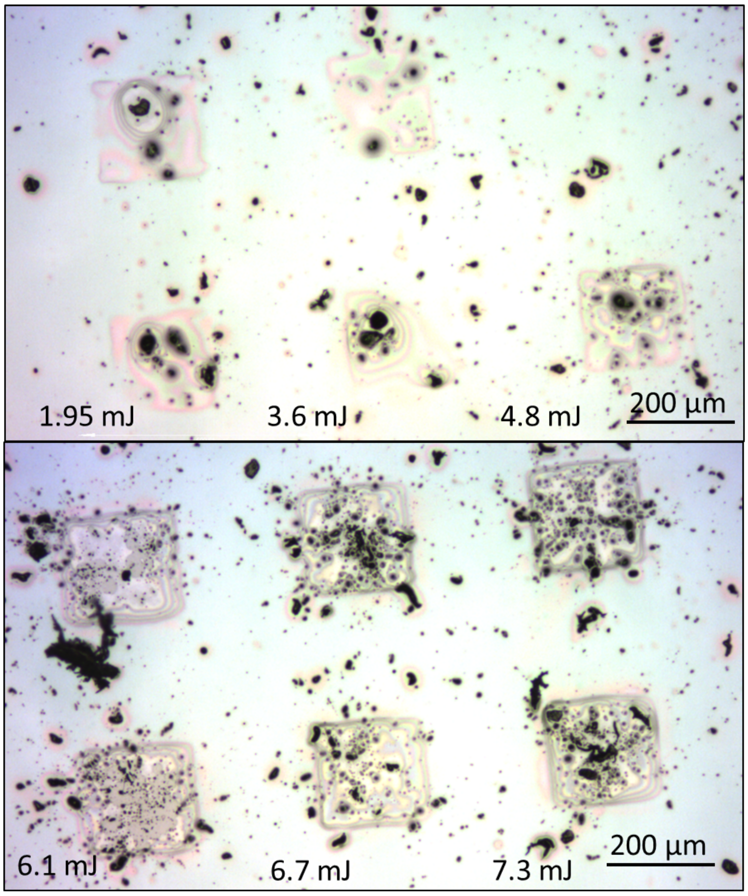

FIGURE 3.6: Microscope images showing areas on the donor film that have been LIFT printed from, using different energies ranging from 2 mJ/pulse to 7.3 mJ/pulse.

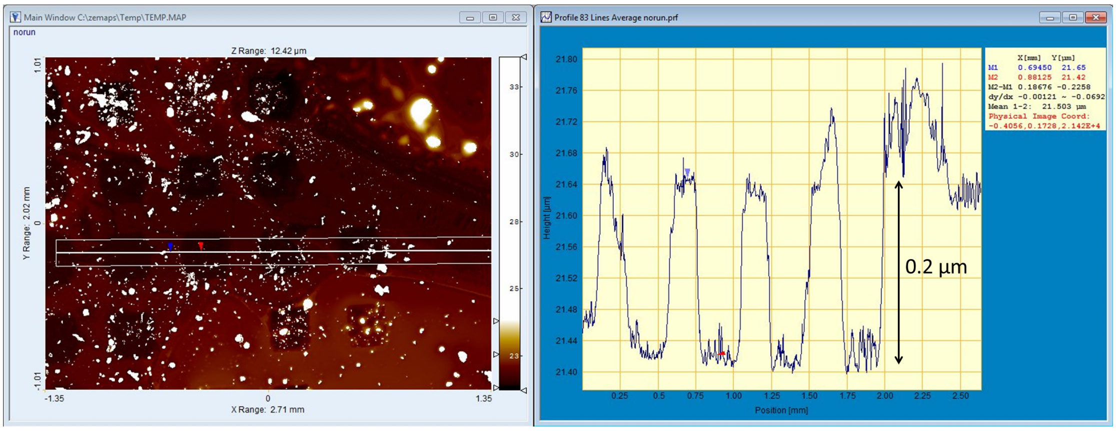

```
       X[mm]   Y[µm]
M1     0.69450  21.65
M2     0.88125  21.42
M2-M1 0.18676 -0.2258
dy/dx -0.00121 ~ -0.0692
Mean 1-2:  21.503 µm
Physical Image Coord:
-0.4056,0.1728,2.142E+4
```

FIGURE 3.7: Images showing the profile of the areas on the donor film that have been LIFT printed from. The spots were 0.2 μm deep whereas the original donor film was ~1 μm.

colour change at the specified LIFT-printed spots, thus confirming that this experiment had not yet succeeded.

Another attempt for LIFT-printing of the gelatine donor was performed with the addition of a DRL. It was found that the gelatine film did not absorb the laser pulse at the wavelength of the KrF excimer, and therefore a DRL film was required. The quartz slides were thoroughly cleaned using a standard cleaning procedure in the cleanroom, and a 25 nm Au layer was deposited with the resistive evaporator to ensure the uniformity and smoothness of the layer. LIFT was conducted as previously, with pulse energies ranging between ∼2 mJ/pulse and ∼7.3 mJ/pulse, keeping the same 100 μm separation, but the spot size was increased to 500 x 500 μm. As seen in Fig. 3.8 that shows the donor film, LIFT worked slightly better, although residue of the film can still be seen inside the spots. The same test using HRP-tagged antibodies and TMB was performed on the paper receivers to see if the antibodies had been successfully transferred, but it did not produce any colour change, and thereby experimenting with LIFT-printing from a gelatine donor was discontinued, as it was deemed inadequate.

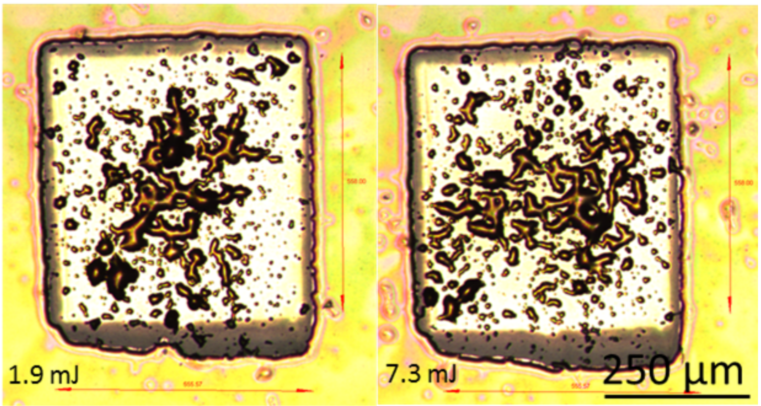

FIGURE 3.8: Spots on an Au-DRL gelatine donor after LIFT-printing using various laser energies, showing the residue remaining on the carrier.

3.4.2 Agar donor films

The following set of experiments described here is on LIFT-printing from solid donors. Agar was chosen as a possible solid donor as it could accommodate and protect the antibodies during LIFT, and also allow subsequent access to them after transfer printing them on paper. In order to prepare the donor, 1 g of agar powder was poured slowly in 100 ml of purified water at a temperature of around 90 °C while constantly stirring the solution until the powder was completely dissolved. The agar was then spin-coated at 300 RPM on the fused silica slide to obtain a thickness of ∼10 μm. The thickness of the film was measured using the ZeScope Profiler as seen in Fig. 3.9. Measurements of the transmittance of light through the Agar film using a spectrophotometer showed that it has more than 95% transmittance at 248 nm, and therefore a gold DRL film was required for LIFT.

The fact that the temperature during the fabrication of the Agar film was high, prohibits us from simultaneously adding the antibodies to the solution at this stage, as the antibodies denature and lose their biological and chemical properties at temperatures over 50 °C [84]. Therefore, the solution containing the antibodies must be added to the agar after the thin donor film was formed on the fused silica carrier slide. Agar is highly hydrophilic and porous, so it can easily and quickly absorb the aqueous solution. 15 μl of HRP-conjugated anti-mouse IgG was diluted in 1.5 ml of PBS for a 1:100 concentration of antibodies. Agar solidifies around $32 - 40$ °C, and since the entire process above was done at room temperature, the agar solution cools down to room temperature in a few minutes only, to form a clear/transparent gel-like film. The antibody solution was then pipetted on the already formed agar film and left to dry. After the film had completely solidified again, the donor film was ready to be used for LIFT.

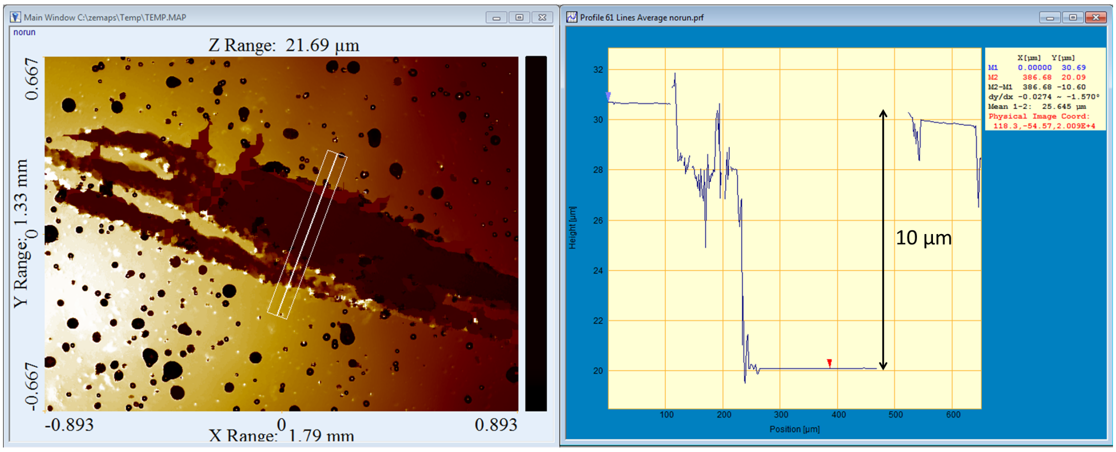

```
        X[µm]   Y[µm]
M1     0.00000  30.69
M2      386.68  20.09
M2-M1   386.68 -10.60
dy/dx -0.0274 ~ -1.570°
Mean 1-2:   25.645 µm
Physical Image Coord:
 118.3,-54.57,2.009E+4
```

FIGURE 3.9: Images showing the profile of the Agar donor film. The thickness of the film was ~10 μm.

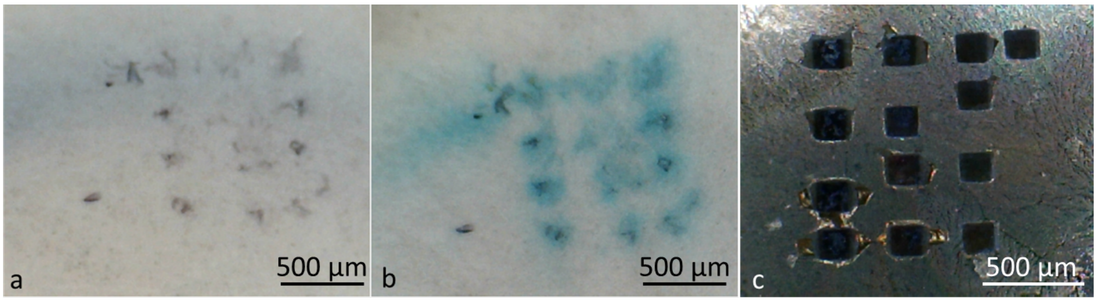

FIGURE 3.10: (a) LIFT-printed spots from an agar donor, (b) Colour change on the agar spots produced by adding TMB, (c) LIFT-produced spots on the agar donor.

During the LIFT experiment using agar, the separation between donor and receiver was about ∼100 μm. Excimer voltages ranging from 19 kV to 30 kV that correspond to energy per pulse ranging from ∼2 mJ to ∼7.3 mJ were used and a line of LIFT-printed squares was formed for each voltage setting in an attempt to determine the optimal parameters for LIFT-printing of agar. Since the agar donors produced exhibited non-uniformities in thickness and quality, and because it also has high porosity, it made it difficult to LIFT-print, and hence it might not be the ideal material for solid-donor LIFT. The laser settings that produced the best results so far were 25 kV corresponding to 5.7 mJ/pulse. These LIFT-printed spots on cellulose paper exhibited a colour change when TMB was added (Fig. 3.10). This verifies that agar can be used as a donor film for LIFT-printing antibodies on paper, but further parametric studies such as the study of the different laser fluences for different thickness of the agar film would be required to optimise this LIFT process. On the other hand, the fact that the produced agar film is non-uniform and porous and because it requires high temperature processing, makes this material not ideal to use for the intended bio-LIFT applications.

3.4.3 Glycerol donor films

A 1 mm thick fused silica substrate, pre-cleaned using a standard solvent cleaning procedure, was coated with a 25 nm Au film DRL using an e-beam or resistive evaporator. In order to improve its hydrophilicity and hence adhesion with the donor film, the Au DRL was treated with O_2 plasma for 20 s using a reactive ion etcher. This treatment allowed the production of films with greater uniformity and stability. Without plasma treatment, it was found that the liquid donor film might break up after its deposition on the carrier due to its surface tension. A liquid donor film, consisting of a glycerol-PBS solution (80% v/v) was then formed on the substrate by containing it in a square well using tape (Fig. 3.11) or by using a wire coater (Gardco, US). In the first case, the adding of the donor solution near one side of the predefined well was followed by spreading it over from one side of the well to the other by a glass slide to remove the excess liquid donor and thereby form a film. Alternatively, about 200 μl of the solution was pipetted on the carrier and spread with the wire coater whilst removing any excess liquid, leading to the formation of a ∼65 μm thick film. The uniformity and reproducibility of the film's thickness using the wire coater method proved to be better, and hence was adopted as the selected approach.

During the first set of LIFT experiments, the donor film was spin-coated on the carrier, in an attempt to achieve donor thicknesses of around a few microns, similar to what the literature suggested for use with solid LIFT donors. Although, this was easily achievable and the reproducibility of the film thickness was excellent when the concentration

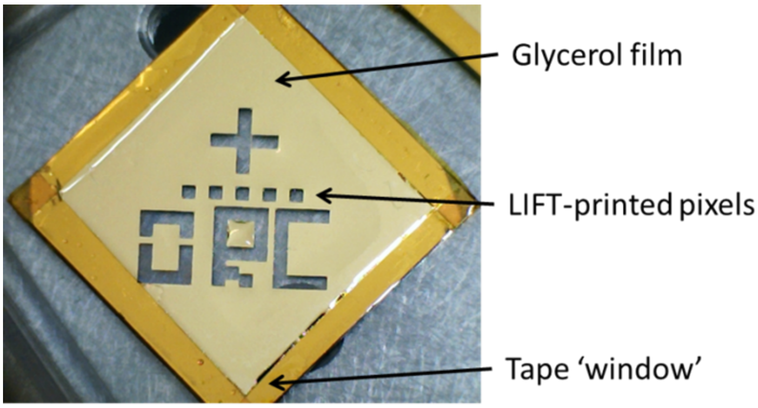

Figure 3.11: Image showing a glycerol donor film on a fused silica carrier after LIFT-printing of specific pixels.

of the glycerol in the film was constant, this method was abandoned as it was found that micron-thick films were not suitable for this application, as they would not carry enough antibodies to create a substantial level of a colour signal on the receiver. Thus, thicker films in the range of 10 s - 100 s of microns were selected for this next series of experiments.

The antibodies, either the secondary (enzyme-tagged anti-mouse IgG) or the primary (untagged mouse IgG), were incorporated in this film in concentrations in the range of ng/ml to μg/ml, prior to the forming of the film on the carrier.

Due to their excellent inherent properties for this work, such as biocompatibility, cost and hydrophilicity, the receiver substrates were Whatman grade 1 filter cellulose paper. Nitrocellulose paper, which exhibits much higher hydrophobicity and results in strong localisation and immobilisation of antibodies and other biomolecules, is another material of choice in many point-of-care sensors. Our results show that similar attributes are observed for LIFT-printing on simple cellulose paper, where antibodies also exhibited high localisation within the LIFT-printed areas. It was also observed that the glycerol was absorbed in the cellulose paper faster due to its hydrophilic nature and with greater efficiency than in the nitrocellulose paper, for which the droplets are not completely absorbed within the volume of the paper, but are adsorbed on its surface with excess liquid evaporating over time as the paper is left to dry under ambient lab conditions.

3.5 LIFT-printing of biomolecules

3.5.1 LIFT-printing of enzyme-tagged antibodies

Two sets of LIFT-printing experiments are presented here. The first included the direct LIFT-printing of enzyme-tagged antibodies on paper. In order to show the viability of the antibody-HRP enzyme conjugate post printing, it is necessary that a change in colour (from white in the absence of HRP to blue in the presence of HRP) is observed at the LIFT-printed positions on paper as a consequence of the presence of the enzyme that induces the colour change on interaction with the chromogenic substrate as seen in Fig. 3.12. This would thus confirm the retention of the biological and chemical properties of the printed antibodies after LIFT-printing. The second set of experiments involved LIFT-printing of untagged antibodies on paper and the subsequent detection of these antibodies via an indirect ELISA test which provides proof of their immunological viability and stability following the LIFT-printing process.

For the first experiment, different concentrations, ranging from 50 ng/ml to 500 ng/ml, of the HRP-conjugated antibodies were incorporated into the donor films and spots were LIFT-printed onto the cellulose paper receiver. These initial tests were needed to determine the lowest concentration that can still provide a sufficiently intense colour change that is detectable with the human eye or a simple mobile phone camera, the two options that we consider convenient and beneficial in the case of point-of-care diagnostics. Spectrophotometry or other more sophisticated and instrument-intensive detection schemes were therefore not used for our viability testing procedures as our aim was to develop a device that operates outside normal medical facilities such as hospitals and furthermore can be read by untrained non-medical personnel/individuals. It was observed that a concentration of the HRP-conjugated antibodies, 50 ng/ml in PBS was the threshold at which detection could still be achieved; concentrations of antibodies lower than this did not induce a colour change intense enough to be observable. Glycerol donor films that contained the HRP-conjugated antibodies have also been used 7 days after they were prepared, and this was to ensure that they can be used later than the day they were formed. The shelf life of these films is considered to be limited by the shelf life of the antibodies they contain, and it is believed that the glycerol does not reduce this time.

The colour intensities of the LIFT-printed pixels were quantified by recording the digital images with a comparatively low-resolution 1.3 megapixel USB camera, followed by analysis of the images using a MATLAB program developed in-house. This program uses a 256-bit colour scale where black corresponds to a colour intensity of 255 and white to a colour intensity of zero. Each pixel of the image is also represented by three values which correspond to red, green and blue colour components of the image. Figure

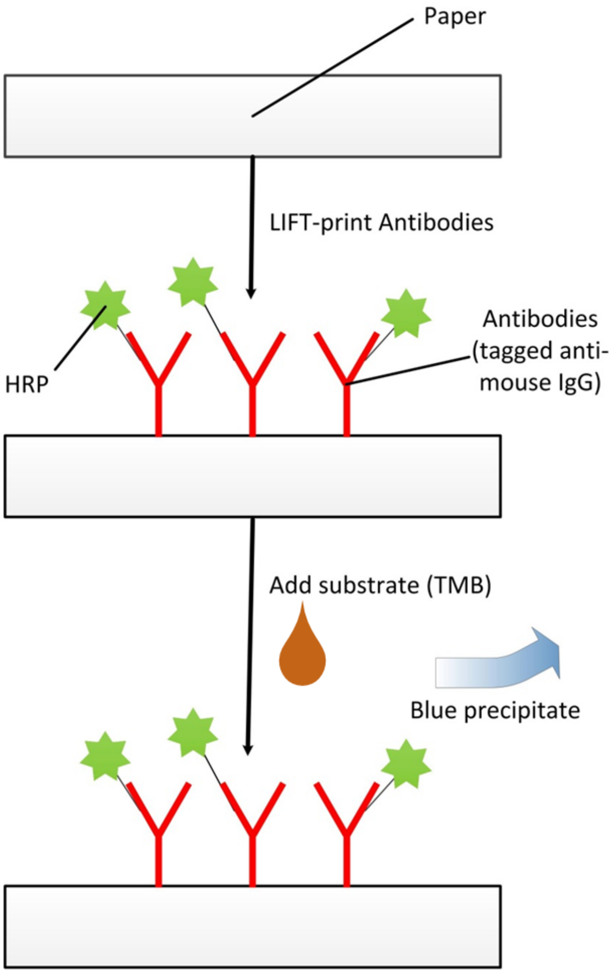

FIGURE 3.12: Schematic showing the LIFT-printing and colour change mechanism of antibodies on paper.

3.13a shows a set of LIFT-printed spots of a known concentration and the red line represents the positions along which the measurement of the colour intensity was taken. The three distinct graphs for red, green and blue components that are the results of the measurement of the colour intensity that correspond to the red line on Fig. 3.13a can be seen in Fig. 3.13b. These results had to be inverted and normalised in order to obtain the average colour intensity value that represents this specific concentration of antibodies.

The dashed calibration curve seen in Fig. 3.14 for all known concentrations of HRP-tagged antibodies was obtained by performing this measurement for several LIFT-printed spots for each known concentration (62.5 ng/ml, 125 ng/ml, 250 ng/ml, 500 ng/ml) and extracting the average colour intensity value for each one. Following the measurements of the LIFT-printed spots, the same concentrations of the HRP-conjugated antibodies were pipetted on another paper substrate, and their images were captured and analysed to create the solid calibration curve of the pipetted IgG. This allowed us

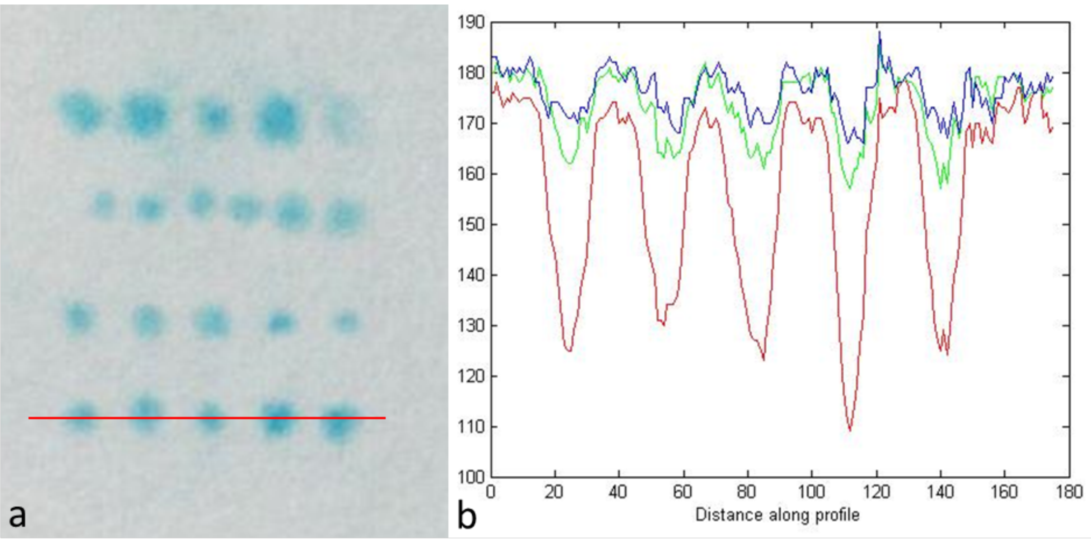

Figure 3.13: (a) Set of LIFT-printed antibodies of known concentration. The red line shows where the measurement of the colour intensity was done. (b) Graphs of the red, blue and green colour intensities corresponding to the set of spots of (a)

to identify any loss of antibodies resulting from the LIFT process. It was found that the colour intensity of the LIFT-printed antibodies is lower by between 2-4% (when normalised to the full scale of 0-100) compared to the colour intensity of the antibodies that have just been pipetted.

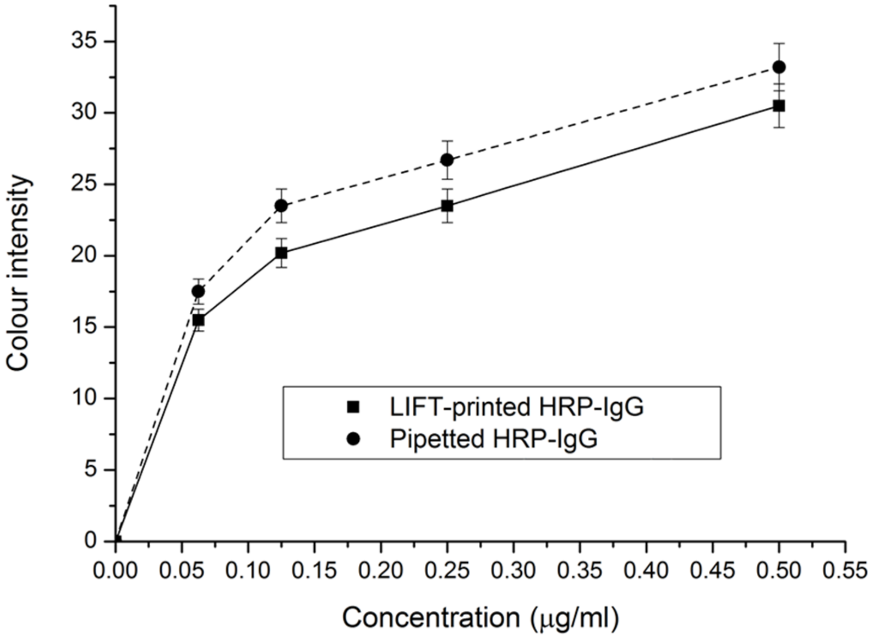

Figure 3.14: Plot of the colour intensity of different concentrations of LIFT-printed HRP-conjugated IgG and of pipetted HRP-conjugated IgG along with their linear interpolation curves.

One of the important properties of direct-write laser processing is that it allows for precise control of the size and shape of both individual printed pixels as well as the resultant multiple-pixel patterns that can be printed. Fig. 3.15a and Fig. 3.15b show the results for a simplistic LIFT-printed trial barcode which further establishes the flexibility inherent to such a laser-based direct write procedure. The bar code patterns were revealed by addition of the chromogenic substrate TMB onto the paper after LIFT-printing of the enzyme-tagged antibody to form the desired pattern. Printing the biomaterial in a shape of a real full-size barcode or QR code would allow additional information to be added to the test, such as patient-specific details, extra controls such as test duplication, or encoding of the result where a positive diagnosis might otherwise produce unintentional patient anxiety. In this latter case, medical intervention may well be needed due to the possible severity of implications of the positive (or negative) outcomes. In practice, through actual implementation of such tests, barcodes can also identify a specific patient. Furthermore, by scanning the test with a mobile phone camera and sending it to the intended recipient, the healthcare professionals can rapidly be alerted of the patient's condition, and in the case of a virus infection, information about their geographical location (available by the GPS feature inherent to modern smartphone devices) would also enable rapid vectorial mapping of the spread of the virus. For simple tests where secrecy or patient confidentiality is not an issue, word patterns such as 'yes/no' that make it easier for immediate read-out by the patient or person taking the test are more suitable. Fig. 3.15c and 3.15d show such LIFT-printed 'yes/no' patterns that have been produced by addition of the chromogenic substrate TMB onto the paper after LIFT-printing the enzyme-tagged secondary antibody to form the desired word patterns.

3.5.2 LIFT-printed paper-based Enzyme Linked Immunosorbent Assay

The second set of experiments involved the LIFT-printing of untagged antibodies from a glycerol donor film onto cellulose paper receivers, and the subsequent validation of their chemical and biological viability through an ELISA as shown in Fig. 3.16. An ELISA is a form of analytic biochemical assay that uses enzymes to detect the presence of an antigen, such as a virus or an antibody, and is mainly used as a diagnostic tool in medicine and plant pathology, as well as a quality control in food and environmental industries. Depending on the type of ELISA (indirect, sandwich or competitive) that is being implemented, LIFT-printing of at least one type of antibody specific to the antigen is required. Typically, an ELISA is conducted in a polystyrene multi-well ELISA plate, which in this report was replaced by plain cellulose paper. This replacement of the

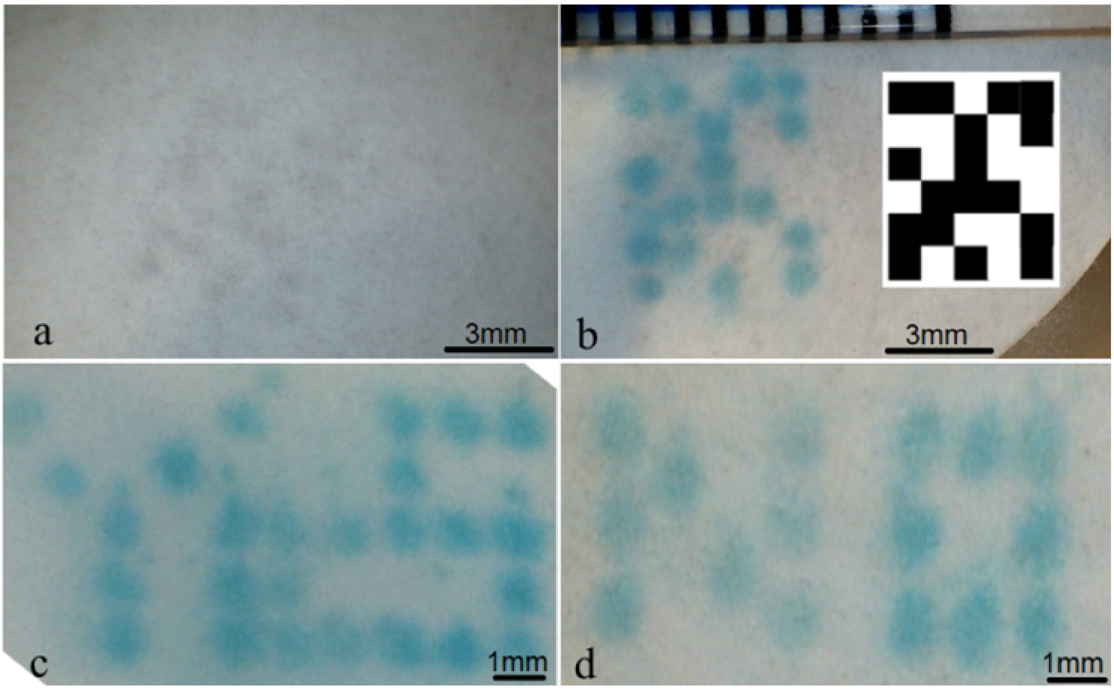

Figure 3.15: LIFT-printed pixels of HRP-conjugated anti-mouse IgG in the form of a QR code, (a) before the detection with the chromogenic substrate TMB and after developing with TMB in the form of (b) a 2-d trial barcode QR code, shown as a black/white pattern in the inset, (c) 'yes' and (d) 'no'.

bulky and relatively expensive ELISA plate with a cheaper, smaller and more versatile medium such as paper, was one of the main incentives for this series of experiments.

Currently in this developmental stage, only the target, a mouse IgG, was first printed on the paper surface via the LIFT-printing step in a specific pattern, and was subsequently immobilised through evaporation. After this, the paper was blocked with Bovine Serum Albumin (BSA) to prevent non-specific binding of the antibodies on the paper during the following steps of the ELISA test. The blocking solution consists of 2% BSA and 0.05% Tween20 in PBS. The paper was immersed in the blocking solution for 1 hour at room temperature. The following step is the tagging of the LIFT-printed antibodies with the enzyme-tagged antibodies (HRP-conjugated anti-mouse IgG). Different concentrations of the secondary tagged antibodies have been used to determine the best result, which in our case means the generation of the highest colour intensity with the minimum background signal and after several optimisation trials, 50 ng/ml was selected as the optimal value. The paper was immersed in this solution and incubated for 1 hour at room temperature followed by a washing step to remove any unbound antibodies from the paper surface. Washing was done three times for five minutes each using a washing solution of 0.05% Tween20 in PBS. After the washing was done, the final step involved the addition of the chromogenic substrate TMB which when combined with the HRP

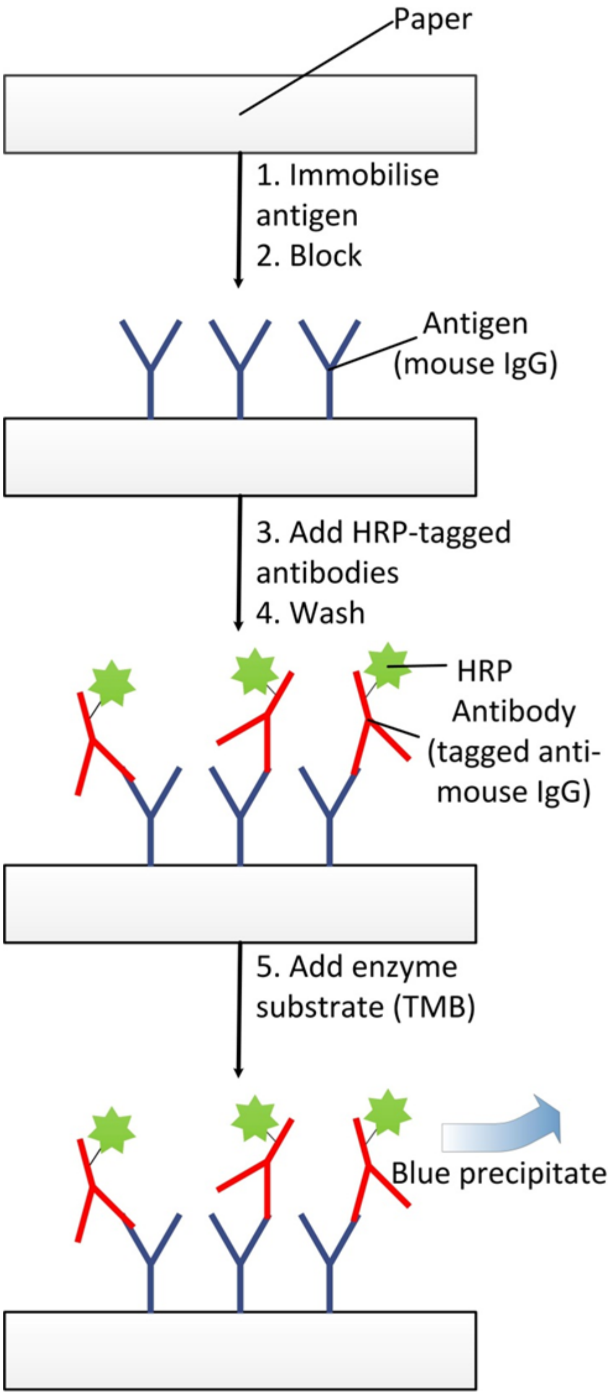

FIGURE 3.16: Schematic diagram of a paper-based indirect ELISA (adapted from [77]).

enzymes, produced blue-coloured pixels, highly localised at the LIFT-printed positions as seen in Fig. 3.17.

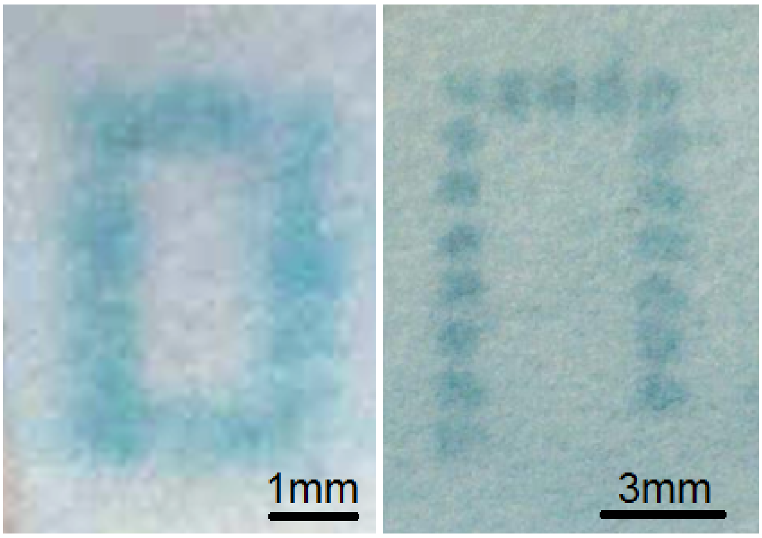

FIGURE 3.17: Optical microscopy images of LIFT-printed mouse IgG following the ELISA test, forming continuous lines and individual pixel arrays.

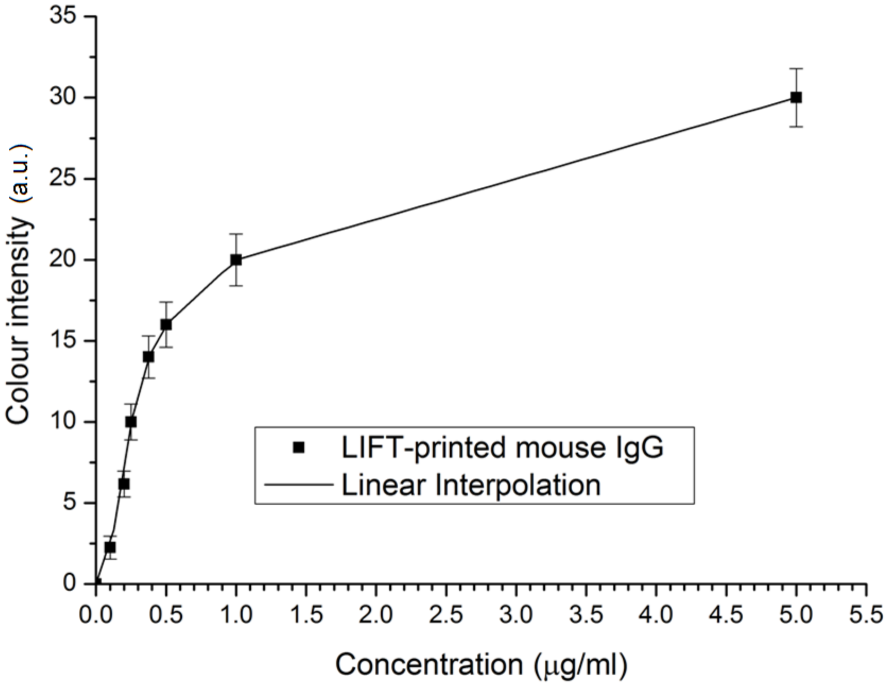

FIGURE 3.18: Calibration curve of the mean colour intensity following the ELISA versus the concentration of LIFT-printed antibodies in each pixel.

The calibration curve for the paper-ELISA using this particular set of antibodies was obtained as described previously, by capturing images of pixels LIFT-printed with known concentrations of antibodies and subsequently measuring their colour intensities (Fig.

3.18). The calibration curve would thus allow the determination of an unknown concentration of the target antibodies in a test-sample. It is clear that the blue colour is highly visible after the ELISA has been performed. For a future complete device however, it is desirable to include a calibration test based on a standard pre-printed blue-coloured control pattern, and we are currently establishing the optimum and easiest protocol that could be used by a patient for POC testing.

3.5.3 LIFT-printing on pre-patterned wax-printed paper

The simple experiment described here involved LIFT-printing onto pre-structured paper-based microfluidic devices. Wax printing [85, 86] and photolithography of polymers [87] are only two of the many methods that have been reported for fabrication of paper-based microfluidic devices. Wax embedded in paper acts as a hydrophobic barrier that creates hydrophilic channels in paper. Any aqueous solution that is subsequently added to the paper will hence be contained in the patterned wax area. The wax printed paper devices that were used in the following experiment were printed with a commercial wax printer and have kindly been provided by our collaborators at the University of Braunschweig in Germany. Each of the used patterns is composed of several wax circles connected through a common channel, as can be seen in Fig. 3.19a.

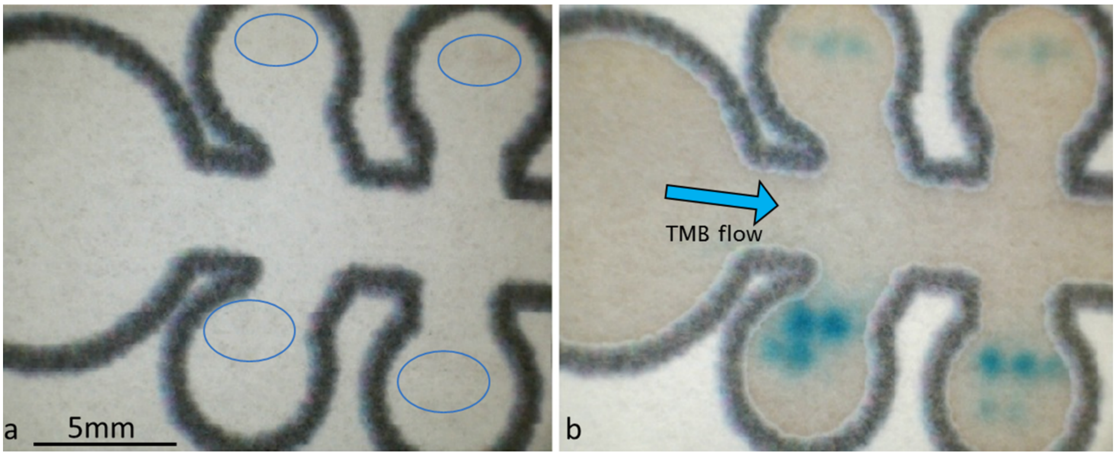

Figure 3.19: (a) LIFT-printed glycerol spots on pre-patterned paper with wax, (b) Spots made visible by adding TMB on the paper channel.

During this experiment, the glycerol solution containing the antibodies was first LIFT-printed on these wax-printed paper strips. Several spots were printed on the small (5 mm diameter) circles and the TMB-substrate was subsequently pipetted onto the large (10 mm diameter) circle and left to wick through the channel in order to produce the colour change at the LIFT-printed areas (Fig. 3.19b). These wax-printed patterns can also be used when fabricating a LIFT-printed paper ELISA test as the circles perform a similar role to the 96-well plates commonly used for standard ELISA tests. It was found that 4 μl of sample solution will completely wick the area of the 5 mm wax circle, thus minimizing the volume of the reagents and reducing the total cost, compared to a standard ELISA test. As reported elsewhere, paper-based ELISA also requires far less incubation and washing times than traditional multi-well plate ELISA [77, 88]. This was the first report on the development of a paper-based ELISA fabricated by LIFT combined with the pre-patterning of the paper device. As can be seen in the chapters that follow, a novel laser-based technique for the patterning was developed by us and therefore experimenting on wax-printed paper devices was discontinued.

3.6 Conclusions

The aim of the experiments described in this chapter was to show the feasibility of transferring undamaged antibodies on paper in order to manufacture paper-based medical diagnostic devices. In order to demonstrate this, the transfer of untagged and enzyme-linked antibodies on paper substrates was performed using Laser Induced Forward Transfer with ns laser pulses. Several different materials, in liquid and solid form, were trialled as the donors that can contain and protect the antibodies during LIFT, and glycerol proved to be the most suitable option, as solid-based donors were found to be difficult to LIFT. In order to ensure the stability of the reagents that were LIFT-printed but also because the donor films used were transparent at the wavelength of the laser used, there was a need to use a thin gold Dynamic Release Layer. After the LIFT-printing process, the functionality and immunological reactivity of the LIFT-printed antibodies was confirmed by developing and demonstrating an ELISA and establishing the standard calibration curves using the LIFT-printed pixels.

Additionally, it was shown that the localisation of the LIFT-printed pixels and immobilisation of the antibodies, which is a pre-requisite for paper-based diagnostic devices, was maintained throughout the wet-bench process which further justifies our use of the spatial patterning ability of LIFT. This immobilisation of the antibodies through the LIFT-printing process on the paper surface, also allowed the use of plain cellulose paper instead of the more expensive nitrocellulose membranes which should help reduce the final cost and more importantly allows for the fabrication of devices that do not need to be confined by hydrophobic barriers in fluidic channels, but can instead work in free-flow conditions. LIFT was proven to be equivalent to commercial dispensing machines (BioDot) in regards to the printed volumes of the reagents which is in the range of nl and also the flexibility of the printed designs, although our current setup would not be able to compete in terms of speed. This work demonstrates that LIFT is a technique capable of transferring antibodies onto a paper substrate accurately and reproducibly, and that LIFT is a promising technology for manufacturing immunologic paper-based point-of-care diagnostic sensors.

Chapter 4

Laser-based structuring of paper-based fluidic devices

4.1 Introduction

Point-of-care (POC) testing plays a vital role for early stage non-invasive clinical detection and diagnosis. One of the principal reasons for its widespread uptake is because it provides an effective and rapid modus-operandi that either excludes or minimises unnecessary delay by providing a prompt exchange of vital information between the clinical care team and the patient undergoing tests. This is achieved through diagnostic testing conducted at the POC at a patients bedside, either in the comfort of their home, at their general practitioners clinic, or in a hospital emergency unit. Such POC testing is facilitated through the use of uncomplicated, user-friendly and portable testing devices and much effort has been directed towards producing diagnostic test-kits that are not only smaller, faster and smarter, but also satisfy the elusive goal of being cost-effective a vital requirement that ensures economic viability, since such POC test procedures may need to be performed repeatedly over potentially very large sample groups, that could even extend to an entire nation in the case of a pandemic.

It has been recognised that microfluidic-based lab-on-chip (LOC) technology has considerable potential, and hence sustained efforts have been directed towards developing LOC-type fluidic systems for medical diagnostic devices [89]. The prime reason for this enthusiasm lies in the obvious advantages presented by these compact LOC devices such as the use of smaller reagent volumes, faster reaction times and portability arising from the device sizes, as well as ease of manufacture and distribution.

Compact LOC devices have primarily been developed on platform substrates such as silicon and glass, using cleanroom-based fabrication processes adapted from the semiconductor processing industry. In an attempt to further reduce the manufacturing costs, a low-cost polymer, polydimethylsiloxane (PDMS), which can be used in a rapid prototyping environment, was also considered as a better choice for implementation of microfluidic-based LOC devices. This material however, still presents certain limitations and entails comparatively high fabrication costs, which has led to a subsequent search for alternatives, that now include paper and thread [90].

In particular, paper, with its varied characteristics, is now considered as a highly suitable alternative for fabrication of LOC-type devices, and many labs have focussed their attention in this direction [64, 73, 91]. Of particular importance is the relatively low-tech nature of paper, which has almost all of the attributes that would help realise low-cost POC diagnostic tests, particularly in the context of poorly resourced locations and environments that exist today within developing countries.

In the previous chapter, we have shown how we can print reagents and biomolecules onto the paper substrates that constitute the POC devices. Following those experiments, we realised that we had to develop a laser-based technique that would allow us to fabricate structures in the paper substrates, thus giving us the ability to create complete paper-based POC diagnostic devices using lasers. In this chapter, this novel technique is described and our results for it are presented. Part of this work has been published in journals [92, 93] and conferences [94–101].

4.2 Paper for point-of-care diagnostics

As a substrate material, paper is inexpensive, abundantly available in a range of different engineered forms and properties, can be stored and easily transported, functionalised and modified in terms of its liquid transport properties, and can be readily disposed of after use via incineration. Additionally, paper-based fabrication procedures can be intrinsically cheap, and paper as a platform technology is mature and well-established, lending itself to routine low-cost large-volume production procedures. Finally, delivery of paper-based items is routinely available to everyone world-wide that has access to a postal service.

Paper is currently used for analytical and clinical chemistry, and chromatographic tests are routinely performed using paper in commercial analytical laboratories for the detection of different chemical species. Two of the most commonly known paper-based chromatographic clinical tests are the pregnancy test and the lateral flow-based urine dipsticks that can simultaneously detect blood sugar, pH, ketone etc. However, clinical tests that can yield quantitative information of a multiplexed nature (i.e. can perform a series of parallel tests) using a single test strip are clearly the way forward, and recent reports of microfluidic paper-based analytical devices (μPADs) suggest that these may be the ideal platform for performing such tests [66].

As their name suggests, paper-based microfluidic devices have either a single or multiple flow channels that are designed to guide and transport an analyte fluid, from a point of entry on the device to a reaction zone that has been pre-treated with specific reagents. Unlike glass, silicon or polymer substrates, where the fluidic channels are surface-relief structures that have been inscribed in these substrates, for paper-based devices the fluidic channels are formed inside and extend throughout the full thickness of the paper. The walls that are required to delineate the separate fluidic channels to contain and guide the flow of liquids have been successfully demonstrated using hydrophobic materials such as SU8, PDMS, polystyrene (PS), alkyl ketene dimer (AKD) and wax [64].

The earliest approach presented by the Whitesides group [68], relied on a cleanroom-based lithographic technique that involved exposure of a UV-sensitive polymer (SU8) impregnated in a paper, through a custom-designed mask, to cross-link it and form the required barriers for the intended fluidic channels. In order to reduce the costs associated with such a conventional lithographic procedure, a subsequent approach they presented involved the use of a modified desktop plotter that dispensed an ink composed of the low-cost elastomeric polymer PDMS [102]. Several other groups have also proposed and demonstrated the usefulness of other paper-patterning approaches such as inkjet printer-based etching of paper impregnated with PS [103], plasma-treatment through a metal mask of a paper impregnated with hydrophobic AKD [104, 105], paper-cutting using a computer-controlled X-Y knife plotter [106–108], printing of wax [85, 86], inkjet-printing [109–112], flexographic printing [113], wax-screen printing [114], and laser-treatment of a paper with a hydrophobic coating [115].

Each of these procedures has its own advantages, as well as some characteristic drawbacks. Techniques such as UV-lithography and plasma-treatment require the use of expensive and fixed-pattern masks as well as dedicated equipment and controlled conditions in labs. The knife-plotting technique requires specialised or custom-modified patterning equipment whereas other techniques sometimes require undesirable post-processing procedures. Another important issue is the limitation on achievable feature size resulting from the lateral spreading of the hydrophobic material (for example with wax printing), and finally the need for specialised chemicals or inks (for ink-jet printing) or the use of harsh chemical etchants.

In this work, we present the use of a laser-based procedure to create the fluidic patterns in a paper substrate that has been previously impregnated with a hydrophobic material. This laser-based direct-write (LDW) approach is non-contact in nature, and this is advantageous when fabricating such biological or biomedical devices as this helps avoid cross-contamination that can arise from contact of the deposition tool with the substrate. It is also a mask-less, non-lithographic procedure, and hence is ideally suited for use in the preliminary trial fabrication stage as well as final device and mass-production stages. As with any laser-based procedure, the technique also offers the possibility to control the patterning process through choice of the laser parameters such as wavelength, pulse duration and repetition rate. More importantly, if desired, it is routinely possible to reduce the dimensions of the patterned features down to a value of 100 μm, or even below, and our current results show that fluidic channels with barrier wall width as small as $\sim$50 μm can be fabricated. Finally, this LDW process can also be scaled up for mass-production, possibly on a roll-to-roll scale. After initial set-up costs required for the laser and other equipment required for pattern definition, production costs for individual tests could be acceptably low.

4.3 Laser patterning of cellulose paper

4.3.1 Experimental section

As described earlier, the inscription of the fluidic patterns in paper is achieved via a LDW procedure that uses the principle of light-induced photo-polymerisation, where the laser beam is scanned over the paper, and/or the paper is moved beneath the laser spot. Before this patterning step, the paper is briefly soaked in the light-sensitive polymer which has been diluted in an appropriate solvent (isopropanol), and then left to dry under ambient laboratory conditions.

The schematic of the experimental setup employed for this LDW procedure is shown in Fig. 4.1, where the UV laser beam is directed towards the polymer-impregnated paper which was mounted on an xyz-translational stage. A cylindrical lens (either f = 36 mm, or f = 25 mm) focussed the laser beam onto the paper surface, and translation in the two planes (x and y) perpendicular to the propagation direction of the incident laser beam allowed inscription of (2D) user-defined patterns on the paper surface. Translation along the third (z) axis of the stages was used to ensure optimum positioning with respect to the focal plane of the lens.

Laser illumination of the impregnated paper induces polymerisation only within the exposed regions through initiation of light-induced cross-linking of the polymer. By

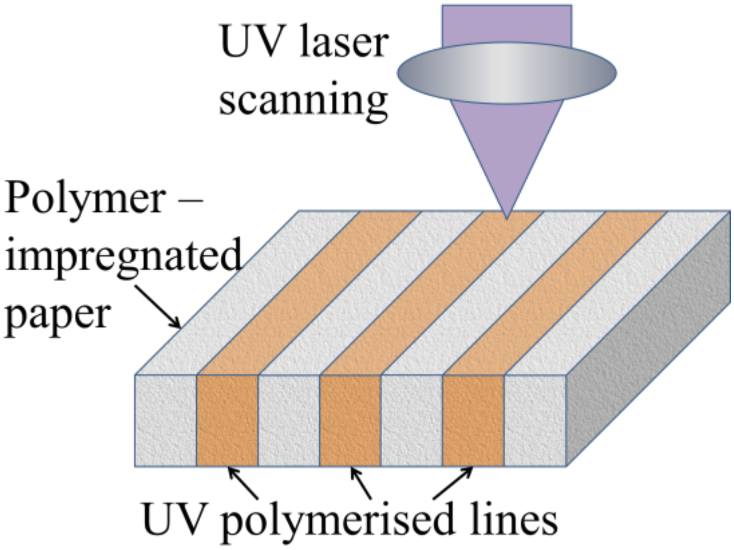

FIGURE 4.1: Schematic showing the laser-patterning of fluidic channels throughout the entire thickness of the paper.

varying the exposure parameters of laser energy density (for pulsed laser sources), or laser power (for continuous wave (c.w.) lasers), and speed of translation of the paper, the extent of this local polymerisation can be precisely controlled. These parameters clearly play a crucial role in determining both the widths and depths of the regions polymerised, and through variations in the incident laser exposure it is possible to produce polymerised structures that extend throughout the desired thickness of the paper substrate. The final step in the fabrication procedure involves washing away any un-polymerised material from the paper substrate by immersing the paper in isopropanol.

The procedure described here results in a paper substrate with user-defined regions that have been selectively polymerised through the direct-write step. Figure 4.2 shows a step-wise schematic depicting the sequential processing steps involved in the creation of these fluidic channels - laser scanning of parallel lines along the surface of the paper substrate under the correct conditions creates photo-polymerisation-induced hydrophobic barrier walls that define a fluidic channel.

The choice of laser used dictates several important parameters of the photo-polymerisation process such as the optical penetration depth in the paper, writing speeds for the barriers and finally the width of both the barriers and the fluidic channels, due to scattering of the incident laser light within the paper matrix, which can lead to photo-polymerisation occurring beyond the width of the focussed laser spot. The first laser used for the direct-write pattern definition step was an Nd: YVO_4 laser (B M Industries, Thomson CSF Laser, France) operating at 266 nm, with a pulse duration of 10 ns, a maximum single pulse energy of 2 mJ, and a repetition rate of 20 Hz. Subsequently, we explored the use of cheaper and smaller c.w. diode-lasers, namely Omicron (Laserage, Germany), operating at 375 nm with a maximum output of 70 mW, and Cobolt MLD (Cobolt AB, Sweden), operating at 405 nm and delivering a maximum output power of ∼110 mW. We also explored two different photopolymers, namely DeSolite® 3471-3-14 from DSM Desotech Inc., and Substance G (SubG) from Maker Juice, USA. A range of trial experiments was then performed to investigate and optimise the exposure parameters and photo-polymerisation characteristics which involved these three laser sources, pulsed and c.w., and two different photopolymers, under varying parameters such as laser pulse energy/power, sample translation speed, and focal spot size for each combination.

For experiments with the pulsed 266 nm laser, the range of translational speeds was varied from 0.05 mm/s to 0.5 mm/s, together with a variation of incident average powers ranging from ∼7 mW to ∼10 mW (corresponding to energies of ∼0.35 mJ to ∼0.5 mJ per pulse). The paper was positioned at a distance of 10 mm away from the focal point of the cylindrical lens (f = 36 mm), and the corresponding dimension of the laser spot (on the paper substrate) was ∼0.3 mm × ∼1 mm. The corresponding incident fluence hence ranged from $\sim$4.6 J/cm^2 to $\sim$66 J/cm^2.

For experiments with the c.w. 375 nm laser, the range of translational speeds was varied from 4 mm/s to 6.7 mm/s, with corresponding variation of incident power ranging from 1 mW through to 50 mW. The paper was positioned at the focal point of the cylindrical lens (f = 25 mm), and the corresponding incident fluence ranged from $\sim$1.9 J/cm^2 to $\sim$156 J/cm^2.

For experiments with the c.w. 405 nm laser, the range of translational speeds was varied from 4 mm/s to 10 mm/s, with a corresponding variation of incident power ranging from 1 mW through to 100 mW. The paper was positioned at the focal point of the cylindrical lens (f = 25 mm), and the corresponding incident fluence ranged from $\sim$1.25 J/cm^2 to $\sim$312.5 J/cm^2.

4.3.2 Results and discussion

4.3.2.1 Patterning with the 266nm pulsed laser

Figure 4.3 shows three sets of parallel lines that have been inscribed using the 266 nm pulsed laser source, at translation speeds of 0.06 mm/s, 0.07 mm/s and 0.09 mm/s with an incident average laser power of 7 mW. The photopolymer used for this was DeSolite®. A blue ink solution was subsequently pipetted into the channels, to test the ability of the structures to contain and wick liquids along the channel. The ink was pipetted from

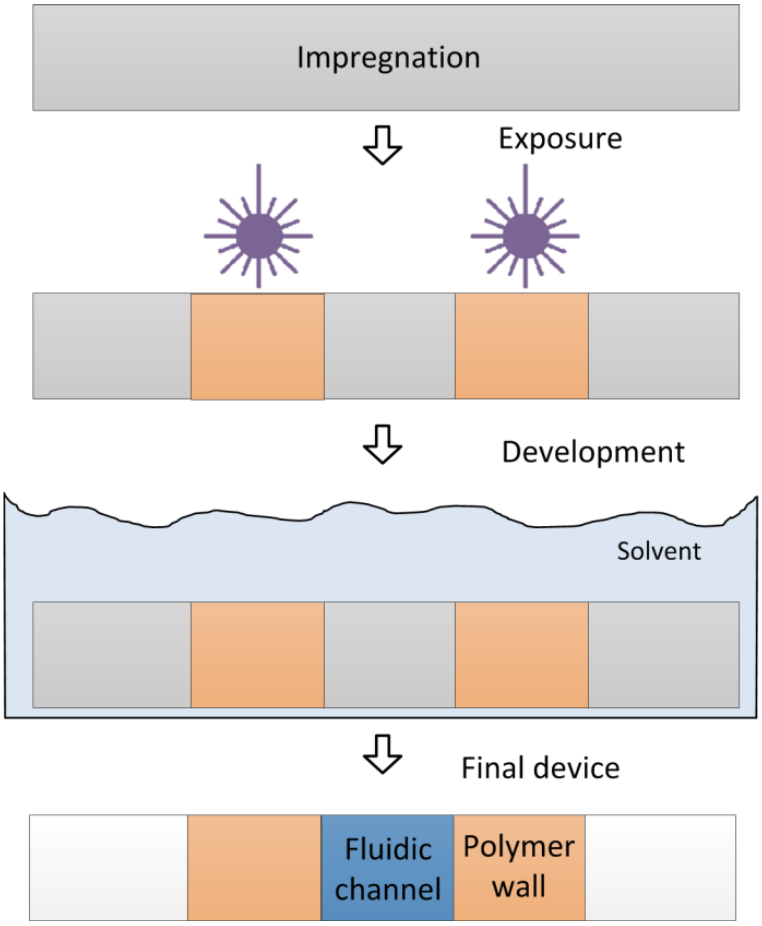

FIGURE 4.2: Schematic of the paper-patterning procedure.

one side of the channel (the top side in the figure shown) in 3 μl droplets, until the channel was filled or a leak was observed.

By looking at the cross-section of the paper under the microscope, it was found that the polymerisation depths of the barrier walls for channel (c) was only about 60% of the thickness of the paper (Fig. 4.4a), whereas for channel (b) this depth was about 75% of the paper thickness. For channel (a) however, the barrier walls extended throughout the full thickness of the paper (Fig. 4.4b), enabling leak-free transport of the ink on introduction at one end of the fluidic channel. In contrast, for channels (b) and (c), whose barrier walls do not extend throughout the entire paper thickness, undesirable and irregular leakage of the ink was seen from either side of the channel walls. For speeds slower than 0.06 mm/s, for this pulsed laser source, ablation along a central section of the barrier wall was observed as the local fluence had exceeded the paper ablation threshold at the peak of the Gaussian laser profile.

Subsequent experiments were performed with the paper held at a distance of 1 mm from the focal point. Translation speeds were trialled ranging from 0.06 to 0.5 mm/s,

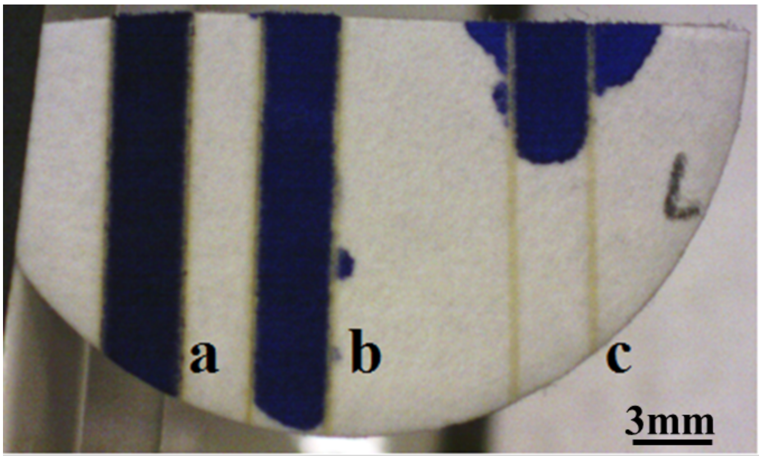

FIGURE 4.3: Three sets of parallel lines that have been polymerised while being translated at three different speeds, namely, (a) 0.06 mm/s, (b) 0.07 mm/s and (c) 0.09 mm/s.

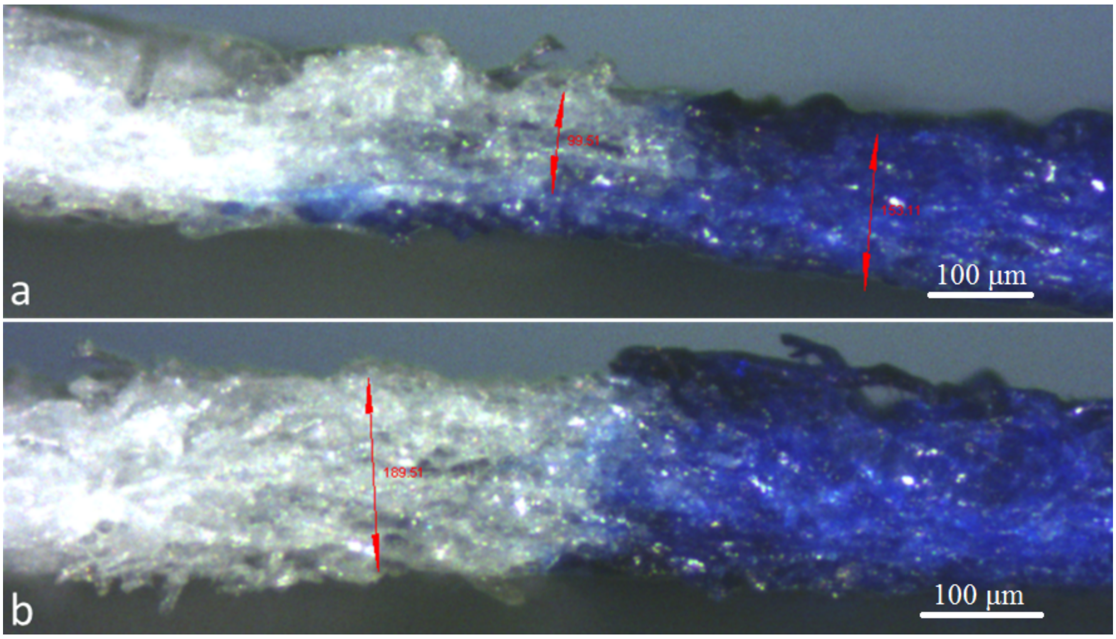

FIGURE 4.4: Microscope images showing the cross-sections of a line polymerised at (a) 0.09 mm/s and (b) 0.06 mm/s respectively.

and for speeds greater than 0.35 mm/s the photo-polymerised structures did not extend throughout the paper, while for speeds slower that 0.25 mm/s ablation occurred along the central region of the scanned lines. For speeds lower than 0.2 mm/s the paper was physically cut through along the length of the scanned line.

From the above results, the correlation between spot size of the incident laser source and resultant size of the polymerised regions is easily determined, and hence for a specific choice of laser and photopolymer it is then possible to deduce the correct exposure regime that will produce any desired line-width. However, for our demonstrations it is important to note that the smallest barrier widths that are able to contain and guide the fluid flow are of order 100 μm. Since there is a minimum fluence requirement for photo-polymerisation at any specific translational speed, this fluence then determines the maximum translational speed (and hence device fabrication) speed. However, the above demonstration clearly shows the ability to build compact fluidic flow-based devices which encompass the basic needs for smaller volumes of expensive reagents in the fabrication of low-cost LOC-type medical diagnostic devices.

4.3.2.2 Patterning with c.w. lasers at 375 nm and 405 nm

In order to explore the possibility of using our paper-patterning procedure with different laser parameters, we then tried other UV lasers which operated continuously (c.w. mode), at wavelengths of either 375 nm or 405 nm instead of 266 nm. One of the primary reasons for choosing c.w. operation was that it would allow us to circumvent the deleterious ablative effects that we observe when scanning with the pulsed laser at higher fluences. Additionally, operation at these longer wavelengths would translate into greater absorption depths for the incident light, hence allowing much higher writing speeds than those possible with the pulsed 266 nm source. As can be seen from the results, the writing speed using the c.w. laser was at least three orders of magnitude higher than using the pulsed laser.

Figure 4.5 shows a set of lines polymerised with the 375 nm laser, where the line-widths obtained are shown as a function of incident laser power and paper translation speed. Figure 4.5a shows results for a fixed incident laser power of 1 mW, and the line-widths are seen to increase from a value of ∼130 μm at 6.7 mm/s to a value of ∼320 μm at 4 mm/s. Similarly, as shown in Fig. 4.5b, for a fixed scan speed of 6.7 mm/s, the width of the polymerised lines increases with increasing incident laser powers from a value of ∼500 μm at 5 mW, to a value of ∼1000 μm at 30 mW. This can be attributed to the fact that with an increase in the incident laser power, a larger fraction of the incident Gaussian intensity laser profile would be above the polymerisation threshold, thus resulting in polymerised lines with larger widths.

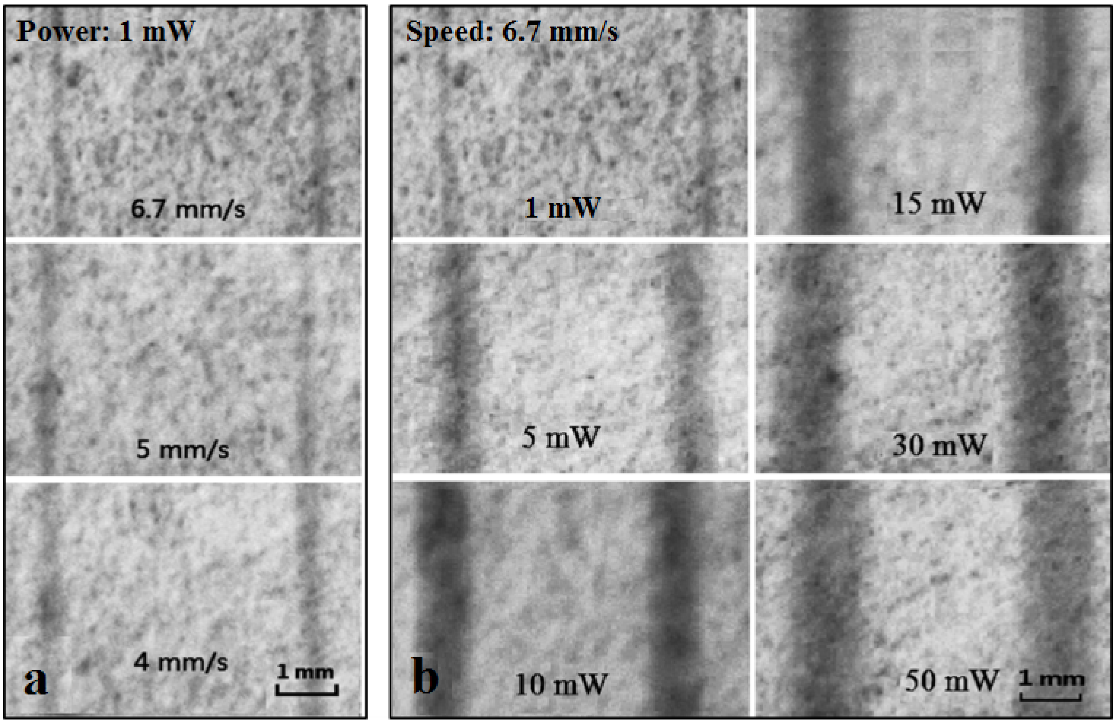

FIGURE 4.5: Images of sets of parallel lines that have been photo-polymerised using a 375 nm c.w. laser under different writing conditions: (a) fixed laser power, variable translation speed, and (b) fixed translation speed, variable laser power. Photopolymer used was DeSolite®.

The graph in Fig. 4.6 summarises the above observations, and presents the relationship between the line-widths of the polymerised regions for different scan speeds and different laser powers. The data presented in Fig. 4.6 show that, for a fixed laser power of 10 mW, the widths of the polymerised lines increased from ~680 μm to ~1000 μm with decreasing scan speeds, and for a fixed scan speed of 6.7 mm/s, the widths of the lines increased from ~130 μm to ~1200 μm with increasing laser powers.

We observed a similar effect for the 405 nm laser, and the relationship between the widths of the lines for different scan speeds and different laser powers is shown in Fig. 4.7. For a fixed laser power of 10 mW, the widths of the polymerised lines increase from ~220 μm to ~330 μm with decreasing scan speeds, and for a fixed scan speed of 6.7 mm/s, the widths of the lines increase from ~80 μm to ~800 μm with increasing laser powers. The smaller line-widths for the irradiation at a wavelength of 405 nm, are a direct consequence of the better beam quality of the 405 nm laser compared to the 375 nm laser and the absence of parasitic lobes in the spatial intensity profile that we saw with the 375 nm source. Although of low intensity, these lobes induce additional photo-polymerisation and therefore produce a broadened line-width compared to the

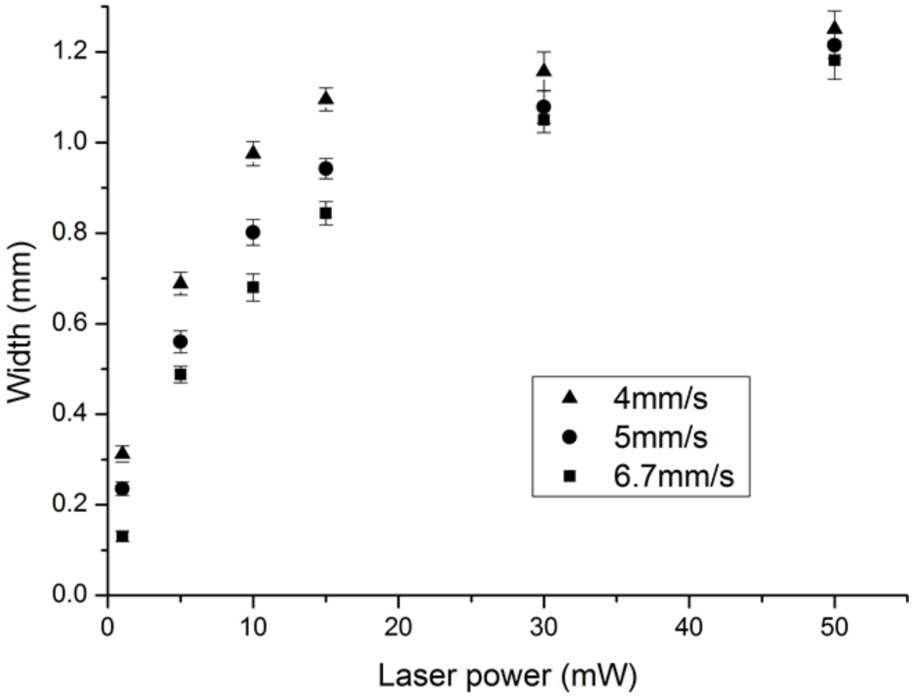

Figure 4.6: Graph showing the widths of the laser-patterned lines for different incident laser powers from the 375 nm source at different scan speeds. Error bars indicate the standard deviation for 5 measurements along each line.

theoretical limit for a perfect single mode laser source. Table 4.1 shows a summary of the resulting line-widths for the lines polymerised with the two c.w. wavelengths under different laser writing conditions.

Table 4.1: Summary of the line-widths for writing wavelengths of 375 nm and 405 nm, at different incident powers up to a maximum value of 50 mW, but a common writing speed of 6.7 mm/s

Laser power (mW)	Line-widths (μm) for 375 nm at 6.7 mm/s	Line-widths (μm) for 405 nm at 6.7 mm/s
5	~ 480± 15	~ 80± 10
10	~ 680± 30	~ 220± 20
15	~ 850± 30	~ 270± 30
30	~ 1050± 30	~ 380± 20
50	~ 1180± 40	~ 550± 20

The immediate observation using c.w. laser sources is the considerable increase in writing speeds possible compared to the pulsed laser source. As an example, to polymerise a line which was 2 cm in length at an incident fluence of 9.3 J/cm^2, the scan speeds for the pulsed laser was ~0.25 mm/s, whereas for the c.w. laser the scan speed was ~40 times faster at ~10 mm/s. These comparatively faster speeds are a very positive attribute that has immediate benefits for increased rate of production if this technology reaches the stage of commercialisation.

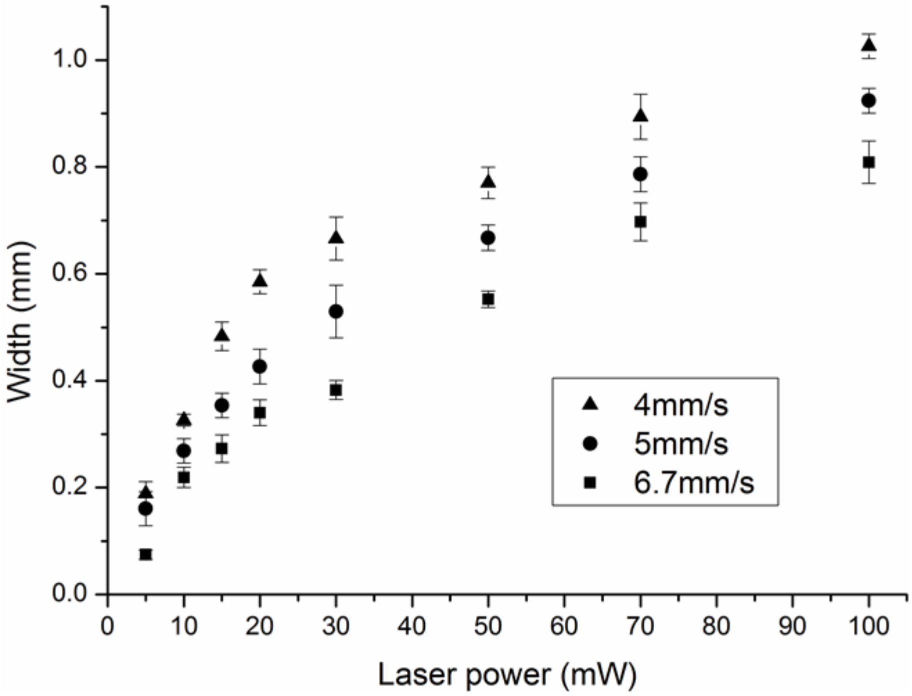

FIGURE 4.7: Plots showing the variations in the widths of the laser-patterned lines for different incident laser powers at 405nm at different scan speeds.

All of the experiments described so far were performed using the DeSolite® photopolymer. However, to make a useful comparison, we repeated our experiments with another photopolymer, SubG. Due to the extremely low viscosity (12cP @ 25 °C) of SubG, we soaked the paper directly with the photopolymer solution without the need for any solvent-based dilution, unlike the case for DeSolite®, which had to be diluted in a solution of isopropanol prior to impregnation into the paper substrates. Fig. 4.8 shows a series of parallel lines that was patterned with the same laser-patterning conditions using two different photopolymers. As can be seen, the lines that were formed with SubG were narrower, and had edges that were more sharply-defined when compared with those written with DeSolite®. Fig. 4.9 shows the variations in width of the lines patterned with the 405 nm laser for the two different photopolymers at different incident laser powers but the same scan speeds of 10 mm/s. As can be seen from both Fig. 4.8 and Fig. 4.9 the widths of lines polymerised using SubG are consistently narrower.

An important advantage offered by LOC-type fluidic devices is their cost-effectiveness, which is a consequence of their much reduced sizes, so an important requirement is to implement the entire device with the smallest possible footprint. Using our LDW procedure for making such compact devices would require finding the smallest dimensions not only for the fluidic barrier walls but also for the fluidic channels. To this effect, we initially investigated the minimum barrier wall widths that could be created with our procedure using a c.w. 405 nm laser. As shown in Fig. 4.10a, under the appropriate

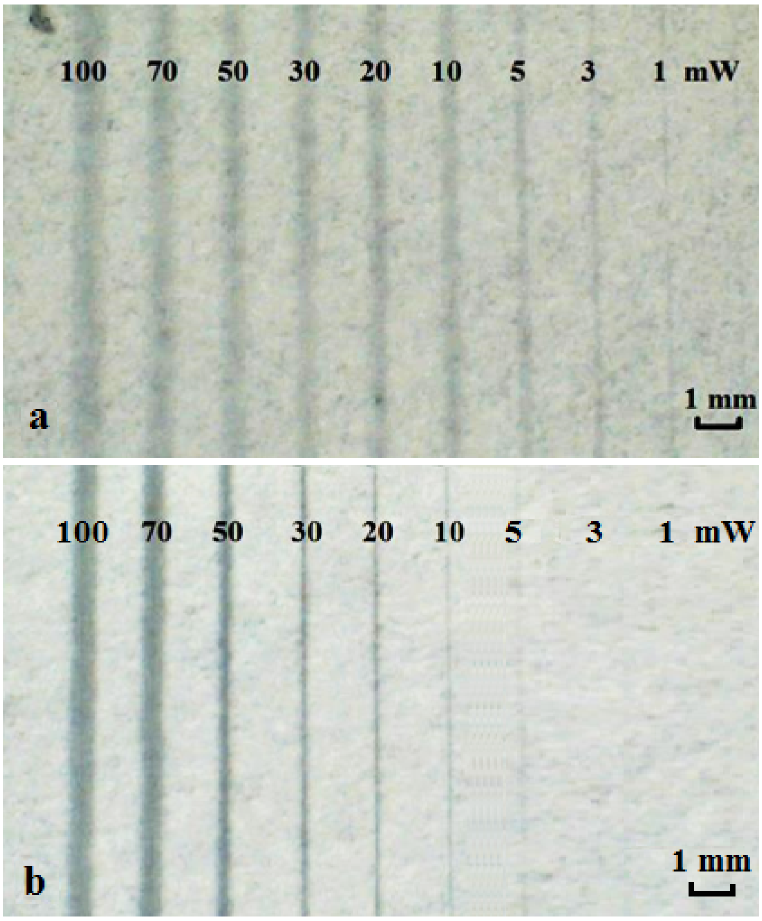

Figure 4.8: Sets of parallel lines that were polymerised using a 405 nm c.w. laser with a scan speed of 10 mm/s and different incident power (100 to 1 mW) using two different photopolymers, (a) DeSolite®, and (b) SubG.

writing conditions (scan speed of 10 mm/s, incident power of 10 mW and corresponding incident fluence of ∼125 J/cm^2), we could polymerise lines with widths of ∼50 μm, which is smaller than the dimensions we could achieve using the pulsed laser, and to our knowledge, is also the smallest line-width reported so far for barrier-walls in paper-based devices. Although such feature dimensions would have been possible through lithographic procedures, our LDW method presents a far less complicated approach as it does not require lithographic masks or cleanroom-intensive processing. However, fluidic channels formed with barrier-walls that had such narrow line-widths were found to be unable to contain and guide fluids, and instead a minimum line-width of ∼120 μm was required.

For this barrier wall width, we then investigated the minimum widths a fluidic channel can have and still guide fluids. We observed that the fluidic channel with a width of ∼80 μm was able to contain and guide the flow of ink along it. Fig. 4.10b shows such a channel having a width of ∼80 μm, and barriers with widths of ∼120 μm, guiding red ink. To

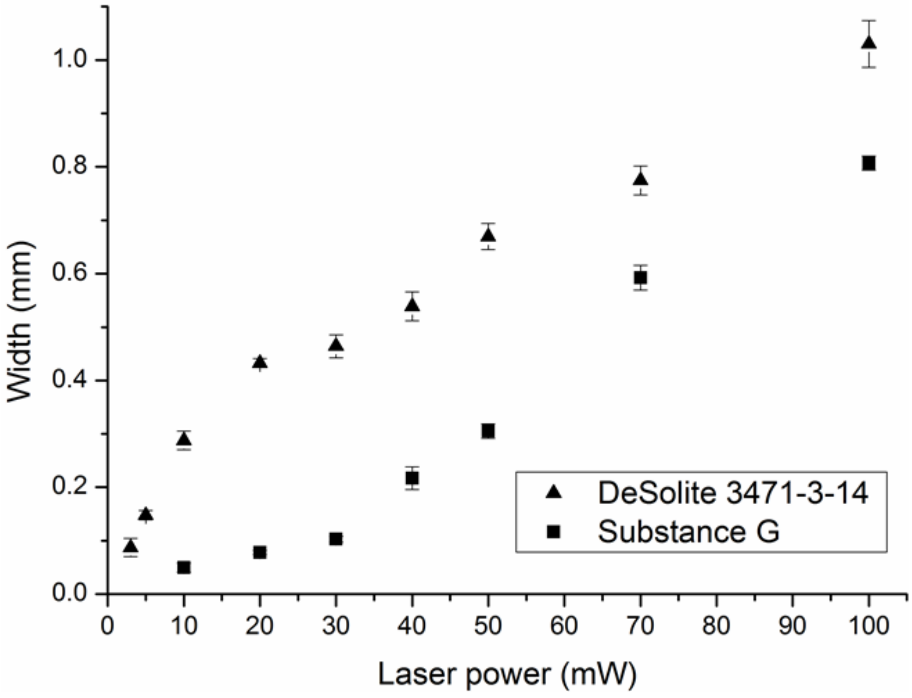

FIGURE 4.9: Graph showing the widths of the laser-patterned lines for different incident laser powers and a scan speed of 10 mm/s. The lines were patterned with a c.w. 405 nm laser and the photopolymers used were DeSolite® and SubG. Error bars indicate the standard deviation for 5 measurements along each line.

our knowledge this is the smallest dimension for a fluidic channel on cellulose paper, and is better than the dimensions that can be achieved with the wax-printing procedure that is currently one of the most widely used for the creation of fluidic patterns in cellulose paper, and for which the dimension limitations are imposed by the undue spreading of wax during the heat-treatment/wax-penetration step. The smallest dimension for fluidic patterns reported recently on a fibre-glass substrate through use of a simple cutting method is ∼137 μm [116].

As described above, a minimum line-width is necessary for a barrier wall to contain fluids, and this was found to be different for the two photopolymers. Fig. 4.11 shows a set of square patterns each with identical dimensions of 5 mm × 5 mm, but with barrier walls that have different line-widths ranging from ∼100 μm to ∼800 μm. These patterns have been written with the same laser (405 nm) but were created using the photopolymer SubG. As seen in Fig. 4.11, squares with line-widths greater than ∼300 μm were able to contain ∼2.5 μL of ink solution.

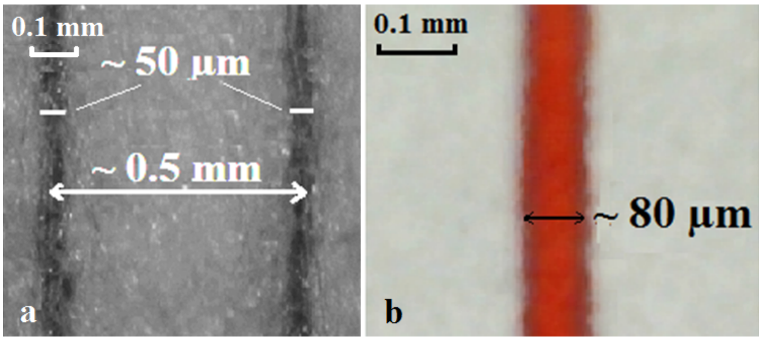

FIGURE 4.10: Microscope images showing: (a) two parallel lines written in DeSolite® via LDW using a scan speed of 10 mm/s and an incident power of 10 mW at 405 nm, and having widths of ~50 μm, (b) a fluidic channel with a width of ~80μm guiding red ink.

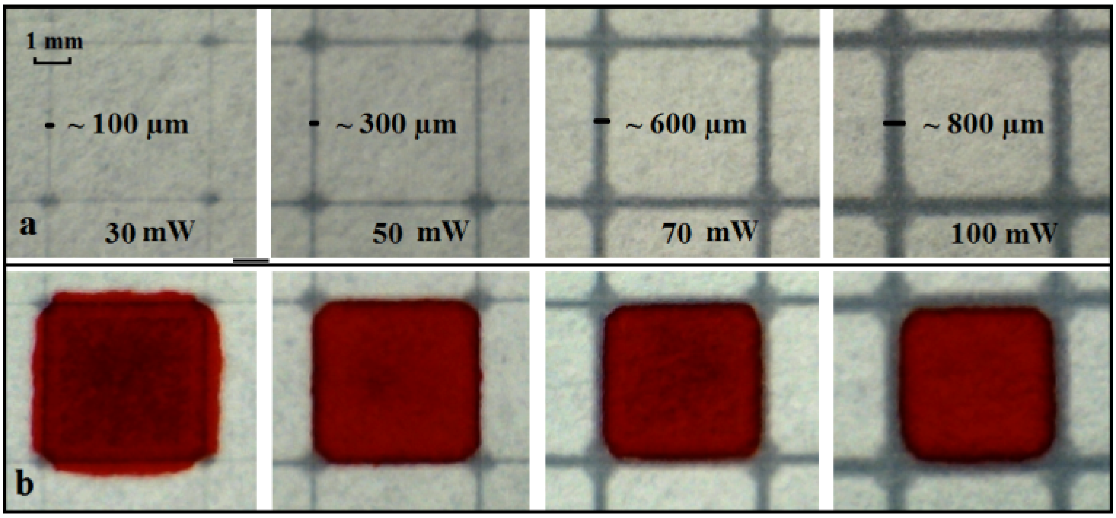

FIGURE 4.11: Camera images (a) of a series of 5 × 5 mm square patterns written in SubG with a 405 nm laser and different output powers (30, 50, 70, 100 mW) at a scanning speed of 10 mm/s, and (b) showing the introduction of 2.5 μl of red ink to each square.

4.3.3 Applications for protein and glucose detection

As our end-goal was to show the feasibility of this procedure in producing fluidics-based diagnostic devices, we patterned paper substrates with two different designs, namely a cross-hatch grid pattern that resembled a conventional micro-titer plate, and a T-junction. These fluidic tests were patterned into the paper substrates using the 405 nm laser and the photopolymer SubG, at a power of 70 mW and a writing speed of 10 mm/s.

First, we tested the use of the grid-like fluidic pattern of square wells (Fig. 4.12) by implementing the detection of Bovine Serum Albumin (BSA) and glucose. For the BSA test, we pipetted 3 μl of a 250 mM citrate buffer solution at pH 1.8 in each square well of the test-pattern. The test paper was then allowed to dry for 1 hour before 3 μl of a 3.3 mM solution of the second reagent, tetrabromophenol blue (TBPB) (Sigma Aldrich 199311) in 95% ethanol was added into each well. After further drying at room temperature for 1 hour, the test-pattern was ready for use in the detection of BSA via the addition of sample solutions into the respective square wells of the test-pattern. We pipetted sample solutions made up in de-ionised water, with BSA concentrations ranging from 0.25-50 mg/ml into each well. Introduction of the sample solutions resulted in a colour change in each well showing different concentration-dependent shades of blue-green colour (as seen in Fig. 4.12a.) which were fully developed after ~10 minutes. The concentration of protein in each sample is labelled in Fig. 4.12a. Comparing the colour change observed for an unknown concentration with a known calibration curve would then allow determination of the concentration for that unknown sample. Using such test patterns with nine wells, it should be possible to quantify nine unknown samples illustrating the utility and simplicity of using such low-cost paper-patterns to perform multiplexed quantitative analysis.

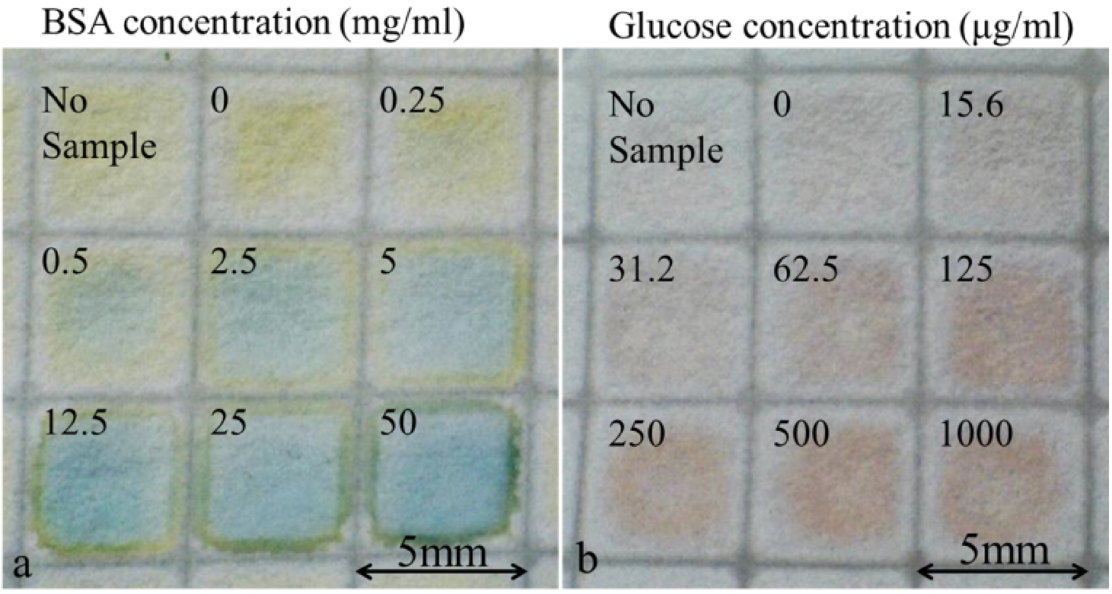

Figure 4.12: (a) Patterned cellulose paper after completion of the BSA detection assay showing different shades of the blue-green colour, corresponding to the different concentrations of BSA pipetted in each well, (b) patterned cellulose paper after completion of the glucose assay showing different shades of the pink-brown colour, corresponding to the different concentrations of glucose pipetted in each well.

The detection of glucose was implemented using an identical square-well pattern, where 3 μl of Glucose Oxidase/Peroxidase reagent (Sigma Aldrich G3660) at a 5:1 ratio and 15 units of protein per ml of solution, were pipetted into each well. As with the BSA test, the reagents were left to dry at room temperature for 1 hour before further use. The test was then executed by addition of sample solutions with different concentrations of glucose into each well of the test-pattern. The concentration of glucose in the artificial solutions made up in de-ionised water ranged from 15.6-1000 μg/ml of D-Glucose (Sigma Aldrich G3285). Introduction of the sample solutions into the wells resulted in a change of colour from white to different shades of pink-brown (Fig. 4.12b). The colours were fully developed after ~10 minutes. The concentration of glucose in each sample is labelled in Fig. 4.12b.

Quantification of the results is very important for medical diagnostic tests, as in most cases, a 'yes/no' answer would not be sufficient. Therefore a way of obtaining the concentration of the analyte from the captured photos was necessary, and we have used the same technique reported in Chapter 3 for the quantification of the LIFT-printed antibodies. The images were processed with the ImageJ software (National Institutes of Health, USA) to extract the respective colour intensities of the blue and brown colour produced within the detection zones for the BSA and glucose respectively. The central part of each detection zone was selected and the average grayscale intensities for each zone were measured. The measured average intensity of the blank control was subtracted from the average intensity of each detection zone, to remove any background colour. By measuring the colour intensities of the known concentrations, we were then able to plot the calibration curves as seen in Fig. 4.13 and Fig. 4.14. Using the same procedure as above, we can find the concentration values of BSA and glucose of unknown samples by measuring their colour intensities and comparing them to the calibration curves.

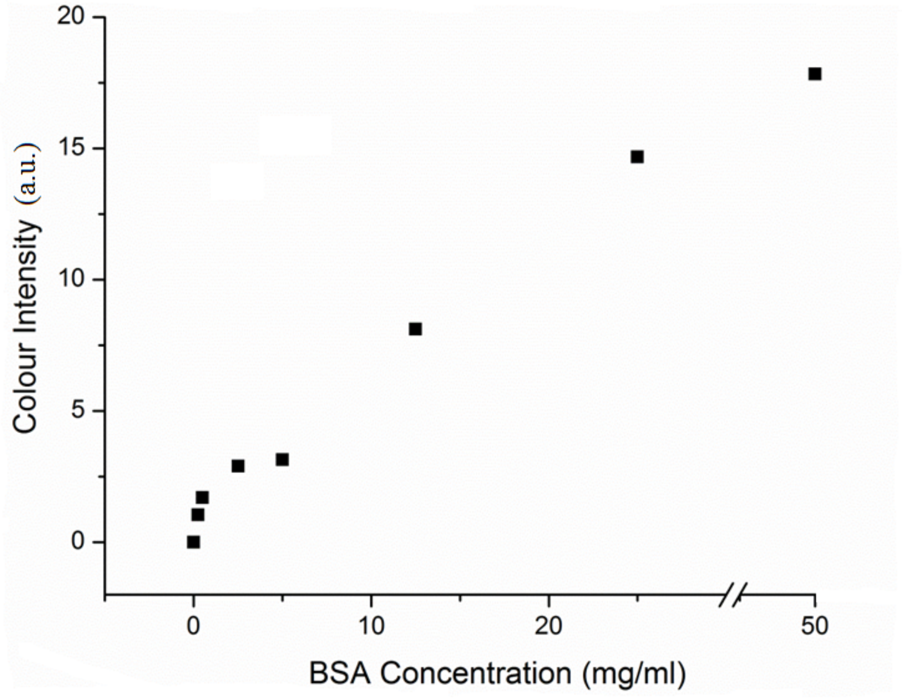

FIGURE 4.13: Calibration curve for the detection of BSA constructed using the grayscale intensity values taken from the image shown in Fig. 4.12(a).

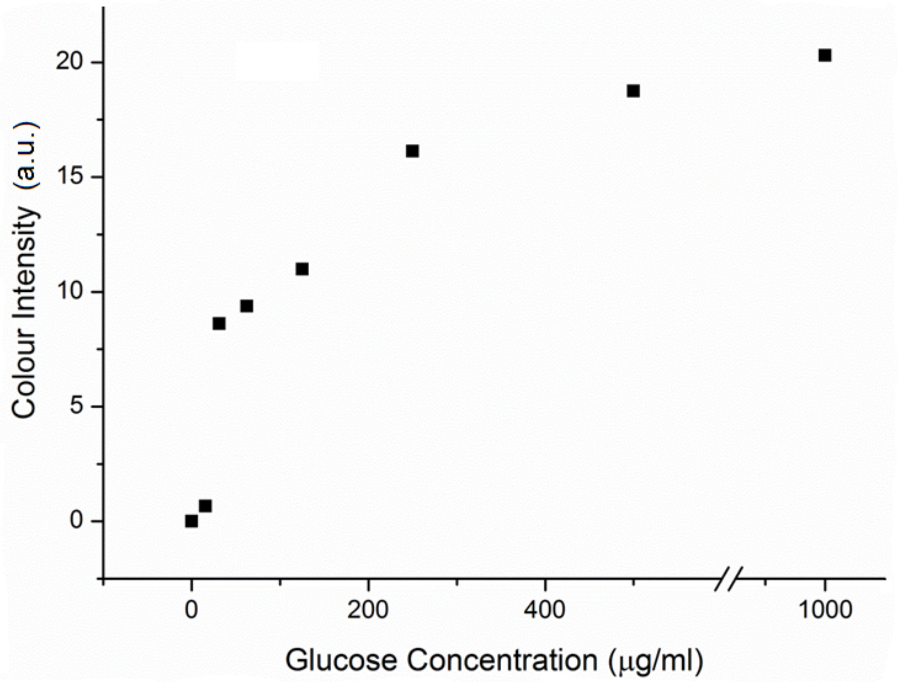

FIGURE 4.14: Calibration curve for the detection of glucose created using the grayscale intensity values taken from the image shown in Fig. 4.12(b).

The final part of our experimental validation involved the use of a fluidic device shaped as a T-junction, for the simultaneous detection of BSA and glucose in the same sample solution, as shown in Fig. 4.15. The lower end of the vertical arm of the T served as the sample inlet point, and the two ends of the horizontal arm of the T served as the test zones. The reagents required for the assays were first pipetted at these two test zones and were allowed to dry. A sample solution (15 μl) containing both BSA and glucose (in concentrations of 50 mg/ml and 1000 μg/ml respectively in de-ionised water), when pipetted at the inlet of the device, flowed towards the test areas, and produced a colour change (blue-green) for BSA and (pink-brown) for glucose with the level of colour change depending on the concentrations of the biomolecules in the sample solution at the respective specified test zones. The dark area, circled in red, (Fig. 4.15a) in the initial section of the vertical arm of the T is the trace produced by the introduction of the fluidic sample solution, and the pale yellow colour of the right end of the horizontal arm of the T is from the dried reagents pipetted into the test zones. Figure 4.15b is an image of the T after completion of the detection assay. For an unknown sample, the concentration of the BSA and glucose in the sample solution can be evaluated by capturing a picture of the T-sensor with a camera, then measuring the intensities of the RGB colours at the test zones [78] and comparing these to a pre-defined calibration curve such as the ones shown in Fig. 4.13 and Fig. 4.14.

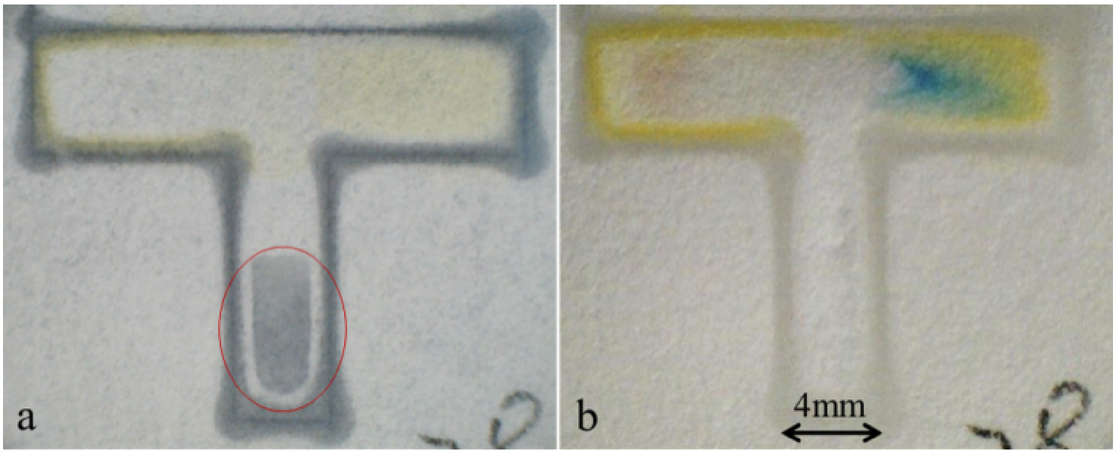

FIGURE 4.15: Camera images of the patterned device, designed for the simultaneous detection of glucose and BSA, (a) at the time of introduction of the sample solution and (b) after detection was completed and measurements taken.

4.3.4 Detection of BSA and glucose with LIFT-printed reagents

Since the main target of this research is to produce a completely laser-fabricated paper-based diagnostic device, it was decided to combine the paper-patterning technique with the previously described LIFT technique. The paper was patterned using the same parameters as in previous experiments of this chapter. Two glycerol donor films were created for LIFT-printing, as described in the previous chapter. One of the donor films contained the reagents for detection of BSA and the other contained the reagents for detection of glucose. LIFT-printing was then facilitated on the pre-patterned paper devices using the 248 nm excimer, as in the previous LIFT experiments. Several spots of both donor films were LIFT-printed in turn on separate and on the same pre-patterned papers.

Two pattern designs were used, the square grid for the separate devices (Fig. 4.16) and the T-shape for the multi-analyte detection devices (Fig. 4.17). A PBS solution containing both BSA and glucose was then pipetted on the paper devices, and blue and brown colour was produced at the corresponding reaction zones. As can be seen from the figures, LIFT-printing allowed for precise printing of the reagents inside the reaction zones. This combination of the two fabrication techniques provides several advantages. LIFT allows for minimal reagent use, as each LIFT-printed spot can be a few nanolitres instead of microlitres that are usually pipetted. Consequently, the area on which the reagents are printed can be less than a mm^2, reducing the footprint of the devices considerably. Both LIFT-printing and the paper-patterning technique are very flexible techniques and are therefore ideal for prototyping.

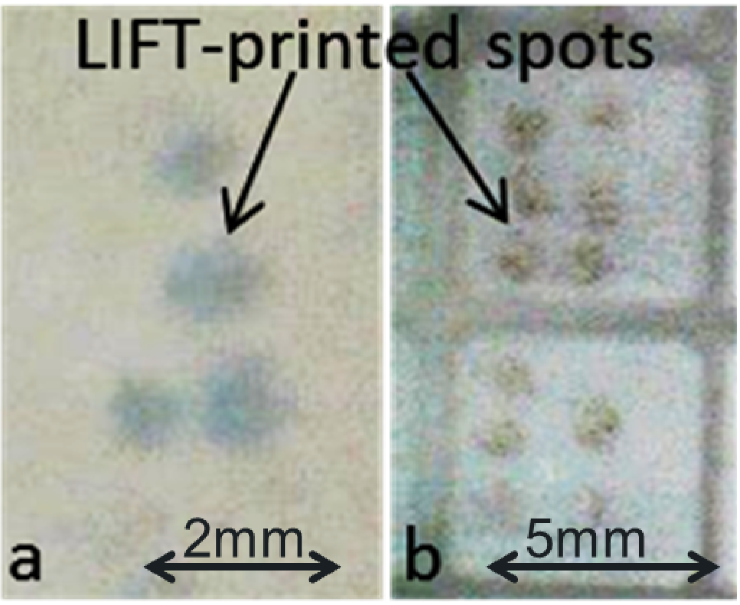

Figure 4.16: LIFT-printed spots on pre-patterned papers for the detection of (a) BSA and (b) glucose.

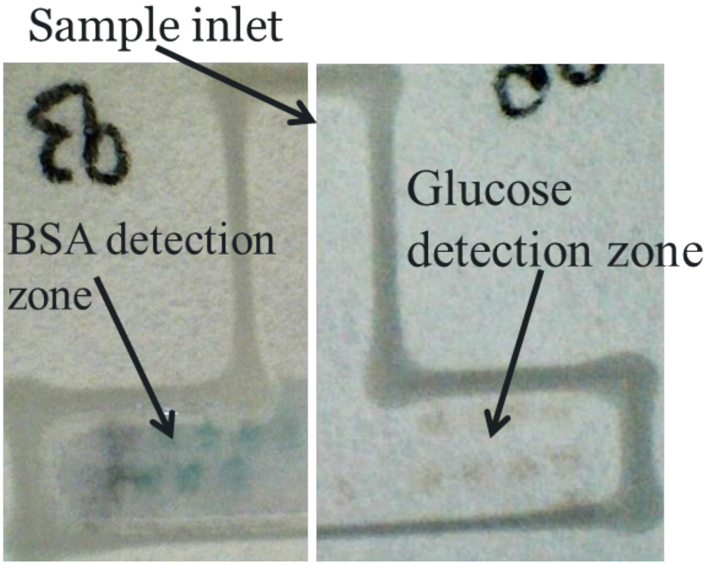

Figure 4.17: Example of multi-analyte detection of BSA and glucose using LIFT-printed spots on pre-patterned paper.

4.3.5 Detection of TNF-α on cellulose paper

The first multi-step sandwich ELISA that was trialled on the nitrocellulose membranes was for the detection of TNF-α. The ELISA kit used in the implementation of the TNF-α detection was purchased from R&D Systems, Inc. (UK). All the antibodies and antigens used were from this kit and were diluted to the working concentrations of 4 μg/mL, 500 ng/mL for capture antibody and conjugated detection antibody respectively. The TNF-α standard was diluted in a range of concentrations between 1ng/ml to 370 ng/mL.

Initially, the assay did not perform as expected. The problem was that when the ELISA was finished, instead of observing a strong colour change only in the areas that the capture antibody was pipetted, there was a blue colour everywhere on the paper as seen in Fig. 4.18. The same result (false positive) occured even when there was no TNFα sample (negative control), so in cases that it was expected that there should be no colour change at all. This problem was attributed to the non-specific binding of the conjugate antibody on the paper and the non-removal of the conjugate antibody during the washing steps. Different blocking solutions were trialled (BSA, milk powder, casein) but none of them solved the problem.

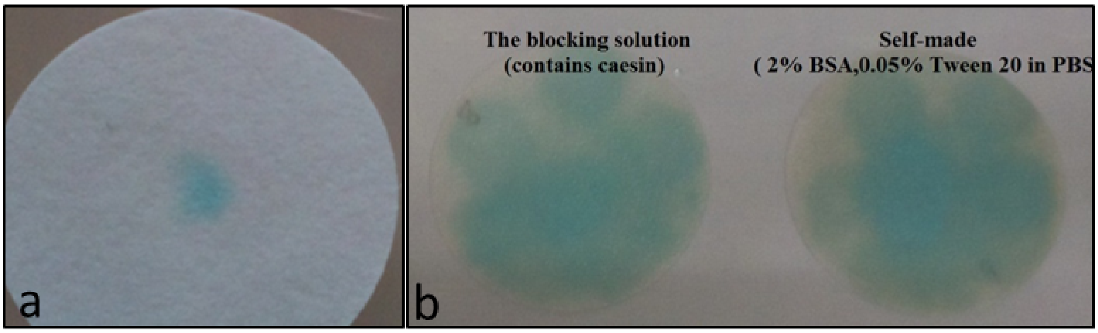

FIGURE 4.18: Images showing (a) the expected result of the TNFα paper-ELISA, and (b) the obtained false-positive result on paper that was blocked with casein and BSA respectively.

Several procedures were undertaken to ensure that the problem was not based on the reagents of the assay, such as testing the assay on the microtiter plate which produced the expected results as seen in Fig. 4.19. Similar problems were encountered when testing different assays on paper, such as ELISAs for diagnosis of IL-1β and PIIINP. Therefore, these ELISAs were deemed not compatible with the paper substrate and these experiments were discontinued.

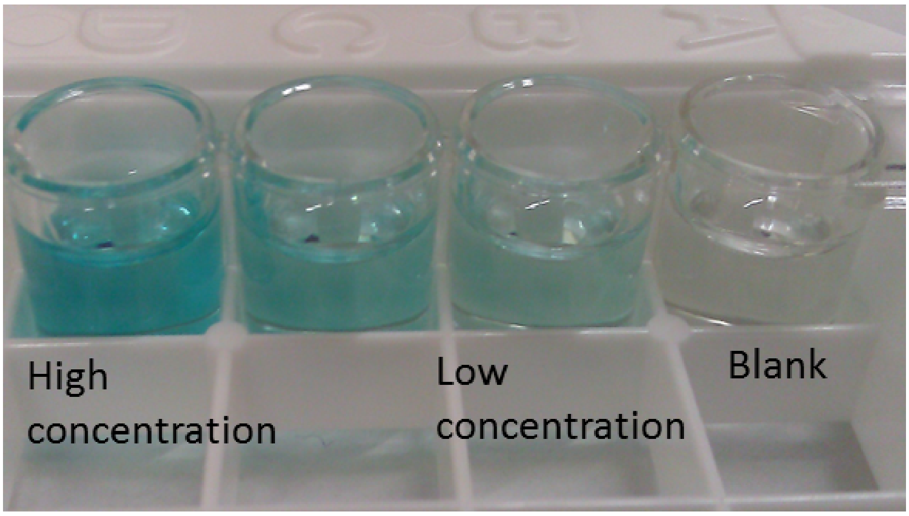

FIGURE 4.19: Image showing the expected result of the TNFα ELISA on the microtiter plate.

4.4 Laser patterning of nitrocellulose membranes

Porous nitrocellulose membranes, since their first demonstration in the 1960s, have been widely used, due to some key features, such as their smooth surface, uniform pore size and high protein-binding capability. A large number of biological assays, namely blotting assays, flow-through assays and lateral flow tests have been developed on these porous nitrocellulose membranes, and hence nitrocellulose-based devices are currently regarded as the best alternative for improving the performance of existing POC assays.

Several methods have already been reported for fabricating fluidic patterns/devices in such materials, and these can be classified into two broad categories: 2D cutting/shaping and physical blocking of pores. The techniques so far reported include the use of photolithography [117], inkjet printing [109, 110], printing of wax [85, 118], and plasma oxidation [104, 119], laser-cutting [120], and shaping [106], each of which has its own merits and drawbacks. In general the ideal technique should be as simple, cheap and fast to implement as possible, and therefore multiple printing steps, the use of specialist chemicals or complex post-processing procedures are to be avoided. The other factor is the feature sizes achievable, which is where procedures such as plotting or wax printing may present restrictions in this context.

In this section, we report on the results of patterning nitrocellulose membranes for low-cost microfluidic devices by employing the laser-based direct-write procedure described earlier in this chapter. As shown later, using this approach, we have successfully demonstrated that it is possible to create microfluidic channels with barriers-walls that have dimensions of ~60 μm a size which has not yet been achieved using other reported methods. Finally, this LDW process is also suitable for a roll-to-roll process, and we believe that this technique presents itself as a promising methodology that can be used for fabricating nitrocellulose-based POC devices.

4.4.1 Experimental section

The laser used for our LDW patterning process was a 405 nm continuous wave (c.w.) diode-laser (Cobolt MLD, Cobolt AB, Sweden) with a maximum output power of ∼110 mW.

The substrates used were Protran nitrocellulose membranes BA85 from Whatman, USA, and the photo-polymer used was DeSolite® 3471-3-14 from DSM Desotech Inc., USA. For this specific photopolymer, the fluence required (for 90% curing) is ∼0.4 J/cm^2. By varying both the laser scan speed and the laser power, a range of experiments was performed in order to find the optimum conditions for forming fluidic structures.

As the extent of the photo-polymerisation process is directly dependent on the incident laser fluence, the widths, depths and the quality of polymerised patterns can be easily controlled by changing the fluence along the exposed area. Thus any desired fluidic pattern can be produced by simply modifying the laser exposure parameters during the LDW process via the laser scan speed and/or laser power.

During the first step of this LDW process, the laser beam was focused onto the nitrocellulose substrate using a spherical lens (f = 15 cm). The substrate was mounted on an xyz- stage, and by controlling the positions in the x and y directions, a user-defined 2D design was patterned on the substrate. The third axis, z, was used to position the substrate at the optimum position (usually, at the focal plane of the lens). For experiments performed in this report, the nitrocellulose substrates were positioned at the focal point, and the corresponding laser spot diameter was ∼8 μm, and the Rayleigh range was ∼125 μm. The range of substrate translational speeds trialled varied from 0.05 mm/s to 10 mm/s, while the incident average powers ranged from 0.3 mW through to 10 mW. The corresponding incident fluences can hence be calculated using the equation:

$$\text{Incident fluence} = \frac{\text{Energy}}{\text{Area}} = \frac{\text{Laser incident power}}{\text{Beam diameter} \times \text{Scanning speed}} \tag{4.1}$$

and therefore ranged from ∼0.375 J/cm^2 to ∼2500 J/cm^2.

The final developing step was to wash off any un-polymerised photo-polymer from the substrate through immersion in a suitable solvent (in this case toluene), which does not affect the intentionally polymerised regions.

4.4.2 Results and discussion

The choice of an appropriate photo-polymer that does not alter the properties of the nitrocellulose substrates is vital, and several, such as SubG from Maker Juice, USA, Norland 61 & 68 from Norland Products Inc., USA, Ablelux A4061T & A4086 from Henkel AG & Co., Germany, were tested in order to find the most suitable. Specifically, photo-polymers that reacted with the nitrocellulose substrate and either dissolved or decomposed it, visibly degraded it, or transformed it into an extremely hydrophobic plastic-like material were rejected. Our current choice, DeSolite® is however extremely viscous, having a viscosity of ∼10,000 mPas at 25 °C, and so we diluted it in toluene in the ratio of 5:3 (v/v) to enable it to soak into the nitrocellulose substrates. These were then left to dry under ambient laboratory conditions, prior to the laser-patterning step. The reason for choosing toluene as the solvent used in these experiments was that other solvents such as acetone or IPA would dissolve the nitrocellulose. This was also the reason we could not use the SubG polymer, as it is a polymer that is pre-mixed with solvents. On the other hand, we found that nitrocellulose does not dissolve in aliphatic and aromatic hydrocarbons such as benzene, xylene and toluene, and therefore toluene was selected as the solvent to be used.

4.4.2.1 Writing of fluidic channels

The first structures to be investigated were simple straight-line channels which would allow determination of some of the basic parameters of laser exposure (scan speed and laser power) required. As shown in Figure 4.20a, two parallel channels were written by scanning at laser powers of 10 and 5 mW under the same scan speed of 10 mm/s, and the fluid containing properties of these channels was tested by flowing red ink through them. As can be seen in Figure 4.20b, the scanned lines form the barrier walls that contain and guide the flow of red ink through these fluidic channels without any observed sideways leakage.

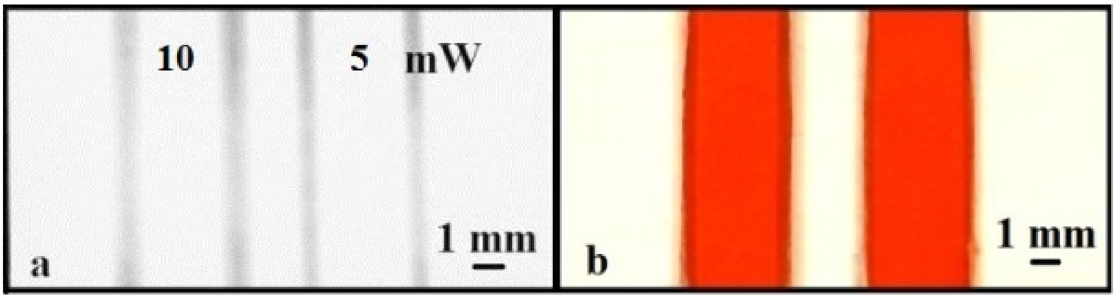

Figure 4.20: Images showing two fluidic channels formed by writing parallel lines with two different laser powers of 10 and 5 mW at a speed of 10 mm/s.

Because toluene is volatile and easily evaporates under ambient laboratory conditions it proved difficult to uniformly soak the substrates with the photo-polymer. As the width, depth and uniformity of the polymerised lines is directly dependent on the polymer concentration in the substrate, any variations would thus translate into lines having undesirable variations. To circumvent this, we chose to soak the nitrocellulose paper directly with the undiluted photo-polymer. However, due to its high viscosity it took ∼20 seconds for the paper to fully absorb the photo-polymer.

Figure 4.21 shows a nitrocellulose substrate that has undergone LDW to polymerise a set of parallel lines, written with different scan speeds (0.05, 0.1, 0.5, 1, 5, 10 mm/s) but with a fixed laser power of 10 mW. The lines shown, after development in toluene, appear as transparent regions of the otherwise white nitrocellulose substrate. This relatively good level of optical transparency of the lines within the otherwise scattering medium is as a result of the induced polymerisation. Lines written with a scan speed less than 5 mm/s have poor definition with irregular edges, which is the result of over-polymerisation due to the unnecessarily high exposures used. However, for scan speeds greater than 5 mm/s, we see that the lines are increasingly well-defined and, as shown in a following section, perform well as barriers to contain and guide fluids.

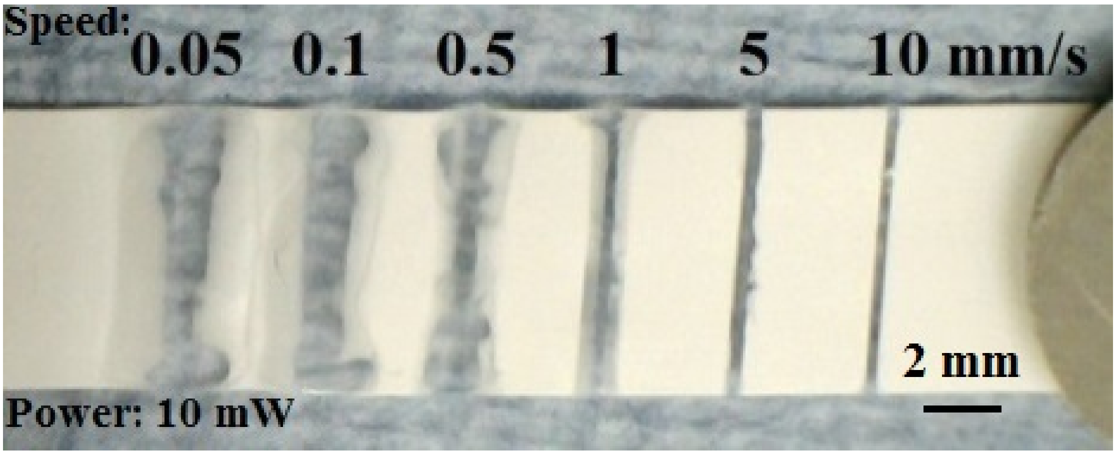

FIGURE 4.21: Photographic image showing a nitrocellulose substrate with a set of parallel lines that were polymerised using different scan speeds of 0.05 - 10 mm/s at an incident laser power of 10 mW.

To further identify the optimum condition in terms of the width and the quality of the patterned lines, we performed a subsequent study by varying the laser power as well as the laser scan speed. The plots in Fig. 4.22 show the relationship between the widths of the polymerised lines and the laser power for three different scan speeds. The line widths obtained increase from ∼70 μm and ∼50 μm to ∼340 μm and ∼270 μm at scan speeds of 5 mm/s and 7 mm/s respectively for an increase in the laser power from 0.2 mW to 10 mW. Similarly, for a scan speed of 10 mm/s, the widths of the polymerised lines increase from ∼50 μm to ∼220 μm as the laser power increases from 0.3 mW to 10 mW.

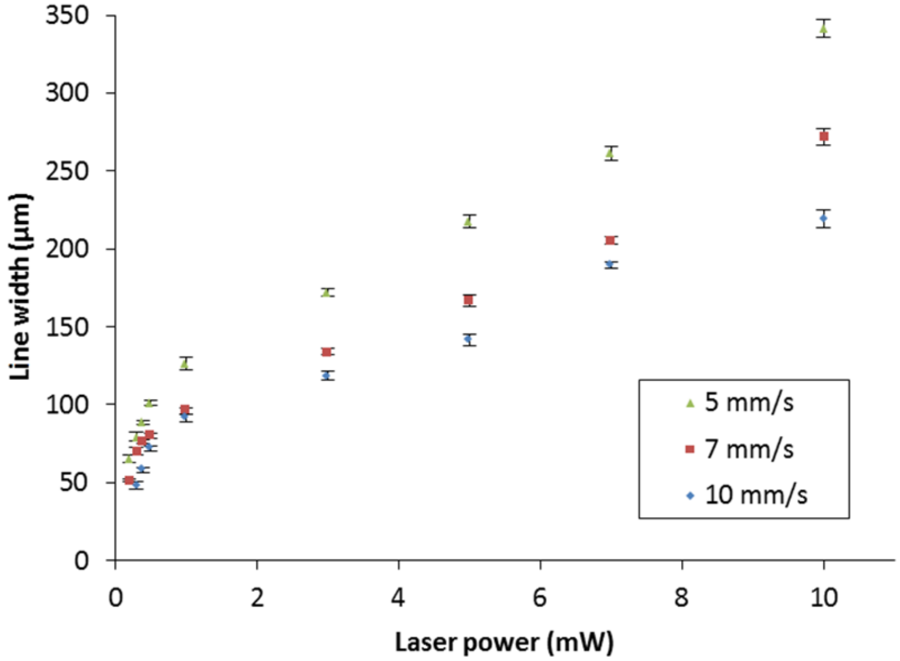

FIGURE 4.22: Plots showing the variations in the widths of the polymerised lines for different laser powers at three scan speeds. Error bars indicate the standard deviation for 5 measurements along each line.

As our final goal was to pattern the nitrocellulose membranes for implementation of LOC fluidic devices, our aim was to identify the optimum conditions for the fabrication of fluidic channels that are able to reliably contain and guide the flow without leakage. Fig. 4.23a shows a set of straight channels having an identical width of 3 mm, written with a constant laser scan speed of 10 mm/s for varying laser powers ranging from 10 mW to 0.3 mW. Fig. 4.23b is an image of the same set of channels after introduction of red ink into each channel. As can be seen from this figure, the ink solution only leaks out of the channel written with the lowest laser power of 0.3 mW, and all other channels contain and guide the flow without any leakage. Using the proposed LDW photo-polymerisation technique, the smallest width of barrier line that we can form in nitrocellulose and which is able to contain and guide the flow, is ∼60 μm - the smallest dimensions reported in literature when compared with other techniques reportedly used to fabricate microfluidic devices such as photolithography, inkjet etching, wax printing etc.[73]

The final step was to determine the minimum width for a fluidic channel that can be patterned via LDW that will successfully allow fluid flow. While the typical widths achieved with the wax printing procedure, which is currently one of the most widely

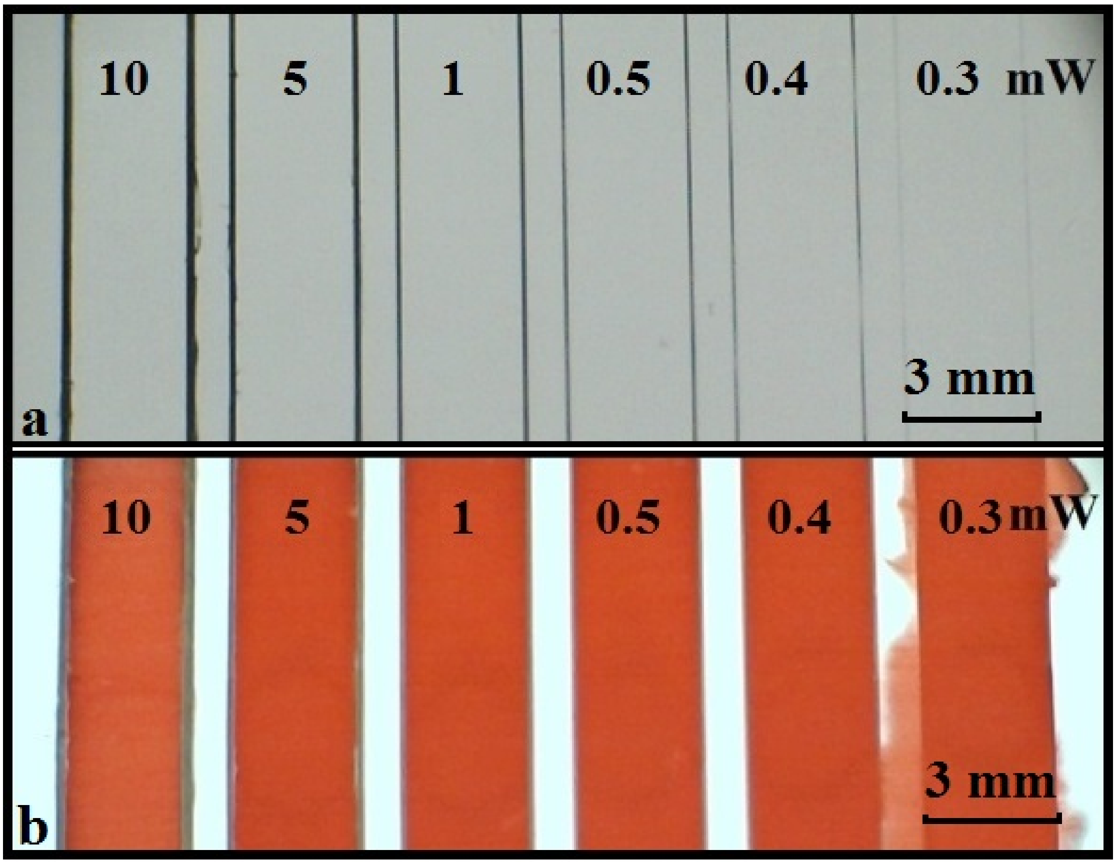

FIGURE 4.23: (a) Image showing a set of fluidic channels formed with pairs of parallel polymerised barrier-walls that were written with different incident laser powers of 10 - 0.3 mW at a constant scan speed of 10 mm/s; (b) after introduction of red ink into each channel.

implemented techniques, ranges from 0.5 mm to 4 mm [64], we anticipated that our LDW technique could produce channel widths that might be around one order of magnitude lower. To identify the smallest widths such fluidic channels can have, as shown in Fig. 4.24a, we patterned several pairs of parallel lines with different channel widths which were fed by the open U-shaped structures that would serve as the fluid reservoirs for the ink used. All these lines were scanned at the same laser scan speed of 10 mm/s and an incident laser power of 1 mW, a condition we had identified as one that produced barrier-walls that reliably contained the fluid. As shown in Fig. 4.24b, after introduction of the ink, channels down to a width as small as ∼100 μm could reliably guide the fluid. This, to our knowledge, is the smallest dimension for any paper-patterned structures reported so far [73].

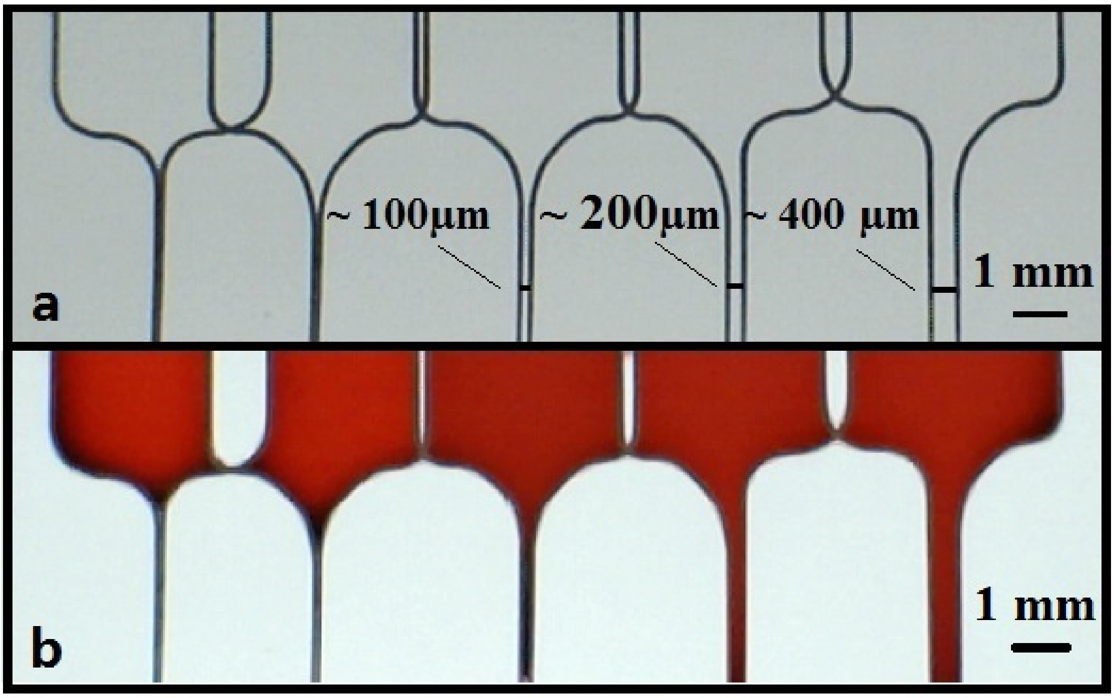

Figure 4.24: Photographic image showing a set of parallel fluidic channels having different channel widths, patterned with a laser power of 1 mW, and a scan speed of 10 mm/s (a) before, and (b) after introduction of 3 μL of red ink into the reservoirs at the top-end of each of these channels.

4.4.2.2 Writing of fluidic wells

The second set of experiments relates to the writing of wells in paper, and their ability to contain fluid. Figure 4.25a shows a set of square wells with dimensions of 5 mm × 5 mm with barrier-walls written using laser powers ranging from 0.3 mW to 10 mW at a fixed scan speed of 10 mm/s. Red ink was again introduced in a fixed volume of 3 μL that was sufficient to fill each square completely. As shown in Fig. 4.25b, we similarly observed leakage only for the wells written with a laser power of 0.3 mW, which we have determined to be the lower threshold value for this fixed scan speed.

The final step was to determine the maximum volume of liquid that these wells could contain without any sideways leakage, a parameter which is important when dealing with actual samples under test, where loss of potentially expensive samples of reagents outside the test area must be avoided. A similar set of squares was written (shown in Fig. 4.26a) into which red ink of different volumes ranging from 1 μL to 15 μL (Fig. 4.26b) was introduced. Even when the volume increased to a value of 15 μL, the wells were still able to hold the ink solutions without any overflow.

On further investigation, we observed that a surface-relief ridge was formed along, and above the patterned lines because of the polymerisation of the photopolymer that was present on the surface of the nitrocellulose membranes prior to the laser-patterning step, and this was investigated through surface-profile imaging measurements. The trace in Fig. 4.26c is a surface-profile scan across a laser-polymerised line, and clearly shows the presence of a ridge (having a width of ∼120 μm and a height of ∼8 μm) along the polymerised line. Hence it can be concluded that the polymerised patterns defined in nitrocellulose using the LDW method not only show excellent ability in containing small liquid volumes, but also show the capability to contain larger liquid volumes without any undesired spill-over, a characteristic that is of immediate interest for practical diagnostic assays.

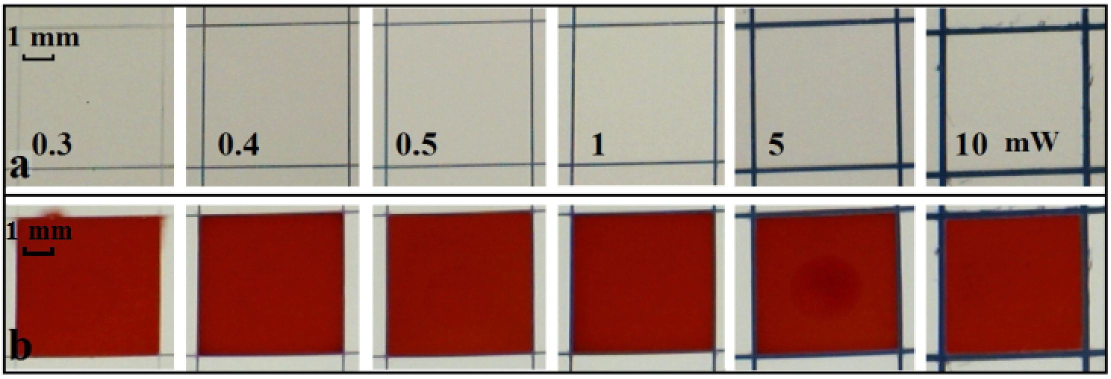

FIGURE 4.25: Photographic image showing (a) a series of 5 mm × 5 mm square-shaped wells patterned with different laser powers of 0.3, 0.4, 0.5, 1, 5, and 10 mW at a constant scanning speed of 10 mm/s; (b) after introduction of 3 μL of red ink into each square.

4.4.3 Applications for chemical and biological diagnostics

4.4.3.1 Detection of nitrite in water

Following these characterization experiments, we chose to validate the effectiveness of our devices as sensors that can be used for the detection of nitrite in water. This is a considerable health concern, as contamination of water sources can occur from fertilizers, animal waste and sewage, which will persist until consumed by plants or other organisms. This experiment served as a useful proof-of-principle, which could equally well be implemented at a relatively cheaper cost on cellulose paper. We performed this detection via the Griess reaction [121, 122], which is a commonly used colorimetric reaction for the detection of nitrite, in which nitrite ions react with a primary aromatic amine under acidic conditions forming a diazonium salt which further reacts with an aromatic compound to form a coloured azo dye.

The Griess reagent was prepared by in DI water dissolving 50 mM sulfanilamide, 330 mM of citric acid and 10 mM of N-(l-naphthyl)-ethylenediamine dihydrochloride.The

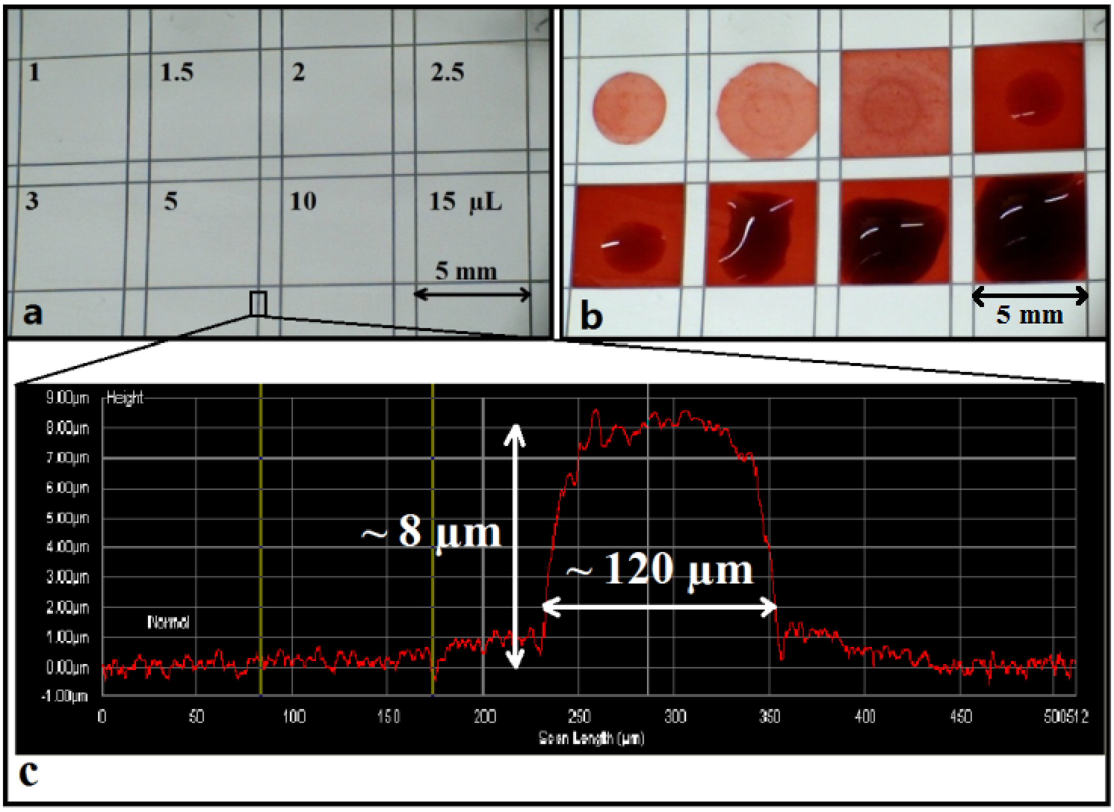

FIGURE 4.26: Image showing (a) a series of 5 mm × 5 mm wells patterned with a laser power of 1 mW and a scan speed of 10 mm/s; (b) after introduction of red ink in different volumes of 1-15 μL into each square; (c) a surface-profiler scan across a polymerised barrier-wall.

prepared Griess reagent (2 μl) was first pipetted into each square-well of the grid-like structure (as shown in Fig. 4.27a) in the nitrocellulose paper, which was then left to dry at room temperature for at least 1 h before use. The grid pattern that formed the square-well detection zones was patterned at a laser power of 1 mW and a scan speed of 10 mm/s, as described earlier. Samples of sodium nitrite were prepared on the day of testing at dilutions of 10 mM, 2.5 mM, 1.25 mM, 625 μM, 312 μM, 156 μM for the known samples and 500 μM, 250 μM for the 'unknown' samples. The samples (2 μl) were pipetted on individual squares, and the colour change produced was imaged by taking a photograph of the paper-device after 1 min with a USB camera as seen in Fig. 4.27a.

The image was then processed with the ImageJ software to extract the respective colour intensities of the pink colour produced within the squarewell detection zones. The central part of each detection zone was selected and the average grayscale intensities for each zone were measured. The measured average intensity of the blank control was subtracted from the average intensity of each detection zone, to remove any background colour. By measuring the colour intensities of the known concentrations, we were then

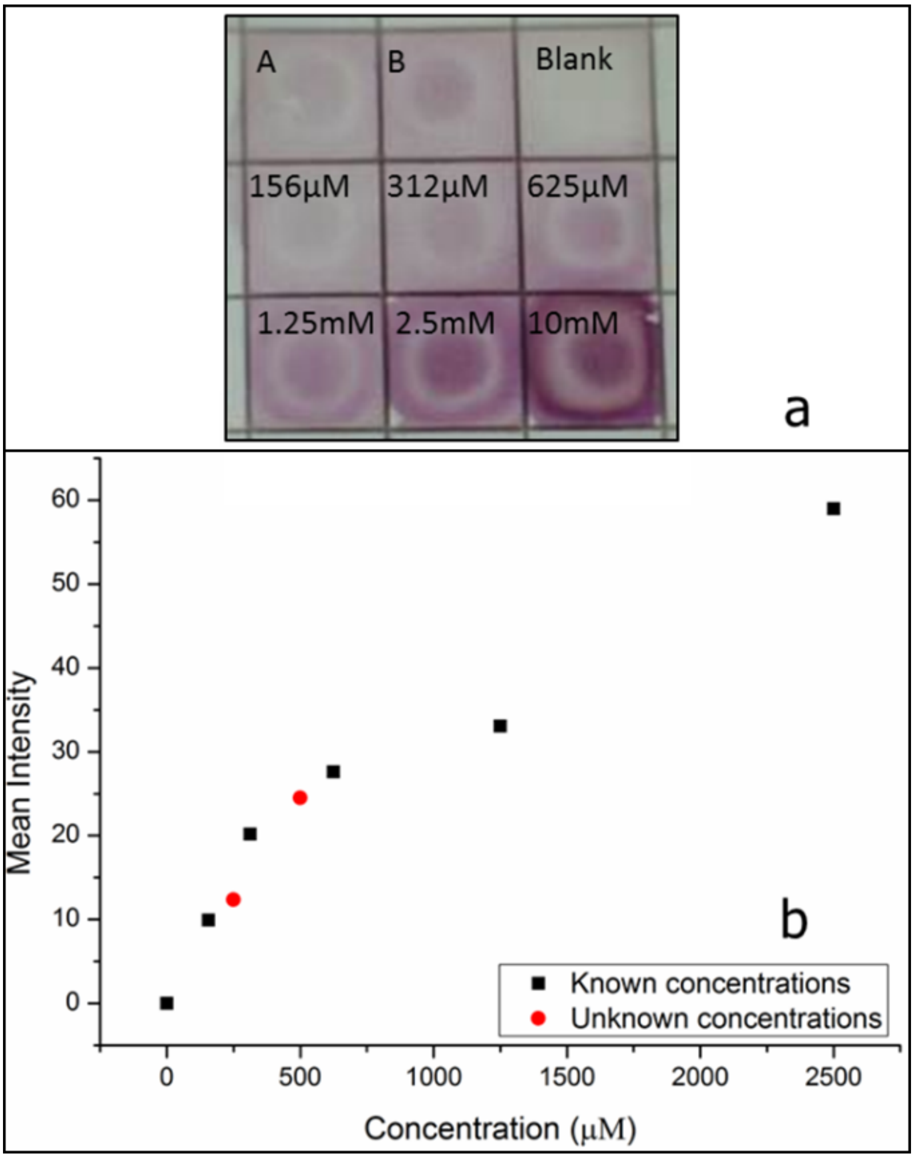

FIGURE 4.27: (a) 5 × 5 mm wells patterned with a laser power of 1 mW and a scan speed of 10 mm/s and prepared for the detection of nitrite by the Griess reagent, after the introduction of the sodium nitrite samples. (b) Calibration curve constructed using the grayscale intensity values taken from the image shown in (a).

able to plot the calibration curve as seen in Fig. 4.27b. Using the same procedure as above, we measured the concentration of the 2 'unknown' samples A and B (plotted in Fig. 4.27b in red) by measuring their colour intensities and comparing them to the calibration curve.

4.4.3.2 Detection of TNF-α on NC

The TNF-α detection assay was revisited using NC as the platform instead of cellulose paper. Reagents, protocol and concentrations used were as described previously in this chapter. Initial tests were done with sample concentrations that are in the clinically relevant range that is pg/ml. The results within this range were unsatisfactory, as the concentration of the antigen was not high enough to produce any colour change, although the problem of non-specific binding observed on cellulose paper did not occur here.

Following that, it was decided to increase the concentration of the antigen to 370 ng/ml, which was the highest possible antigen concentration. By greatly increasing the antigen concentration, the result was as expected and it can be seen in Fig. 4.28: the specific blue spots illustrate the presence of TNF-α in the tested sample. However, these results show that our tested device is far from the sensitivity that can be achieved with commercial ELISA tests performed on their standard platform (microtiter plates), which are normally able to detect TNF-α in the range of pg/mL.

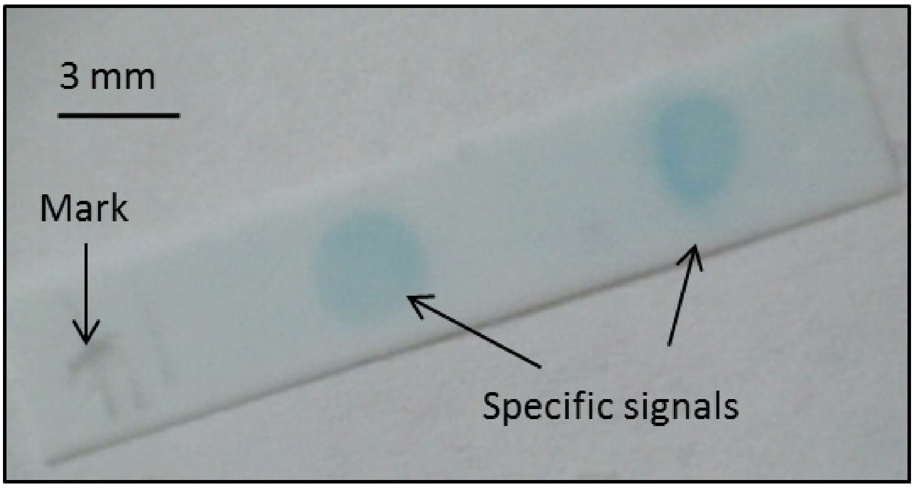

Figure 4.28: Image showing the result of implementation of a sandwich TNF-α ELISA on a nitrocellulose membrane with the sample concentration of 370 ng/mL.

The detection of TNF-α is normally required in the pg/mL range, which is extremely low and thus requires very high sensitivity that increase the difficulty in implementation on paper platform. As a result, we then changed our target to another biomarker CRP, which has a much higher detection level at ng/mL range that makes it easier to detect.

4.4.3.3 Detection of C-Reactive Protein in PBS

Previous experiments showed that a simple one-step chemical diagnostic test can be easily implemented on the patterned NC devices, as well as multi-step biological tests for high concentrations of antigen. It was imperative that the devices were validated further for their effectiveness as medical diagnostic sensors, and the analyte that was chosen as the target was C-reactive protein (CRP), which is an annular protein found in the blood plasma and is mainly used as a marker of inflammation. Measuring and charting CRP levels can provide useful information in determining disease progression or the effectiveness of treatments. Additionaly, the physiological range of CRP is μg/ml, well within the sensitivity capabilities of these devices. This experiment served as a useful proof-of-principle and we performed this detection via the sandwich ELISA (4.29), which is one of the most common reactions used for medical diagnostics.

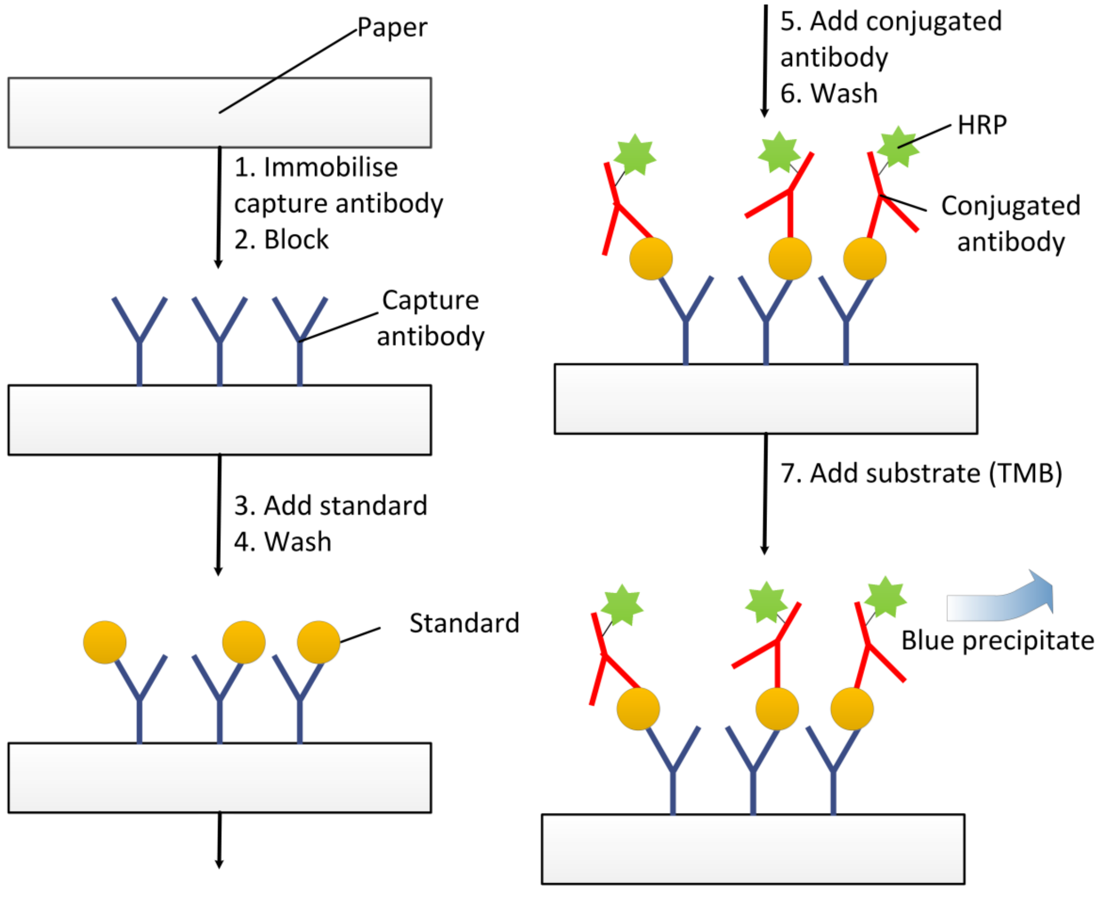

FIGURE 4.29: Schematic of the CRP-ELISA procedure.

The grid pattern that formed the square-well detection zones was patterned at a laser power of 1 mW and a scan speed of 10 mm/s, as described earlier. The solution of mouse IgG primary antibody (2 μL at 360 μg/mL) was first pipetted into each square-well of the grid-like structure (as shown in Fig. 4.30a) in the nitrocellulose paper, which was then left to dry at room temperature for at least 1 hour. The whole paper-device was blocked using a blocking solution of 5% bovine serum albumin (BSA), in phosphate buffered saline (PBS) for 1 hour. Following this, the device was washed 3 times with PBS. Sample solutions of CRP were prepared at dilutions of 1 ng/mL, 10 ng/mL, 100 ng/mL, 1,000 ng/mL, 10,000 ng/mL and 100,000 ng/mL. The samples (2 μL) were then pipetted on individual squares and were incubated for 1 hour. Then the device was washed again for 3 times with PBS and a solution of anti-human CRP antibody (2 μL at 22.5 μg/mL) was pipetted into each square-well. The whole device was again left for

1 hour for incubation and this was followed by washing 3 times with PBS. In the next step, the HRP (horseradish peroxidase) conjugated streptavidin was added into each well and the device was left in the dark for 20 minutes of incubation and then washed again using PBS. Finally, the chromogenic reagent TMB (3,3‘,5,5‘-Tetramethylbenzidine) was pipetted on the whole device and the colour change produced was imaged by taking a photograph (as seen in Fig. 4.30a) of the paper-device after 2 min with a USB camera.

The image was then processed with the ImageJ software to extract the respective colour intensities of the blue colour produced within the square-well detection zones. By measuring the colour intensities of the known concentrations, we were then able to plot the curve (as seen in Fig. 4.30b) that can then be used for calibration.

4.4.3.4 Detection of C-Reactive Protein in urine and blood plasma

In the previous sections of this chapter, we have shown the techniques required to fabricate paper-based and NC-based medical diagnostic devices. In order to prove that these devices can be used in a real setup, they had to be tested for their ability to diagnose analytes in human bodily fluids and more specifically in human urine and human blood plasma. Again, the analyte of interest was CRP, as the protocol was known and well-developed in this format.

The urine samples were obtained from healthy subjects and were spiked with known concentrations of CRP. These spiked samples were then tested in the grid-like devices shown earlier, using the same protocol as before. For comparison, on the same device, the healthy non-spiked samples were also tested. Along with the spiked and healthy urine samples, samples of known concentrations of CRP and blanks in PBS were tested on the same devices to ensure consistency with the previous results. The results of these tests can be seen in Fig. 4.31, and these confirm that indeed these laser-patterned devices can be used for the detection of CRP in human urine samples.

In the following experiment, human blood plasma samples were used for the detection of CRP. The human samples were kindly provided by our collaborators at the Southampton University General Hospital. These were samples from patients that had conditions such as heart attacks and therefore their CRP levels were elevated, and had been measured at the hospital by other traditional techniques. Therefore, a direct comparison of our technique with the one commonly used by the doctors could be performed. Furthermore, blood plasma of healthy subjects was obtained that could be used as the negative control for our tests. The healthy blood plasma was also spiked with CRP of different concentrations. The results of the tests using human blood samples can be seen in Fig. 4.32. All unhealthy clinical samples produced a signal which is also consistent at the

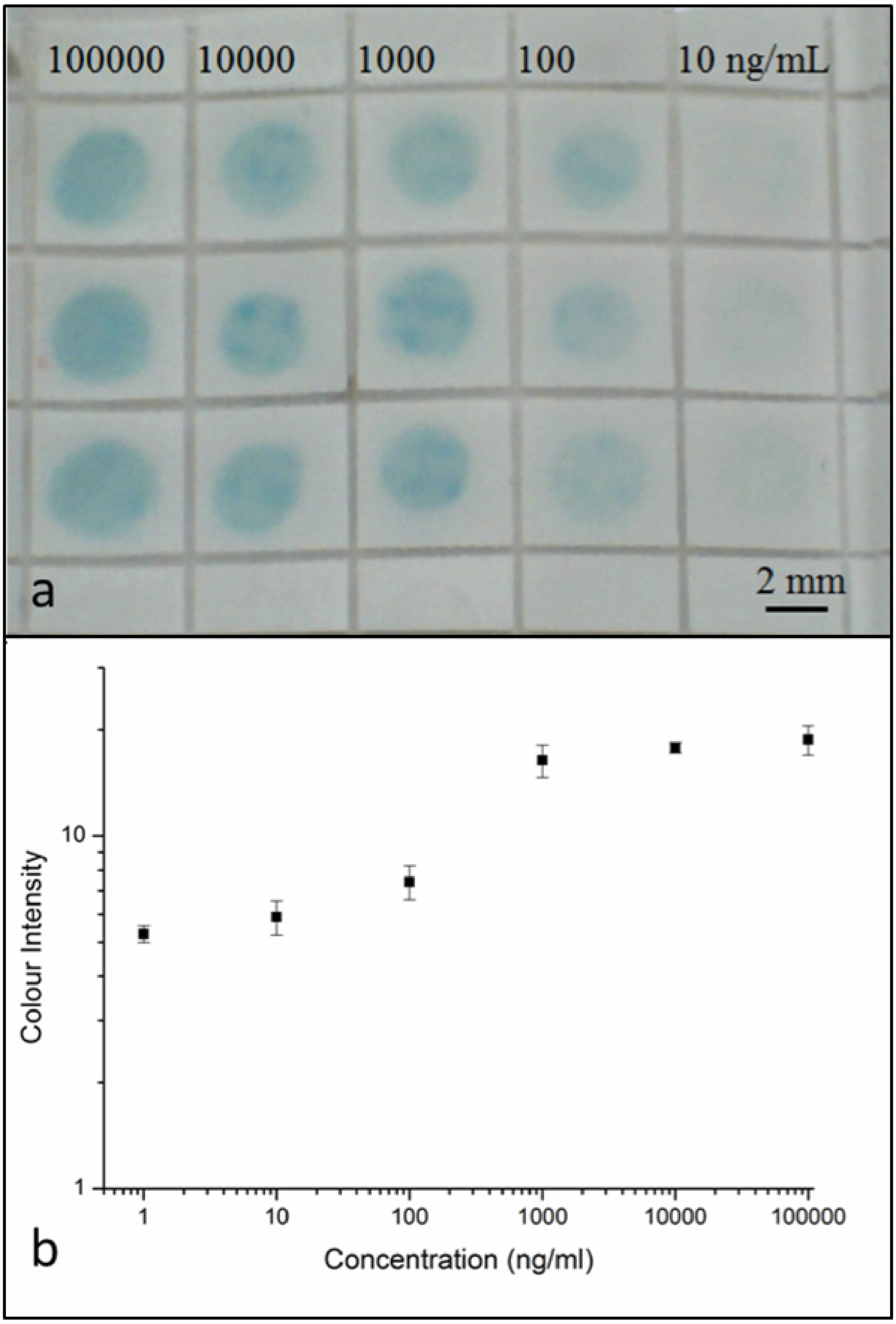

FIGURE 4.30: (a) Selected area of 5 × 5 mm well structure patterned with a laser power of 1 mW and a scan speed of 10 mm/s showing results for the detection of CRP by the sandwich ELISA. (b) Calibration curve constructed using the grayscale intensity values taken from the image shown in (a). Error bars indicate the standard deviation for 4 individual measurements.

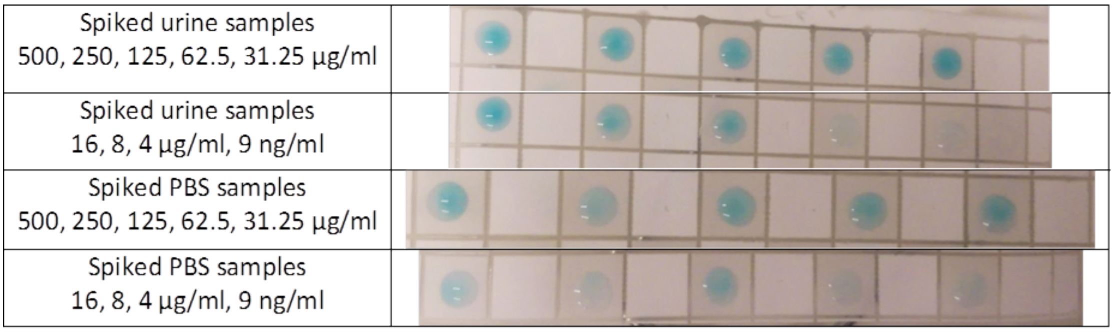

Figure 4.31: Detection of CRP in human urine on laser-patterned nitrocellulose. The first two rows show detection of various concentrations of CRP in spiked healthy human urine, and the two last rows show detection of the same concentrations of CRP in spiked PBS.

different wells that contain the same sample. Moreover, there is a distinct degradation of the colour intensity of the spiked healthy samples as the concentration of the CRP is decreasing, and finally, the non-spiked healthy samples show a very low signal that can be used as the negative control.

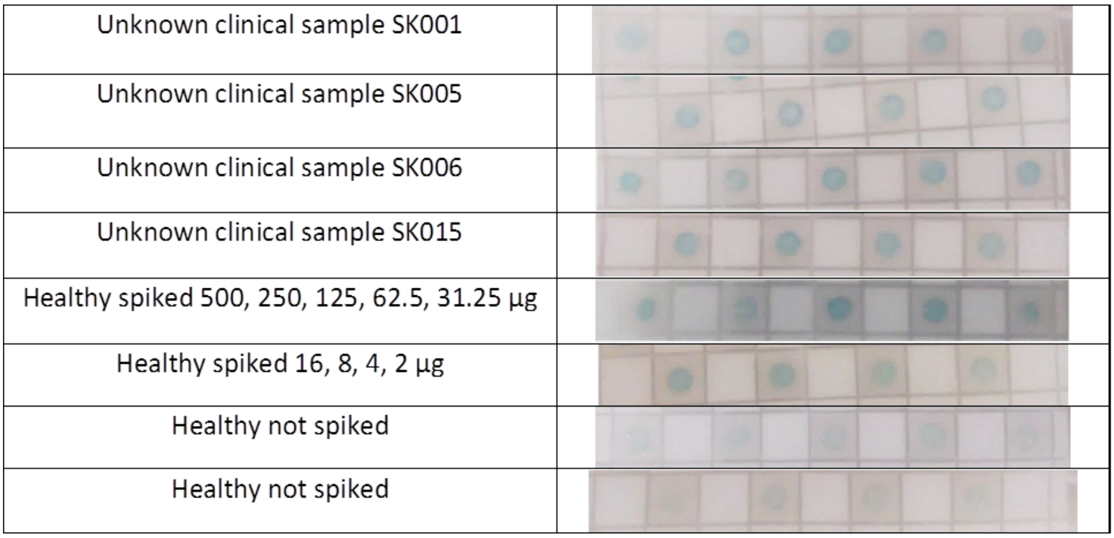

Figure 4.32: Detection of CRP in blood plasma on laser-patterned nitrocellulose. In this trial, both unhealthy clinical samples and healthy samples were used.

4.4.3.5 Detection of IL-6 in PBS.

Another analyte of interest that we trialled with our laser-patterned devices was Interleukin 6 (IL-6), a cytokine that is not only involved in inflammation and infection responses, but also in the regulation of metabolic, regenerative and neural processes [123]. Similar to CRP, IL-6 is elevated in most, if not all, inflammatory states and it has been recognised as a target in medical diagnostics. In many cases, both of these analytes would have to be tested simultaneously, which makes them ideal for our multiplexed diagnostic devices.

The whole paper device was blocked using a blocking solution of 5% BSA in PBS for 1 hour. The capture antibody used in this assay was an anti-human IL-6 mouse monoclonal antibody (R&D Systems, MAB206) at a working concentration of 2 μg/ml in PBS with 1% BSA, that was pipetted at the wells and left overnight to dry in room temperature. The analyte used was recombinant human IL-6 (R&D Systems, 206-IL-CF) in concentrations ranging from 1.2 pg/ml to 75 pg/mlin PBS with 1% BSA, that was incubated in the wells of the paper device for 1 hour. The detection antibody was anti-human IL-6 goat polyclonal biotinylated antibody (R&D Systems, BAF206) in a working concentration of 0.1 μg/ml in PBS with 1% BSA, that was incubated for 1 hour. Finally, streptavidin-conjugated HRP was incubated for 20 minutes and TMB was used to produce the blue colour change at the positive samples. Washing steps with the PBS buffer were performed between each incubation step.

Although the assay has worked correctly, it still requires some optimisation of the protocol, in order to reduce background noise and false-positive results. It is very important though, that in this case the concentration range was in the order of pg/ml, at least 3 orders of magnitude lower than our previous results. That confirms not only that paper-based devices can be used similarly to an ELISA microtite plate test, but also that their sensitivity can be high and comparable to standard lab-based tests.

4.5 Laser-patterning of other porous materials

To further explore the compatibility of this technique, some initial experiments were conducted, that involved patterning of other porous materials. The photopolymer and solvent used here were SubG and acetone and the laser was a 405 nm c.w. laser. The results of these patterning experiments for the different materials are shown in Fig. 4.33. First of all, the result of patterning glass fibre filter is shown in Fig. 4.33a, the patterned channels (with different barrier widths) were able to contain and guide the red-ink through them. In addition, a T-shape structure shown in Fig. 4.33b was patterned in fabric, which faithfully contained and guided the flow. Finally, Fig. 4.33c and 4.33d show the polymerised patterns in Polyvinylidene fluoride (PVDF) and printing paper respectively.

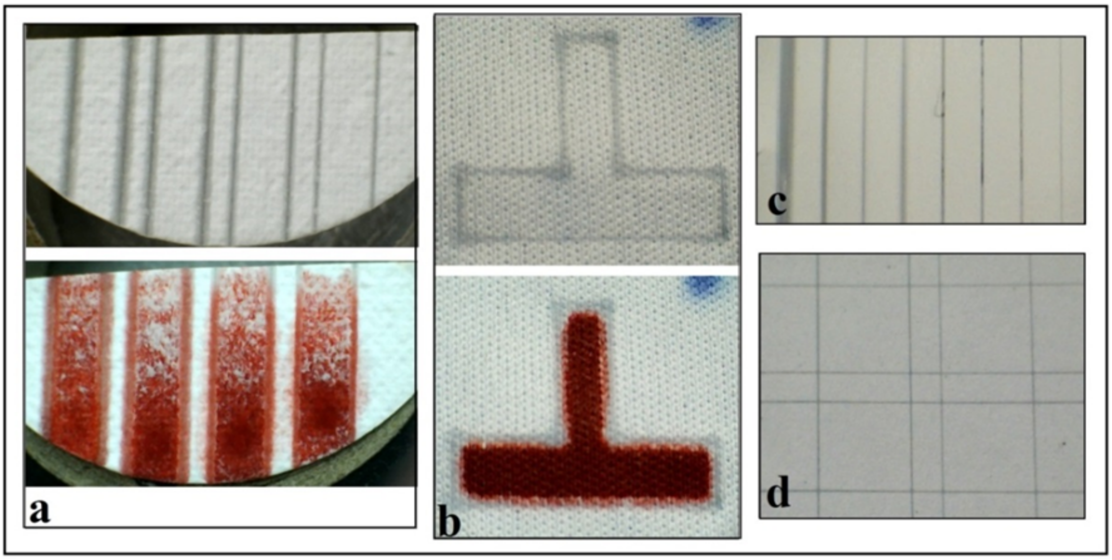

FIGURE 4.33: Images showing the results of patterning different porous materials using the LDW technique such as (a) glass fibre filter, (b) fabric, (c) PVDF, (d) printing paper.

4.6 Conclusions

In this chapter, we have demonstrated laser-based patterning of cellulose paper for the creation of fluidic structures via photo-polymerisation. This LDW procedure is non-contact, thus it offers the advantage of minimizing cross-contamination that could arise during fabrication, it is non-lithographic and mask-less and we have shown its utility in the fabrication of diagnostic tests for protein and glucose detection. The width of the walls/barriers and the width of the channels are at the level of $\sim$100 μm, the smallest that have been reported so far in the literature, which will allow for miniaturisation of the diagnostic sensors, and therefore a corresponding minimal use of reagents. The process is ideal for rapid prototyping at preliminary trial-device fabrication stages and also for final device optimisation. Since the laser energies used are relatively low, the laser required for the process is relatively inexpensive. This means that the infrastructure required for this technique is not expensive and several lasers could even be used in parallel to speed up the process considerably and increase the production volumes. We believe that this technique is therefore ideal for use in mass-manufacturing of paper-based medical diagnostics.

We have additionaly demonstrated that this laser-based direct-write technique based on the principle of light-induced polymerisation can be used for the rapid fabrication of fluidic structures in nitrocellulose membranes. Compared with other methods used in the production of microfluidic devices in nitrocellulose, the technique is also well-suited for up-scaling to mass-production. We have shown that using this method it is possible to create microfluidic channels and barrier-walls with dimensions of ∼100 μm and ∼60 μm respectively, the smallest values that have been reported so far in the literature. We believe that this technique could be an ideal choice for rapid fabrication and mass-production of nitrocellulose-based microfluidic devices that can be used for a variety of applications such as clinical diagnostics and analytical chemistry.

We have also demonstrated that these devices can be used for different detection tests, either simple step in the case of BSA, glucose and nitrite detection, or multi-step in the case of CRP detection. More importantly, we have demonstrated that these devices can be used for the detection of CRP in human bodily fluid samples, whether these were spiked, healthy or with elevated levels due to a condition of the subjects. There are also several advantages of using a laser-patterned paper-based device for these assays. Most important is the fact that the reagents and sample volumes used are only 2 μl per square well which is much lower than the usual 100-200 μl used in a standard ELISA test. This cuts down on the cost of the assay considerably, as reagents are typically very expensive. Another significant advantage is the reduction of the time required to perform this assay. After the incubation of the capture antibody on the paper device, the assays presented here require about 3 hours in total to complete, compared to 6 or more hours required for a standard ELISA test. Additionaly, the cost of the paper device is smaller (∼0.05 GBP per device) compared to the cost of the plastic multi-well plate (∼1 GBP) commonly used in ELISA tests. Finally, the whole footprint of the device is greatly reduced, allowing for easier and cheaper transportation.

Chapter 5

Laser direct-write of advanced structures in paper-based devices for fluidic delays

5.1 Introduction

Ever since the first proposal from the Whitesides group in 2007 [68, 124], the field of paper-based microfluidics has been widely researched and many different lab-on-chip (LOC) type devices have been developed for implementing a wide range of analytical assays. The demand for low-cost alternatives to conventional diagnostic tools has been the driving force that has spurred significant developments in this field. A range of diagnostic assays, ranging from lateral flow type semi-quantitative diagnostic assays to multiplexed tests have already been implemented using such paper-based fluidic devices [64, 66, 78, 87].

Several approaches which include photolithography [117], followed by wax printing [85, 118], inkjet printing [109, 110], plasma oxidation [104, 119], laser cutting [120] and flexographic printing [113] have been used for fabricating paper-based fluidic devices. We have recently reported the use of a laser-direct-write (LDW) approach for creating fluidic patterns in porous media, namely cellulose paper and nitrocellulose membranes [92, 93]. When compared to alternative techniques, the LDW method presents important advantages: it does not need expensive and fixed patterning masks, custom-modified equipment, specialist chemicals or inks, and it overcomes the limitation on achievable feature size that can result from the lateral spreading of the hydrophobic material used to form the fluidic channel walls. Since it is non-contact in nature, the possibility of contamination being introduced during patterning procedures is thereby significantly reduced. Finally, and most importantly, it is suitable for scale-up towards mass-production, possibly on a roll-to-roll basis. Using this approach, we have shown that it is possible to fabricate paper-based fluidic devices, which consist of interconnected hydrophilic channels demarcated by hydrophobic polymerised barrier walls that extend through the thickness of the paper, with feature dimensions below a value of 100 μm.

Research into the development of methodologies to control, and in particular delay the flow of fluids in these devices is a much needed requirement that would enable greater functionalities in such paper-based devices. The introduction of control over the transport of fluid could enable a number of other diagnostic detection tests that have multiple timed analytical steps, for example a multistep test such as the enzyme-linked immunosorbent assay (ELISA), which is most often performed under controlled laboratory environments and has a protocol that requires either a machine or skilled personnel to perform the sequential steps at specific time intervals [125, 126]. In addition to this, a number of additional attributes could be incorporated though controllable fluid flow, such as fluidic diodes and valves [127, 128], timers and metering [129, 130], fluidic batteries [131, 132], and such desirable multi-step sample processing sequences have already been reported in the literature [133, 134].

Current methods that have already been reported for manipulating fluid flow in paper-based fluidic devices can be classified into four main categories: manually activated control [104, 128], modification of the topology and geometry [125, 135], addition of dissolvable chemicals [126, 127], and creation of physical barriers [136], and each of these procedures has its own advantages, as well as some characteristic limitations. Techniques that use manually activated control and physical barriers require additional fabrication steps while adding dissolvable chemicals has the dual drawback of additional processing steps and introduction of chemicals such as sugar in the flow-path which might alter or limit the intended function of the devices. Finally, flow control through modifications of the topology and geometry can increase the fluidic path dimensions, which in turn leads to both a decrease of the fluidic wicking rate and an increase of the required sample and reagent volumes.

In this work, to control fluid flow or delivery, we report the use of a new approach that is an extension of the basic LDW technique that we have earlier reported for creating fluidic patterns and devices made up of interconnected channels and reaction chambers. The LDW method (described in references [92] and [93]) uses lasers to create fluidic patterns in paper via the light-induced polymerisation of a photopolymer previously impregnated in the paper. Laser-scanning of the paper substrate results in the creation of hydrophobic photopolymer tracks that extend throughout the thickness of the paper, and form the boundary walls of the laser-defined fluidic patterns. To produce flow-control the approach presented here relies on use of physical barriers that run across the flow-path (i.e. perpendicular to the fluidic channels) and hence introduce a delay in the fluid flow. As was the case for our LDW method where we demonstrated the use of laser light to form patterns in paper through light-induced photo-polymerisation, the flow delay barriers in this report are created using the same principle of light-induced photo-polymerisation. Part of this chapter has been published in [137]

The schematic in Figure 5.1a shows a simple fluidic geometry that can be used to produce delay barriers via either of the two following methods, (1) by controlling the depth of solid/impermeable barriers (as shown in Figure 5.1b) that are patterned across the flow and which simply impede the fluid flow by reducing the depth of the fluidic channel or, (2) by forming porous barriers (as shown in Figure 5.1c) that allow controlled leakage of the fluids. As described and discussed in the later sections, the control over the depth of the barriers of the first type or the porosity of the barriers of the second type is obtained by simply adjusting the laser-writing parameters such as the laser output power and scan speed. Unlike other paper-patterning methods, the approach presented here does not require any additional processing equipment or specialist materials and as described earlier uses the same fabrication approach that defines the fluidic channels themselves.

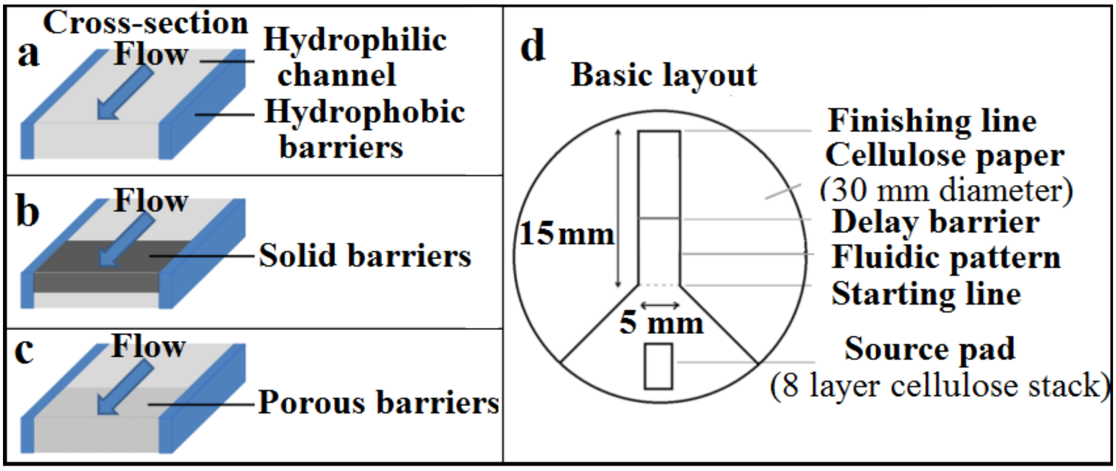

FIGURE 5.1: Schematic representation of: (a) cross-section of a fluidic channel, (b) cross-section of a fluidic channel with solid barriers, (c) cross-section of a fluidic channel with porous barriers, (d) layout of a pre-defined fluidic structure.

5.2 Experimental section

5.2.1 Laser setups and materials

The lasers used for the direct writing process were a Q-switched Nd: YVO_4 laser (B M Industries, Thomson CSF Laser, France) operating at 266 nm, with a pulse duration of 10 ns, a maximum single pulse energy of 2 mJ, and a repetition rate of 20 Hz (used for method 1 as outlined above, and shown in Figure 5.1b) and a 405 nm continuous wave (c.w.) diode laser (MLDTM 405 nm, Cobolt AB, Sweden) with a maximum output power of ∼110 mW (for method 2, shown in Figure 5.1c).

The paper substrates used were Whatman No. 1 filter paper from GE Healthcare Inc. The photopolymer chosen for these experiments was Sub G, from Maker Juice, USA. The sample solution used for characterising the flow delivery delay was Tris Buffered Saline (TBS, 20 mM Tris, pH approx. 7.4, and 0.9% NaCl), which is a buffer commonly used in diagnostic assays.

5.2.2 Creating Fluidic Delays

We first patterned fluidic channels with the design geometry shown in the schematic of Figure 5.1d, using the LDW technique, which we have previously optimised via a systematic study. The width and length of the fluidic channel was 5 mm and 15 mm respectively, and the inlet end of the channel was designed to replicate the shape of a funnel. These fluidic channel patterns were defined using the c.w. laser operating at 405nm [92]. We subsequently patterned the fluidic barriers within the channels using either of the two lasers described previously.

The channels were patterned using the c.w. laser due to the much higher writing speeds achievable (almost three orders of magnitude greater than that for the pulsed 266 nm source). To ensure that there was sufficient fluid to wick the entire length of the channel, we cut and stacked multiple (8 in this example) pieces of paper (of 3 mm x 5 mm), and positioned them at the wider end of the funnel-shaped inlet of the channel, and loaded it with a comparatively large volume of fluid (∼40 μL) the stack serving as a continuous reservoir of liquid.

During our earlier studies into the fabrication of fluidic channels using pulsed laser irradiation, we observed that by controlling the scanning speed (and therefore the effective exposure) of the laser beam, we could polymerise lines of various depths inside the paper substrate as illustrated schematically in Figure 5.2a. Slower scanning speeds produced polymerisation through the full depth of the paper, while faster scanning speeds led to photo-polymerisation only in the upper portion of the paper, thus creating partial barriers that the liquid had to overcome. These fluidic delay barriers can therefore decrease the flow by a rate that is proportional to their depth, and hence this principle can be used to impose a user-defined variable time-delay in the wicking of the liquids and test samples.

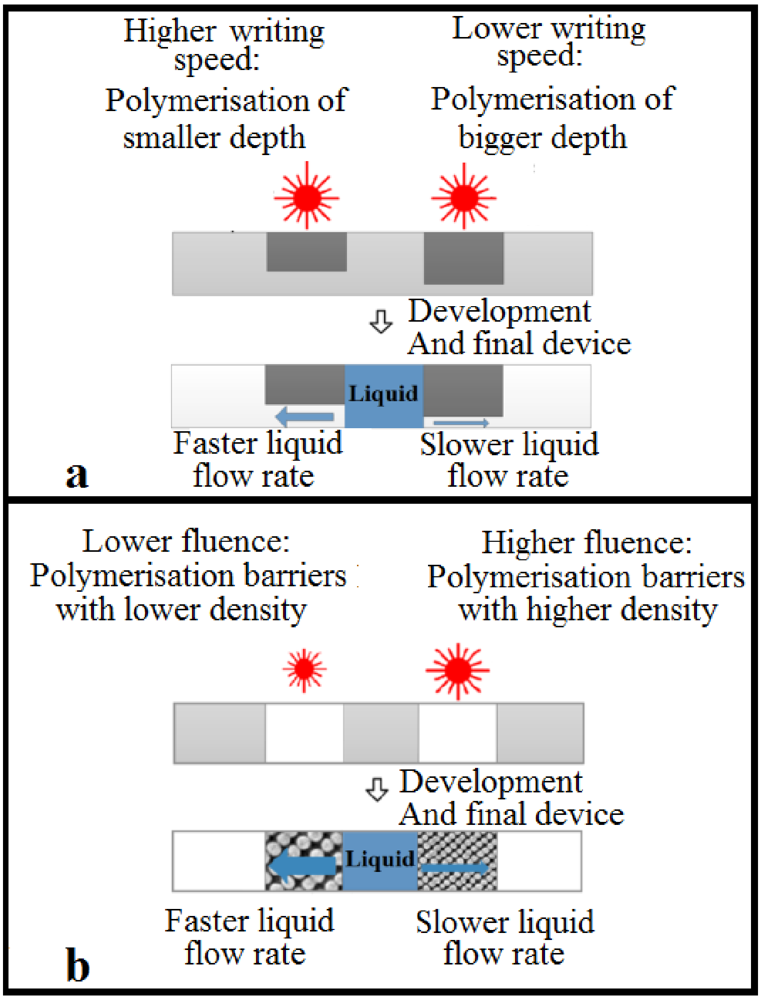

FIGURE 5.2: Schematic of the fabrication of polymerised barriers of: (a) variable depth inside the paper substrate; (b) variable degree of polymerisation extending throughout the full thickness of the paper. Both methods allow for controlled wicking, and variable flow delays.

An alternative approach, as illustrated in Figure 5.2b allows the writing of barriers via manipulation of the extent or degree of polymerisation using c.w. laser exposure. In this case however, the barriers produced extend throughout the full paper thickness, but the degree of polymerisation can be engineered to form barriers whose porosity can be controlled. For these less dense, leaky barriers, the polymerised material does not completely fill the voids within the paper matrix, and instead the polymerised material simply coats the fibrous strands, without forming a completely impermeable barrier.

Figure 5.3 illustrates the difference between such solid and porous polymerised barriers. As shown in Figure 5.3a, the polymerised regions for solid barriers written with a pulsed laser could only be observed on the top, and not the lower face of the paper, suggesting partial polymerisation through the thickness of the paper. However, the polymerised regions for porous barriers written with a c.w. laser always extended throughout the entire paper thickness, as shown in Figure 5.3b. Blue ink was added to the sample in Figure 5.3a to enhance the contrast between the paper substrate and the lines.

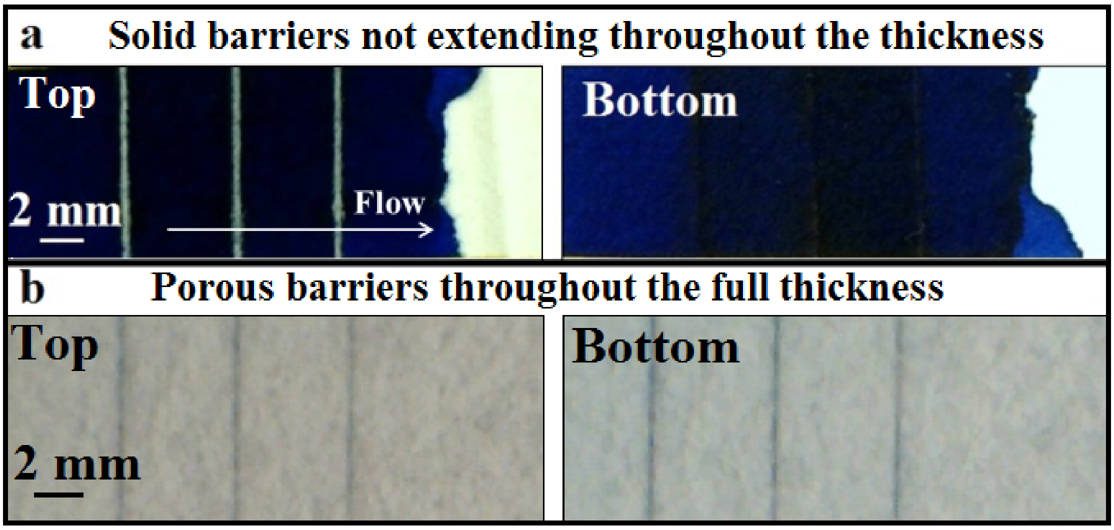

Figure 5.3: Images showing the delay barriers from both sides of the cellulose paper. (a) Depth-variable solid barriers formed by pulsed laser exposure; (b) porosity-variable barriers formed by c.w. laser exposure.

As described below, we compare both of these methods for generating controllable flow delay in fluidic channels. The study was aimed at characterising the influence of the laser fluence and exposure on the depths and porosity of the barriers for methods 1 and 2 respectively, including an investigation of delay as a function of positions and numbers of barriers. Since both the fluidic channel walls and delay barriers can be patterned using the same LDW process, this technique should have immediate appeal to manufacturers wishing to develop such paper-based devices on a large scale where production speed and cost are two of the main considerations.

5.3 Results and discussion

5.3.1 Method 1: Delay via solid barriers created by pulsed laser writing.

In order to explore the relationship between the depth of the solid barriers and the incident fluence, which depends on both the laser average power and the laser scan speed, we first fabricated a set of polymerised barriers written with a fixed incident average power (7 mW) but different speeds from 0.1 mm/s to 1.5 mm/s. We then measured the depth of these barriers by cutting the paper substrates along a line that intersects the barriers, and then imaged the cross-sections of the paper using an optical microscope. The relationship between the depth and the barrier writing speed is plotted in Figure 5.4, which shows that an increase in the writing speed from 0.3 mm/s to 1.5 mm/s leads to an decrease in the depth of the barrier from ∼90% to ∼10% of the thickness of the paper.

To understand and quantify the usefulness of these solid barriers with variable depths in both delaying and even completely stopping the fluid flow, we fabricated a set of 4 channels, as shown in Figure 5.5a, and then patterned barrier lines perpendicular to the flow direction. Each of the fluidic channels was inscribed with two barriers, both of which had been written under the same writing conditions. Importantly, for each of the fluidic channels (1 - 4) these pairs of horizontal lines were written with the same incident average power (7 mW) but different speeds namely, 1 mm/s, 0.7 mm/s, 0.5 mm/s and 0.3 mm/s, thus forming solid barriers with differing depths, which can be calculated from the plot in Figure 5.4.

As shown in Figure 5.5b and 5.5c, blue coloured ink introduced from the inlet of the channels, (marked in the image) experiences a flow rate that is a clear function of the presence and strength of the inscribed barriers, with channel 4 being the slowest, and channel 1 the fastest. The ink was introduced at the same time in each of the four channels. Figure 5.5b and 5.5c are images taken 2 min and 3 min after the introduction of ink, and as seen in Figure 5.5b, the ink has already flowed past the two barriers of channel 1, is leaking past the second barrier of channel 2, has just reached the second barrier in channel 3, while it has just crossed the first barrier in channel 4.

To quantify the flow delay versus writing conditions, we used the arrangement of figure 5.1d, which is shown in greater detail in Figure 5.6, using TBS (pH = 7.4), a reagent conventionally used as a buffer in bio-chemical assays, as the liquid medium. The fluid delivery time was defined and measured as the time the TBS solution needed to travel from the starting line to the finishing line, a distance of 15 mm in total. The channel

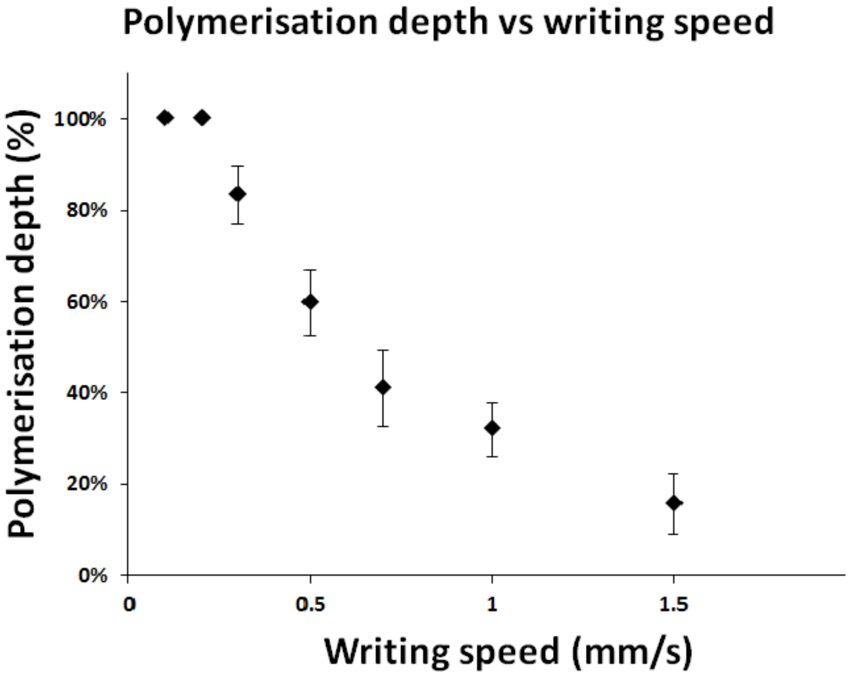

Figure 5.4: Comparison between the depth of the polymerisation in the paper and the delay barrier writing speed. Error bars indicate the standard deviation for 3 measurements.

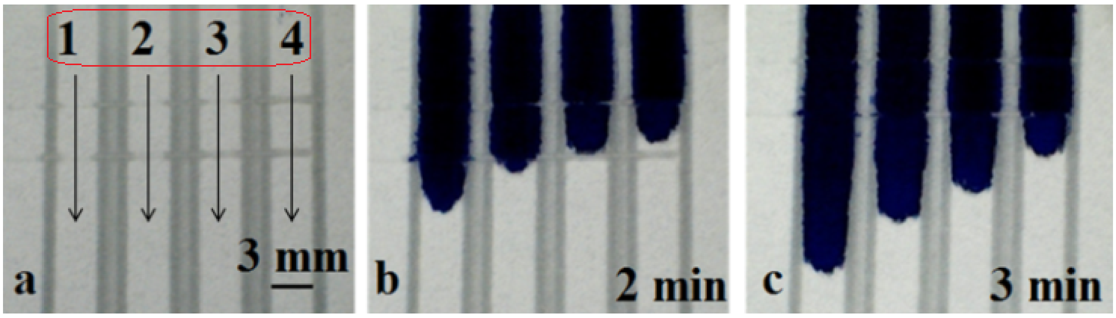

Figure 5.5: Image showing the delay of the liquid flow after introduction of blue ink in fluidic channels with barriers created using different writing speeds.

walls were written with the 405 nm c.w. laser (20 mW, 10 mm/s), whereas the barriers were written with a pulsed laser at writing speeds from 1 mm/s to 0.3 mm/s.

First, we studied the consequence of having solid barriers with different depths in the flow-path, however with only one delay barrier at position P1 (as shown in Figure 5.6a) in each of the pre-defined device. Several devices, each with one single delay barrier were written under different writing conditions, by changing the scan speed (from 1 mm/s to 0.3 mm/s) at a constant laser average power of 7 mW, which corresponded to creation of solid barriers with depths ranging from ∼20 % to ∼90% of the thickness of the paper (as shown in Figure 5.4). We have quantified the ability of the barriers to delay the fluid flow using a normalised delay factor, which we define as the time to flow (from the starting line to the finishing line) in a channel that has barriers, divided by the time to flow in a channel without barriers:

$$\text{Delay factor} = \frac{\text{Flow time for a channel with barriers}}{\text{Flow time for a channel without barriers}} \tag{5.1}$$

The results for the delay factor are plotted in Figure 5.7 which show an increase in the delay factor from ~1.1 to ~1.6 with an increase in the barrier depth from ~20% to ~90%.

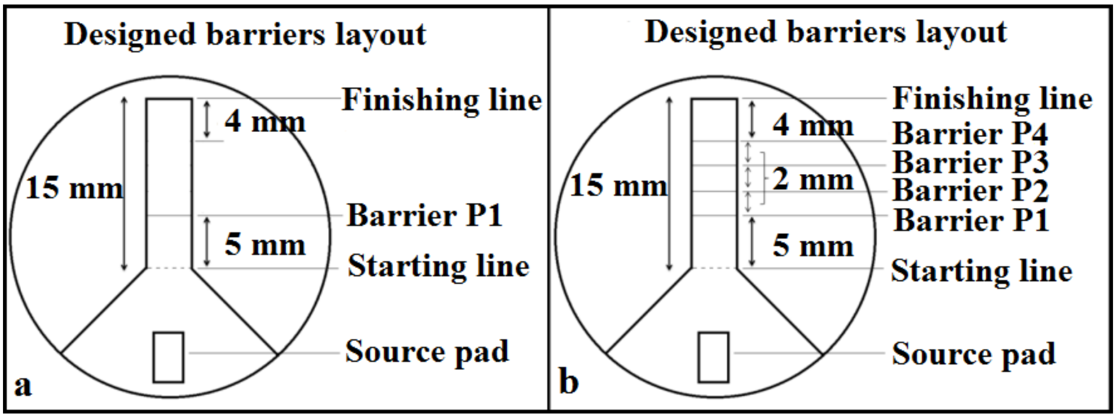

FIGURE 5.6: Schematic representation of designed barrier layout showing the position of delay barriers (P1, P2, P3 and P4).

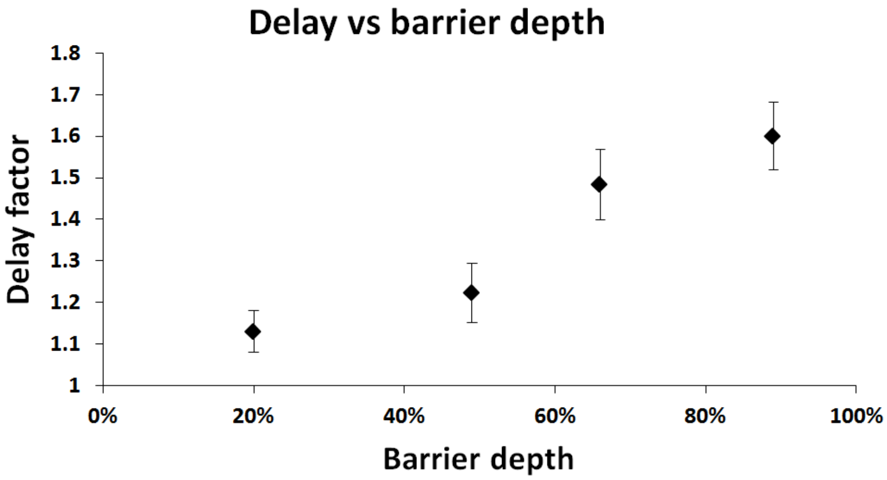

FIGURE 5.7: Plots showing the delay factor for devices with barriers having different depths. Barriers were written with different writing speeds at a fixed average power of 7 mW. Error bars indicate the standard deviation for 3 measurements.

5.3.2 Method 2: Delay using porous barriers created by a c.w. laser

In this case, both the fluidic channels and the flow delay barriers were written with the same c.w. laser (in a common programmed writing step) by simply changing either the laser output power or writing speed. To allow for a direct comparison with the results for the solid barriers, fluidic devices that were tested had the same design as in Figure 5.6.

In this case however, four porous barriers were written across the fluidic channels, to explore the role of number and position of barriers as shown in Figure 5.6b. A comprehensive study was performed to explore the flow delay induced through barriers written with a range of different writing conditions. The fluid delivery time and the percentage delay were calculated as for method 1.

We first did a comparative study for barriers patterned with different writing conditions, namely different laser powers and scan speeds. Subsequently, we then changed the number of the barriers to explore the relationship between the delay and the number of barriers in the flow path. As in Figure 5.6b, a one barrier design refers to a device with a single barrier patterned at position P1 in the channel; a two barrier device refers to a channel with two barriers patterned at P1 and P2; and so on.

As shown in Figure 5.8a, for barriers written with a fixed scan speed of 100 mm/s, the fluid delay gradually increased with an increase of the laser power, and progressively decreased for barriers written with an increasing scan speed at a fixed laser output power of 20 mW, as shown in Figure 5.8b. These results show that the porosity of these barriers is a clear function of the laser fluence used and that any targeted delay (within the experimental error) can be achieved by choosing the correct fluence. Similarly, for the plots shown in both Figure 5.8c and 5.8d, which are based on the use of multiple barriers, we observe identical trends - for barriers written with the same writing conditions, the delay increases with an increase in the number of barriers.

In addition to this dependence on the porosity of the barriers and the number of barriers, we observed that the fluid delay also depended on the position of the porous barrier. We introduced a single porous delay barrier written under the same writing conditions (200 mm/s scan speed and 20 mW laser output power) at different positions (P1 P4) as show in Figure 5.6b, and then studied the fluid delay. The plot of the fluid delay versus the position of the porous barrier is shown in Figure 5.9. As the delay barrier was shifted further from the starting line towards the finishing line, the delay factor rapidly dropped from ∼2.5 (for position P1) to ∼1.3 (for position P4). We believe this is because of the geometry of the device, since the volume of the paper that serves as the reservoir for the fluid flow changes with a shift in the position of the delay barrier.

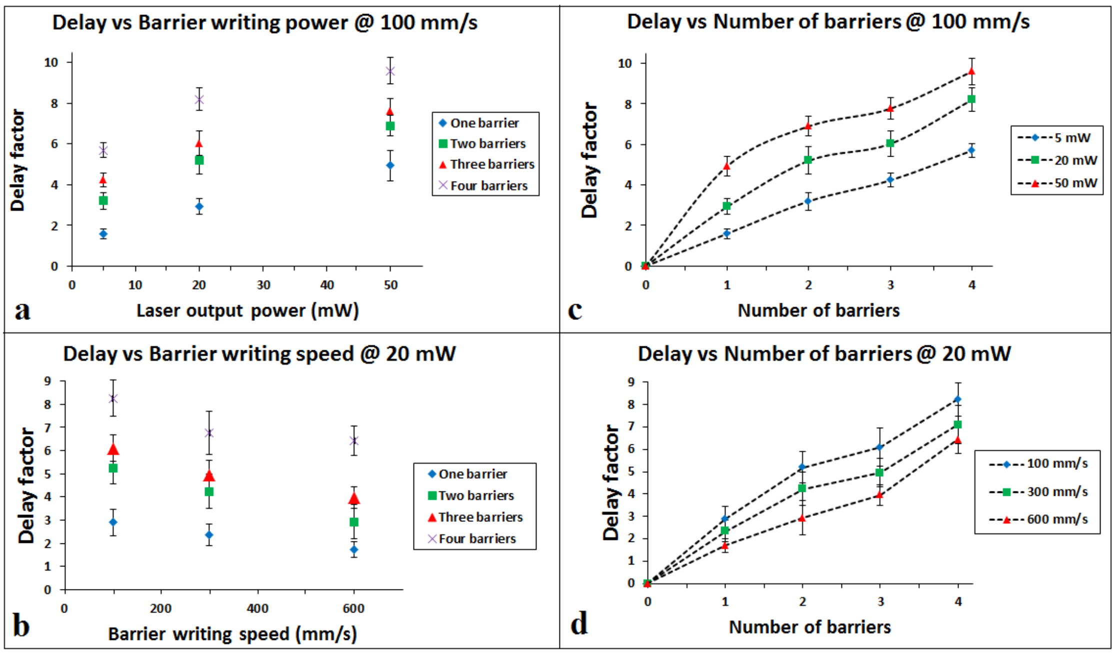

Figure 5.8: Plots showing the delay factor of delay-barrier-designed devices. (a) Barriers written with different laser output powers at a fixed scan speed; (b) barriers written with different scan speeds as a fixed laser output power; (c) different number of barriers written at a fixed scan speed; (d) different number of barriers written at a fixed laser output power. Error bars indicate the standard deviation for 3 measurements, and lines are a simple guide for the eye.

The volume before the delay barrier acts as a pump for subsequent flow, thus affecting the flow rate after the barrier. As shown in Figure 5.6b, the closer the barrier is to the starting line, the smaller the source volume is, and this leads, we suggest, to a lower pump force and hence a lower flow rate and larger fluid delay.

5.3.2.1 Weight measurements of porous barriers

In order to establish the difference in porosity or polymer-filled volume, weight measurements of the polymer lines were considered. Several same-size samples were prepared with the same number of lines but different laser fluences, ranging from ~0.1 J/cm^2 to ~1.7 J/cm^2. The paper substrates were weighted before and after the laser-based patterning, specifically before the introduction of the polymer (blank paper) and after the unpolymerised polymer was removed and the paper was dried to remove any remaining solvent. The first weight measurement was then subtracted from the second to obtain the total weight of the polymer on every paper substrate. The polymerised lines though, have different widths depending on the laser fluence used for their fabrication. Therefore the weight/volume had to be calculated from the total weight of polymer for each paper substrate. The results of these measurements and calculations are shown in Fig. 5.10,

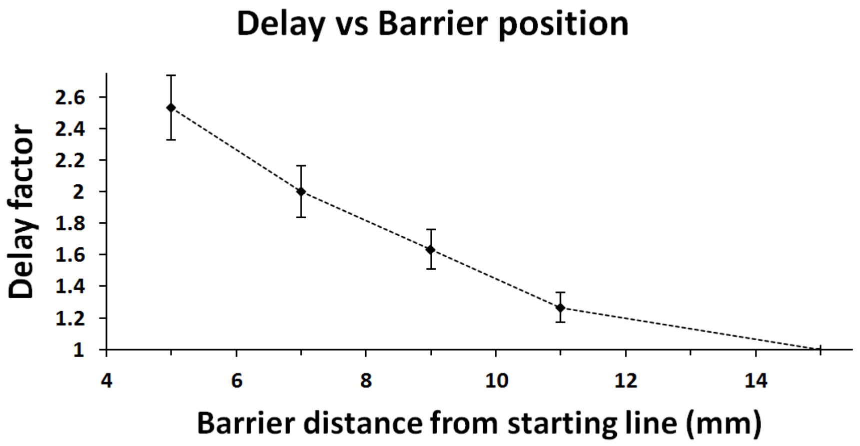

FIGURE 5.9: Plots showing the relationship between the fluid delay factor and the position of the delay barriers (distance to the starting line) with the same condition of 200 mm/s scan speed and 20 mW laser output power. Error bars indicate the standard deviation for 3 measurements, and the line is a guide for the eye.

and they clearly show the correlation between the weight/volume unit of the polymer and the laser fluence used. This shows that indeed, the higher the laser fluence used for the fabrication of the polymer structures, the higher the density of the polymer, and therefore its capability as a flow-delay mechanism.

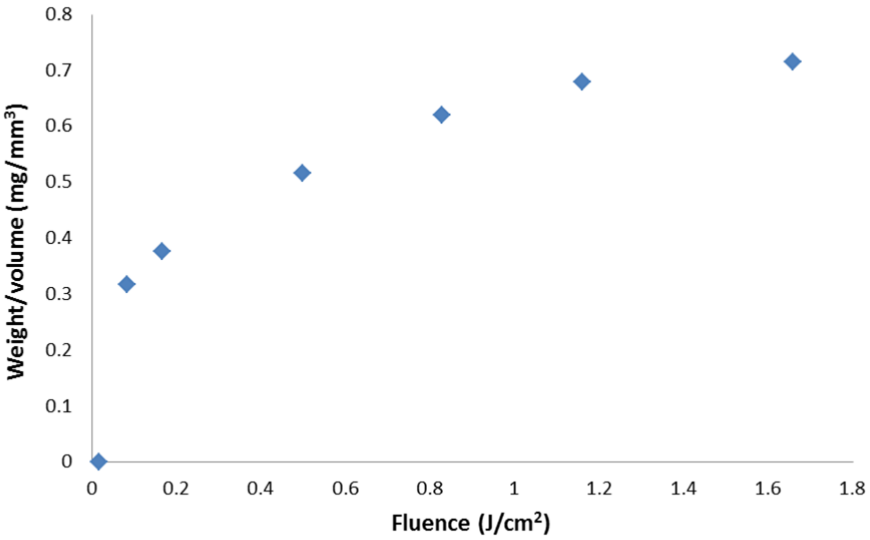

FIGURE 5.10: Plot showing the correlation between the fluence used to prepare polymer structures and their weight/volume.

5.3.3 Multiple fluid delivery using delaying barriers

Implementation of automated paper-based devices (as described by Apilux et al. and Lutz et al. [125, 126]) that are user-friendly and need minimal intervention from the patient or an unskilled user need strategies that allow control over the flow of several liquids (reagents and sample) along their pathways. Such devices allow the implementation of a multi-step assay (such as an ELISA), and in this section, using fluid delay strategies effected using the flow-barriers described earlier, we demonstrate the usefulness of our method to fabricate such automated paper-based tests. Figure 5.11 shows a device that uses a network of three identical channels for sequential delivery of three fluids to a common detection or reaction point. As shown in Figure 5.11, sequential delivery of each of these fluids is made possible by introducing (a set of three identical) porous barriers written with a c.w. laser across the fluid channels. By changing the porosity of each set of delay barriers through simple adjustments of the laser parameters, different delays can be introduced into each channel.

To show the operation of our devices, as also described earlier, we first introduced a source pad (a stack of 8 cellulose papers) into each channel that allows us to load a comparatively large volume of fluid ($\sim$40 μL) in to each channel, and also serves as a continuous reservoir of liquid (Figure 5.11). We first tested the performance of our devices using TBS as the test-fluid which was introduced into the source pad in each of the three channels. Figure 5.11a is a set of images that are snapshots taken sequentially at different times after introducing the TBS into the source pads. The fluid in channel 2 (that does not have any delay barriers) arrived at the intersection zone first (after 5 min) and continued to flow onwards until the fluid in channel 3 (with weaker delay barrier) arrived at the intersection (after 10 min). Thereafter, the fluids from these two channels mixed and flowed forward until the arrival of the fluid from the third channel (with the stronger delay barriers) after 20 minutes. Finally, the mixture of three fluids then wicks through the reaction pathway in the following 10 minutes.

To further illustrate the dynamics related to the mixing of the different fluids and to make the concept of flow delay more obvious, we instead used three different coloured inks to source the three separate channels (black for channel 1 and 3 and red for channel 2). The sequential images that show the flow through the device are shown in Figure 5.11b. When compared to the (blank) channel 2 that did not have any delay barriers, the fluid delivery through channel 1 and channel 3 were delayed by 15 and 5 minutes respectively. The results for both of the devices that were either tested using TBS or the coloured inks show clear evidence that our laser-patterned delayed-fluid flow strategy can be used to make paper-based automated devices. As a final step, we demonstrate the use of this strategy to fabricate devices that can implement multi-step ELISA protocols.

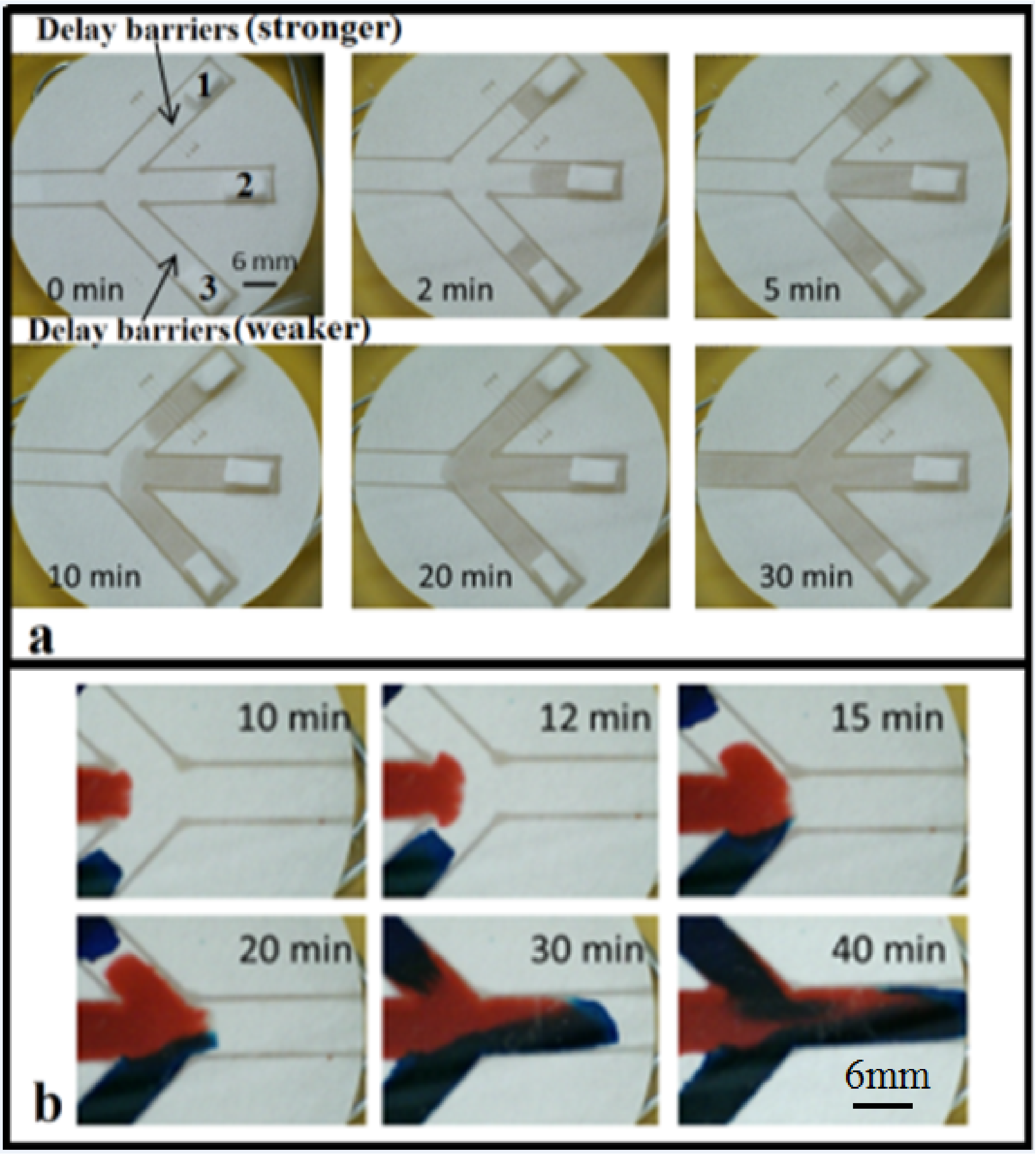

Figure 5.11: Image showing a 2D multi-channel fluidic device used for sequential delivery of three fluids. It has three identical channels (6 mm width and 23 mm length) modified with different delay barriers (1.Stronger delay barriers; 2. No barriers; 3.weaker delay barriers). (a) Sequential images showing the arrival of BSA from each channel at different times; (b) Sequential images showing the arrival and mixing of black and red ink from three separated channel and the subsequent mixing of the inks.

5.3.4 Automated multistep assay for CRP detection by sandwich ELISA

This section describes the use of our fluid delay strategy to implement a multiple step ELISA that enables the detection of CRP (C-reactive protein). We have chosen CRP as an example for evaluating this automated paper-based device because it is an important and realistic analyte which is frequently measured for early-stage diagnosis. Devices (with the 2D multi-channel geometries) identical to that shown in Figure 5.11 were used to realise a multistep enzyme-based immunoassay that allowed for the detection of CRP. As shown in Figure 5.12a, the three individual arms of the device were used to sequentially deliver the three different reagents - channel 1 delivered streptavidin-HRP; channel 2 delivered the sample; channel 3 delivered the detection antibody through to the capture antibody which was immobilized in the detection zone (identified in the image with a rectangular frame). As mentioned earlier, the device geometry and the delay mechanism used were the same as those in Figure 5.11, except that an additional cellulose absorbent pad was attached at the end of the detection pathway for collection of the excess fluid.

The ELISA kit used in the implementation of the CRP detection (DuoSet Human C-Reactive Protein/CRP) was purchased from R&D Systems, Inc. (UK). All the antibodies used were from this kit and were diluted to the working concentrations of 3.6 μg/mL and 162 ng/mL for capture antibody and conjugated antibody respectively. The CRP human standard (C1617) was purchased from Sigma-Aldrich (UK) and diluted to working concentrations using calibrator diluent (1% BSA in PBS).

The capture antibody was pipetted at four distinct spots within the detection zone, and then left to dry for one hour at room temperature. The whole device was then immersed in a blocking solution (5% BSA in PBS) for one hour at room temperature, followed by three sequential washing steps using PBS. After subsequent drying, the device was ready to use.

In order to implement the assay, 40 μL of each reagent was simultaneously pipetted onto the source pads in each channel and the device was left in a covered petri dish at room temperature to allow for the timed, sequential delivery of the individual solutions along each channel, into the detection zone for reaction with the capture antibodies immobilized therein. After 30 minutes, the whole device was washed three times using PBS for five minutes each. Finally, the colorimetric substrate TMB (Tetramethylbenzidine) was added at the reaction zone and the result was read after 20 minutes. Ideally, such a device should also enable the sequential delivery of TMB to the detection zone via another fluid flow channel, and that would then be a true example of a sample-in-result-out type device, however, for this initial proof-of-principle experiment where we intend to show the usefulness of delays, we have not yet manufactured such a test. In the case of several routinely employed assays, the detection antibodies are tagged either with a gold nanoparticle or coloured beads, and if we choose to use detection antibodies labelled in this fashion, then there would not be the need to have this additional delivery path.

Figures 5.12b and 5.12c show the results for the detection of different concentrations of CRP, and the clearly visible and distinct four blue spots that appear in the detection zone (with minimal background colour noise) confirm the presence of CPR in the sample. Figure 5.12d shows the result for a control device tested with a sample solution that did not have CRP. As shown in the figure, for this negative result, we do not observe any specific blue spots in the detection zone. The colour intensity of the spots in Figure 5.12b is greater than that in Figure 5.12c, and this relates to the higher concentration of CRP in the corresponding samples that were used in the two different cases. For some of the spots, their non-symmetric circular shape is as a result of the spotting of the capture antibodies more towards one edge of the channel walls, resulting in a clipping of their circular shape. The images in Figure 5.12b and 5.12c clearly demonstrate the successful detection of CRP on our laser-patterned paper-based device with incorporated fluid delay mechanisms. This device is an example of a semi-automatic type test that still requires intervention from a user, but we are planning on developing this concept further in the immediate future to enable a fully-automated device which would then be a true example of a sample-in-result-out type device. In addition, using our devices, we were also able to detect CRP with concentrations of less than ∼10 ng/mL, which we believe is close to the limit of detection.

5.4 Conclusions

In this work, we report a new method based on our LDW technique that allows the fabrication of pre-programmed or timed fluid delivery in paper-based fluidic devices without any additional equipment or minimal actions from the user. Barriers, aligned perpendicular to the flow-path, and used to control the fluid flow in a channel were either solid barriers with differing depths, or barriers with differing porosity, and these could be fabricated by simple adjustments of the laser patterning parameters, such as the laser power and the writing speed. Both types of barriers yield similar results for control over the fluid flow. These programmable fluid delay techniques should help to further improve the functionalities of paper-based microfluidic devices as such control can be used to enable semi-automated multi-step fluidic protocols. In contrast to other methods reported for controlling fluidic transport, our approach eliminates the requirements for cleanroom-based steps, or custom-designed equipment, or the need for long flow paths,

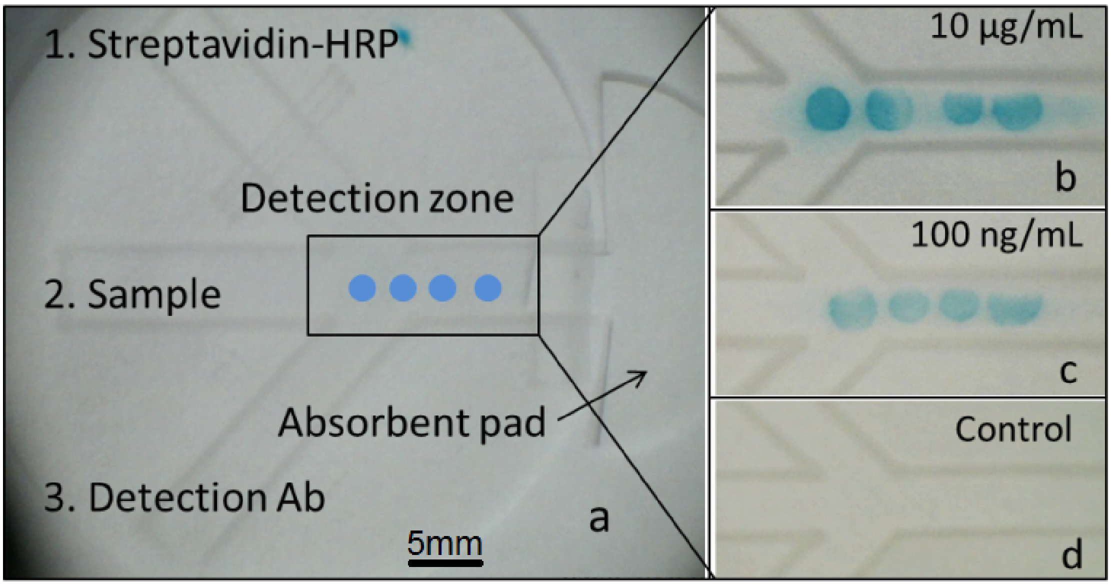

Figure 5.12: Automated multi-step ELISA for CRP detection in a 2D multi-channel fluidic device. (a) Image of a device showing its design and indicating reagent locations for the assay. Four blue spots, shown schematically in (a), represent the position of immobilized capture antibody in the detection zone. (b), (c) and (d) are photos of the CRP ELISA result on the device for different sample concentrations of 10 μg/mL, 100 ng/mL and no sample respectively.

which can then translate into requirements for larger analyte volumes. Most importantly, since the delay-mechanism can be an integral part of the fabrication of the fluidic devices themselves, we believe this integrated process presents a considerable manufacturing and hence commercial advantage. Above all, we believe that this method could be an ideal choice for rapid fabrication of custom-designed paper-based microfluidic devices for realizing single or multistep analytical tests.

Chapter 6

Rapid and mask-less laser-processing technique for the fabrication of microstructures in polydimethylsiloxane

6.1 Introduction

The general idea and target of the work described in this thesis, as can also be seen in the previous chapters, was the utilisation of laser direct-write techniques for the fabrication of devices with biomedical applications. In a similar vein, the following chapter shows the results of our work on developing a novel technique for the creation of micro-contact printing (μCP) devices.

More precisely, we report a rapid laser-based method for structuring polydimethylsiloxane (PDMS) on the micron-scale. The novelty of this method is that it is mask-less as it uses a digital micro-mirror device (DMD) (Fig. 6.1) to create arbitrarily shaped structures via either ablation or multi-photon photo-polymerisation in a master substrate, which is subsequently used to cast the complementary patterns in PDMS. This patterned PDMS mould was then used for micro-contact printing of ink and biological molecules.

A range of methods such as wet chemical etching, reactive-ion etching [138, 139], light induced patterning [140], decal transfer microlithography [141], the bond-detach method [142], and print-and-peel [143] approaches (such as photo-copying [139] and solid-object printing [144, 145]) have been utilised for creating patterns in PDMS through the use

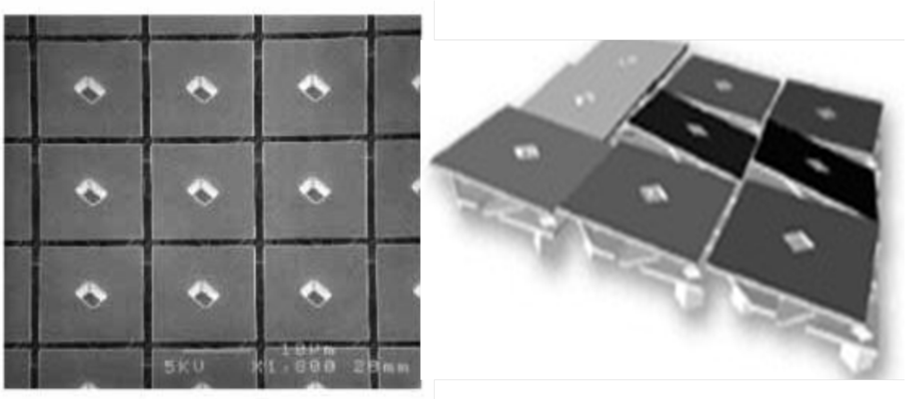

Figure 6.1: Photographs showing micromirrors of a DMD.

of a master. However, one of the most commonly used approaches for the structuring of PDMS for such applications is through the creation of a pattern in either a photoresist (SU8), or in a film of SiO_2 or Si_3N_4 or metal on a Si or SiO_2 substrate to produce a master mould that is used to cast the PDMS [146, 147]. This more often than not involves the use of a clean-room based UV-lithographic procedure that utilizes custom-designed masks for the creation of a master-mould. The structures that are formed in the master are then duplicated by casting PDMS on it to produce a secondary-mould of PDMS which is then used for end applications in micro-contact printing or, by itself as a fluidic substrate.

Even though this lithographic procedure can routinely produce high-resolution micron-scale structures, the procedure, by its very nature, is both expensive and time-consuming. Instead, in this chapter, we demonstrate, for the production of the master and hence the secondary PDMS-mould, a rapid and flexible alternative to the expensive UV-lithographic procedure. The method described here is a mask-less laser-based direct-write procedure that does not rely on cleanroom access, but can rather be done in a traditional laboratory setting. As in soft-lithography, the creation of the PDMS-mould via the mask-less approach shown here, occurs in two steps, and allows the creation of high-quality micron to millimetre-scale features in PDMS. The process is generic, and the mould material is not limited to PDMS, but can also be used to create structures in a wide range of other materials, with the added advantage of being able to fabricate complex and differently-shaped structures adjacent to one another, in a single laser patterning step. Furthermore, through a simple step-and-repeat procedure it is then possible to stitch together a 2D array of complex patterns over a larger area of several cm^2.

This laser-based direct-write method uses a DMD as an intensity spatial light modulator in order to produce a user-defined laser light pattern for the creation of the complex structures. The master-mould with user-defined pattern was created by either laser-ablation or multiphoton polymerisation [148–151], which are commonly employed laser-based techniques extensively used in materials patterning. Patterns that are complementary to the two-dimensional surface relief patterns created in the master-mould were then produced in a PDMS mould. To demonstrate the applicability of this laser-based procedure, we also present the results from the use of a laser-patterned PDMS mould for micro-contact printing of ink and fluorescently-tagged biomolecules. Part of of the work presented in this chapter has been published in [98, 152–154].

6.2 Micro-contact printing

Soft lithography is a technique complementary to photolithography. Whereas photolithography was mainly developed and adapted to fabricate semiconductors in the microelectronics industry, soft lithography extends its possibilities as it can process a wide range of elastomeric and mechanically soft materials. Materials such as polymers, gels and organic monolayers can be used with soft lithography, although PDMS has been the material of choice due to its inherently useful properties such as low cost, biocompatibility and low toxicity, chemical inertness, as well as mechanical flexibility and durability. Soft lithography is not a single fabrication technique, but rather a collection of fabrication methods based on using patterned PDMS.

Microcontact printing is a form of soft lithography that uses the relief patterns on a master PDMS stamp to form patterns of molecular ink on the surface of a substrate through conformal contact (Fig. 6.2). In this case, the patterned PDMS is used as a stamp. The side of the PDMS that has the patterned features is first immersed in the ink and then brought into contact with a substrate in order to transfer the ink onto the substrate surface. Therefore, only the ink from the raised features of the PDMS mask will be transferred.

Creation of the master is done using traditional photolithography techniques as seen in Fig. 6.3. The master is typically created on silicon, but can be done on any solid surface. Photoresist is applied to the surface and patterned by a photomask and UV light. The master is then baked, developed and cleaned before use. In typical processes the photoresist is usually kept on the Si wafer to be used as a topographic master template for the stamp. However, the unprotected silicon regions can be etched, and the photoresist stripped, which would leave behind a patterned wafer for creating the stamp. This method is more complex but creates a more stable template.

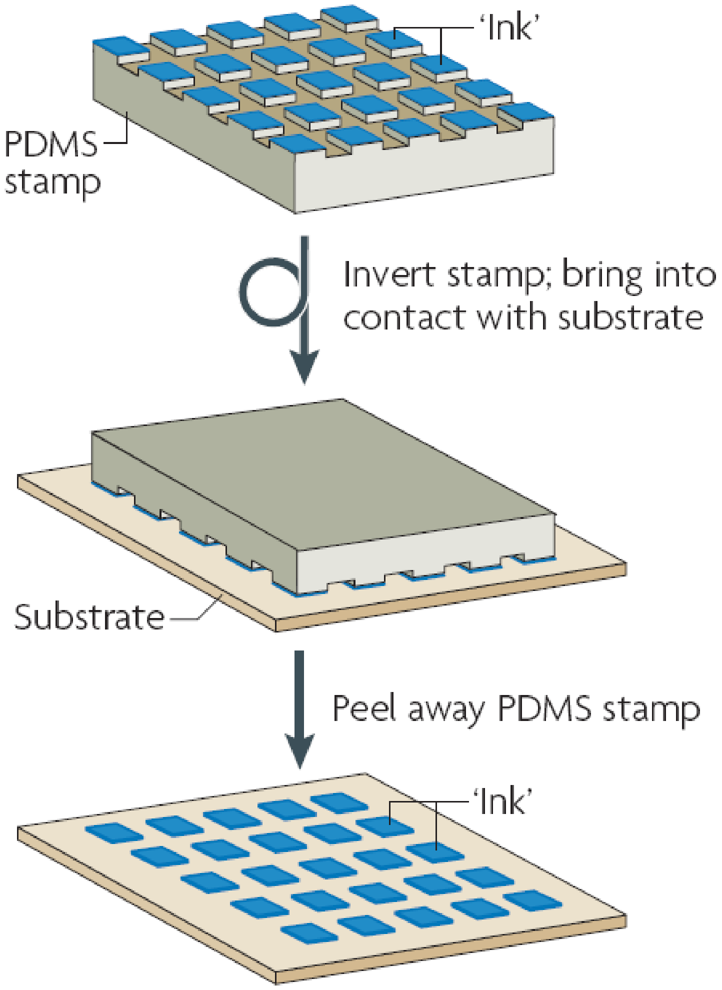

Figure 6.2: Schematic showing the micro-contact printing technique (From [155]).

After fabrication, the master is placed in a walled container, typically a petri dish, and the PDMS mixture is poured over the master. The PDMS mixture, in most applications, is a 10:1 ratio of silicone elastomer and a curing agent. This mixture consists of a short hydrosilane crosslinker that contains a catalyst made from a platinum complex. After pouring, the PDMS is cured at elevated temperatures to create a solid polymer with elastomeric properties. The stamp is then peeled off and cut to the proper size. The stamp replicates the complementary features of the master: elevated regions of the stamp correspond to indented regions of the master and vice versa.

Inking of the stamp occurs through the application of a solution to it, either by immersion or by coating of the stamp. The highly hydrophobic PDMS allows the ink to be diffused into the bulk of the stamp, which means the solution stays not only on the surface, but also inside the stamp material. This diffusion into the bulk creates an ink reservoir which allows the stamp to be used for multiple prints before having to re-ink it. The

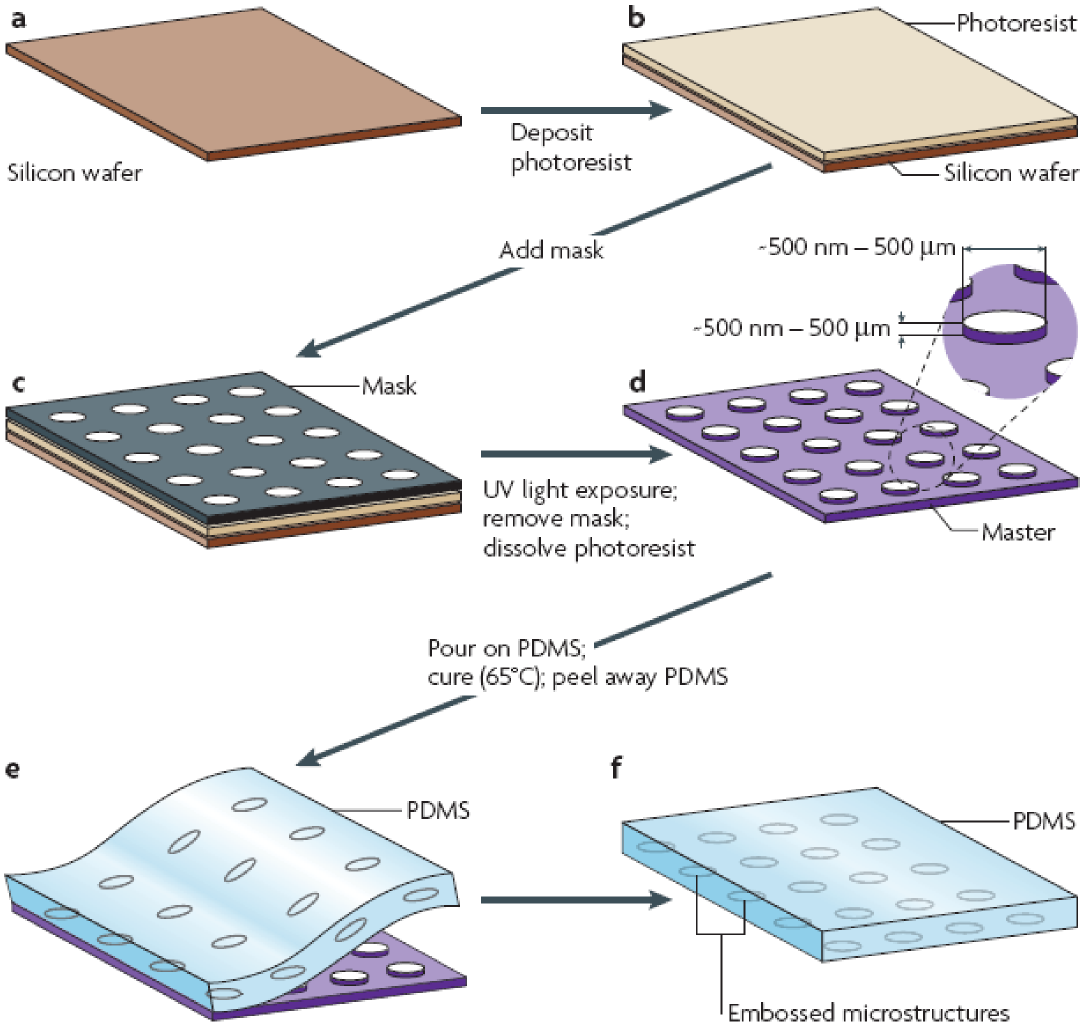

FIGURE 6.3: Schematic showing the traditional fabrication technique of the master and mould for micro-contact printing (From [155]).

stamp is left to dry until no liquid is visible on the surface and an ink reservoir is thereby created. The stamp is then ready for contact printing.

The application of the stamp to the substrate is easy and straightforward which is one of the main advantages of this process. The stamp is brought into physical contact with the substrate and the solution is thus transferred to the substrate. The solution is therefore area-selectively transferred to the surface based on the features of the stamp. Printing can also take place on a planar surface by using a rolling stamp and can even happen on curved surfaces, as the stamp is flexible.

Microcontact printing has several advantages which makes it a good candidate for patterning surfaces. It is very simple and easy to create patterns with micron-scaled features, stamping can be done in a normal laboratory instead of a cleanroom, the same master can be used to create multiple stamps and individual stamps can be used many times with minimal degradation.

6.2.1 PDMS

PDMS finds widespread use as the platform for the fabrication of microfluidics-based LOC devices [146, 156]. It is also a material of choice in micro-contact printing for the creation of a mould that is then repeatedly used for stamping an array of specifically desired biological molecules [147, 157]. The popularity of PDMS in such biological applications stems from some of its distinctive characteristics which include biocompatibility, elasticity (which allows it to be flexibly moulded into the desired shape and be released from a rigid and complex 3D master mould), optical transparency down to ∼230 nm, chemical and thermal stability, isotropic nature, homogeneity, durability and low-cost [146, 147, 156]. These characteristics lead to its selection as a material of choice for microfluidics-based LOC devices and applications in micro-contact printing. However, its ability to be moulded or structured is the key advantage, as this allows the formation of embedded structures, such as fluidic channels, and surface relief structures, such as upstanding blocks or pillars.

There are, though, several limitations in using PDMS as a μCP stamp. It is highly hydrophobic which does not allow polar inks to be used, while proteins tend to denature on such hydrophobic surfaces [158]. Hydrophobic surfaces also require longer inking times to create homogenous films on the substrate. Another drawback is its mechanical stability, which leads to stamp deformation during removal from the master and during the printing on the surface, thus limiting the resolution of the features. The aspect ratio of the features influences the deformation of the features: if the aspect ratio is high, buckling and lateral collapse is possible (Fig. 6.4a), and if the aspect ratio is low, roof collapse may occur causing contact between the stamp and the substrate in regions where it is not desirable (Fig. 6.4b). Moreover, diffusion along the surface and through the gaps between the features reduces the resolution significantly and produces background noise (Fig. 6.4c) [159]. Finally, although many chemicals do not react with PDMS as it is relatively inert, most organic solvents induce swelling, making it unusable as the dimensions of the features are changed.

6.2.2 Applications of micro-contact printing

The micro-contact printing technique has many different applications including in microelectronics, surface chemistry and cell biology, depending on the type of ink and substrate used [160].

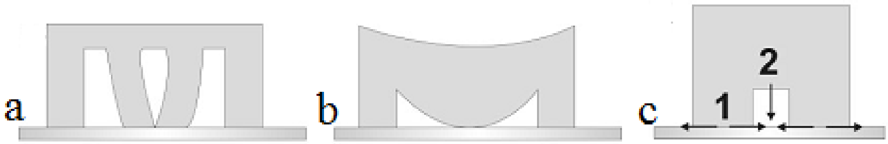

FIGURE 6.4: Pattern resolution on a PDMS stamp can be limited by (a) buckling, (b) roof collapse and (c) diffusion phenomena.

Microcontact printing has also applications in micromachining [161] with inking solutions commonly consisting of a solution of alkanethiol. This method uses metal substrates with the most common metal being gold. However, silver, copper, and palladium have been proven to work as well. Once the ink has been applied to the substrate the printed layer acts as a resist to common wet etching techniques allowing for the creation of high resolution patterns. Because of the microcontact printing technique, no traditional photolithography is needed to accomplish these steps.

The patterning of proteins has helped the advancement of biosensors [162], cell biology research [163], and tissue engineering [164]. Various proteins have been proven to be suitable inks and are applied to different substrates using the microcontact printing technique. Polylysine, immunoglobulin antibodies, and different enzymes have been successfully placed onto surfaces including glass, polystyrene, and hydrophobic silicon. Microcontact printing has also been used to advance the understanding of how cells interact with substrates. This technique has helped improve the study of cell patterning that was not possible with traditional cell culture techniques. Successful patterning of DNA has also been done using this technique [165]. The reduction in time and DNA material, as well as the reusability of the stamp, are the critical advantages provided by this technique.

6.3 Experimental setup and methods

Figure 6.5 shows a schematic of the laser-based patterning set-up used for this work. The laser used was a Ti:sapphire ultrafast amplifier (Coherent Legend-F, seeded by a Coherent Mira-900 oscillator), with a central wavelength of 800 nm, pulse length of 150 fs, repetition rate of 1 kHz, and a pulse energy of ~2 mJ. Patterning was effected by reflecting the laser light from a digital micro-mirror device, which is a pixelated programmable mirror array. DMDs are widely used in video projectors, and can operate in the visible and near-infrared spectrum, have fast switching speed of up to 32 kHz, and they are quite inexpensive (a few 100 GBP). The DMD used in these experiments was from Texas Instruments (DLP3000), had an array of 608 × 684 mirrors, each of width ~7.6 μm and horizontal and vertical centre-to-centre distances of ~10.8 μm.Each mirror in the array was individually programmed to either turn on or off (by loading a static black and white bitmap onto the DMD), corresponding to a change in the angular deviation of the mirrors on their supporting-hinge by an angle of either +12° or -12° with respect to the surface of the device. This pattern was then used for subsequent laser machining of the sample, at a typical fluence of ~1.7 J/cm^2.

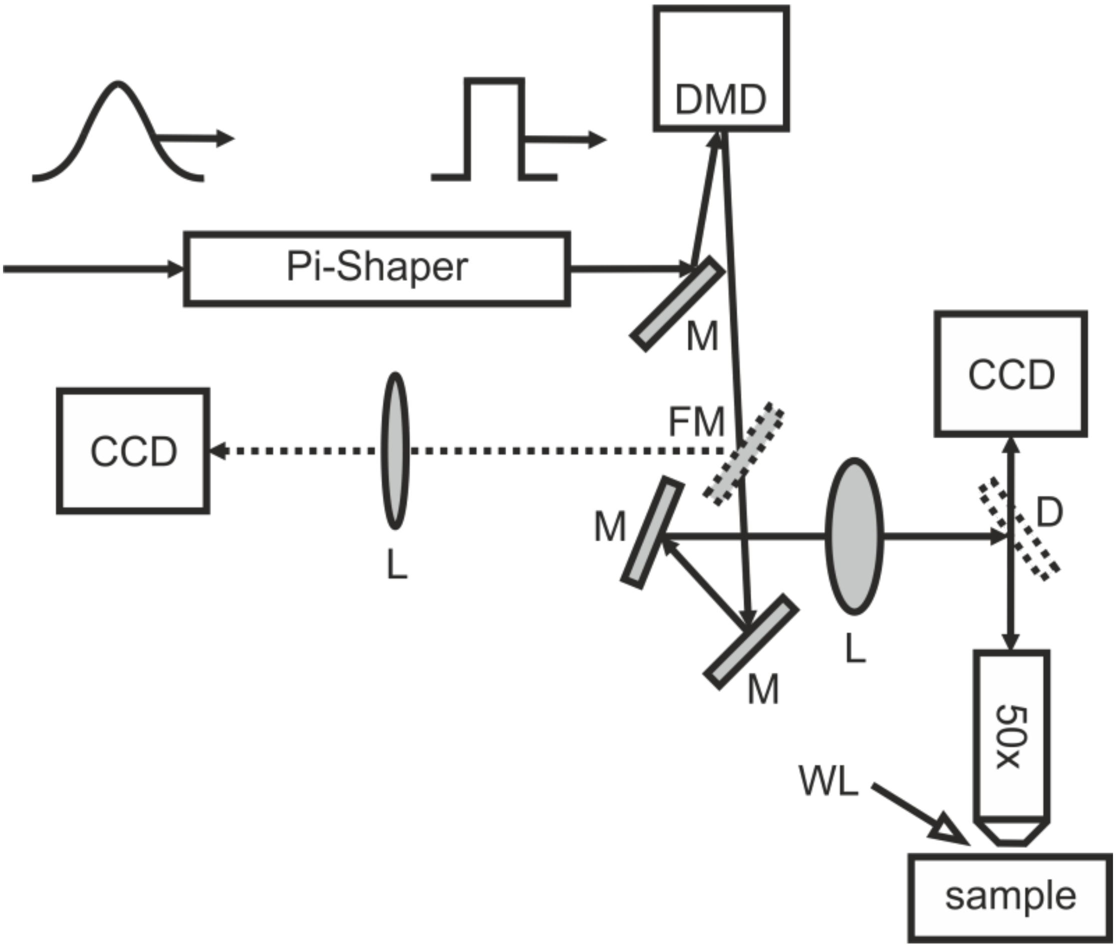

Figure 6.5: Schematic of the DMD-based laser patterning set-up.

In order to ensure illumination of the DMD by a uniform light intensity pattern, the Gaussian spatial beam profile of the laser was homogenised and transformed into a top-hat intensity profile using a refractive element (π-shaper, model 6_6, from www.pishaper.com). As shown in Fig. 6.5, using appropriate relay optics (mirrors M, flip mirrors FM, lenses L, dielectric mirror D) and imaging optics (a 50× objective, NA=0.55, Nikon) the intensity pattern immediately after the DMD was de-magnified onto the sample. A co-axial imaging setup that used a white light (WL) source and a CCD camera allowed real-time observation of the DMD-assisted laser-machining of the work-piece. The sample was mounted on a computer-controlled three-axis translation stage to allow precise positioning of the sample within the image-plane, and for stitching together an array of individually created patterns. Using this DMD-based laser-machining set-up it was possible to pattern an area of ∼30 μm × 30 μm via a single laser pulse. However, when combined with step-and-repeat techniques, at laser repetition rates of 1 kHz and single pulse energies of ∼1 mJ, it is possible to achieve a final patterned area of around 1 cm^2 (with micron-scale feature sizes) within reasonable (less than 1 hour) time scales.

In standard UV-photolithography, in addition to the time required for the fabrication of a custom-designed mask, the subsequent steps of spinning, patterning, developing, deposition or evaporation and wet-etching can be time-consuming, and will then produce only pre-specified patterns. As a direct comparison with regards to cost and time, the approach presented here is a mask-less procedure, with complete freedom over feature design, and hence the cost, availability and fabrication of designer or one-off structures compares very favourably.

In order to create a master-mould with the desired set of patterns, experiments using two distinct approaches (Fig. 6.6) namely laser-based ablation and laser-based multiphoton polymerisation have been performed.

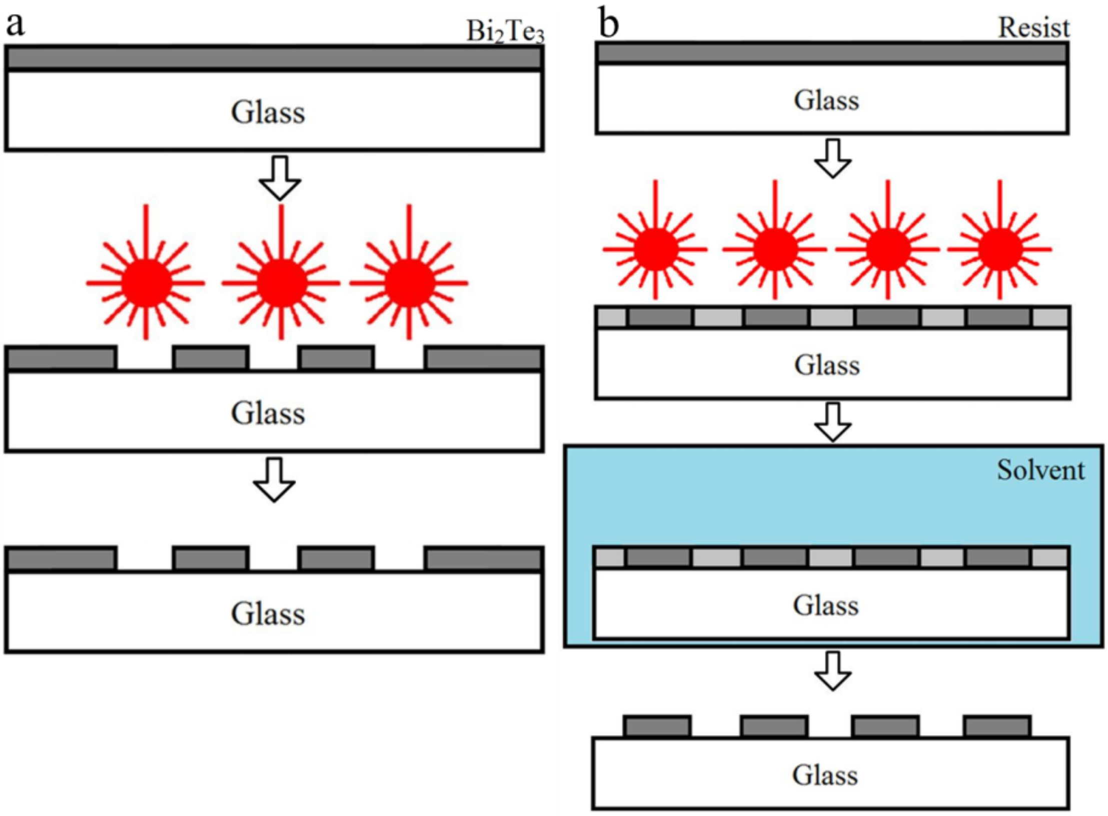

Figure 6.6: Schematic of the two DMD-based routes used to pattern a master via (a) ablation, and (b) multiphoton-polymerisation of the DMD-based laser patterning set-up.

6.4 Results and discussion

6.4.1 Laser-based ablative patterning

For the first case we chose to fabricate the master via ablation of a ~1 μm thick bismuth telluride (Bi_2Te_3) film that had been sputter-coated onto a glass substrate, although any material that can be ablated could have been used. The first set of experiments included ablation of a two-dimensional array of 10 × 10 square trenches, with each square having a dimension of 30 μm × 30 μm and a centre-to-centre separation of ~50 μm. Each square trench was ablated in the Bi_2Te_3 film using 10 sequential laser pulses with a fluence of 1.7 J/cm^2. We chose to create an array of simple square patterns so that, following PDMS casting, the secondary-mould would have the complementary square pillars which are best suited for the subsequent contact printing experiments. Also, these initial set of experiments allowed us to identify the laser conditions required for the creation of well-defined features. It was found that 10 pulses was the minimum number required to produce structures with shapes having good fidelity with the DMD-projected image pattern, good verticality and extended throughout the entire thickness of the Bi_2Te_3 film. The size of the features ablated were on the order of microns, however, using the same set-up, features with sizes of <400 nm were demonstrated [56].

To demonstrate the advantage offered by this direct-write procedure in the production of an array constituted of features with varied shapes and sizes, the second set of ablative-patterning experiments involved the ablation of different shapes (a square, a triangle and a circle) in a single step, via a different DMD pattern. The incident fluence was kept at 1.7 J/cm^2 however 100 pulses were used to ablate the pattern-set. It should be noted here that 10 pulses were actually sufficient to ablate the pattern-set but additional pulses were employed as a means to clean up any debris that might have remained on the underlying glass substrate. Multiple step-and-repeat ablations resulted in the formation of an array within ten minutes, with lateral dimensions of a few hundred microns. Fig. 6.7a shows an image of DMD-ablated BiTe film acquired using an interference-based surface profiler (ZeScope from Zemetrics). The inset in Fig. 6.7a shows the black/white bitmap pattern that was loaded onto the DMD. In this work, white regions of the bitmap correspond to the presence of laser light on the target sample, whilst black regions correspond to no laser light.

These ablated patterns were then used to form a secondary-mould in PDMS. A 10:1 mixture of a PDMS base and a curing agent was mixed thoroughly, de-gassed to remove trapped air-bubbles, and poured onto the patterned Bi_2Te_3 film. The mixture was allowed to set at 90 °C for one hour. As shown in Fig. 6.7b, this led to the creation

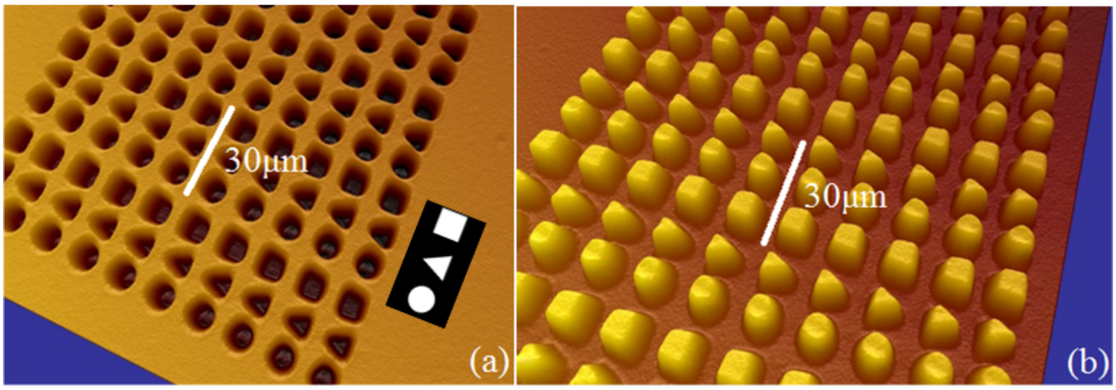

FIGURE 6.7: Image (a) shows a 2D array of 10 × 30 shapes formed in a ∼1 μm thick Bi_2Te_3 film via DMD-ablation. The black/white inset shows the bitmap loaded onto the DMD for ablation of the Bi_2Te_3 film; (b) shows a complementary 2D array of 10 × 30 shapes (circles, triangles and squares) formed in PDMS using the Bi_2Te_3 mould in figure 6.7a. Images have been taken using an interference-based surface profiler. The depths of the ablated features, and hence the corresponding heights of the upstanding PDMS structures was measured to be ∼1 μm. They however appear to be >1 μm because the images have been adapted through the profiler software for better visualisation.

of a complementary micron-scale two-dimensional pattern of upstanding structures in PDMS.

In order to show that this technique can be used for different and more complex shapes, a different image that included a star and a polygon was used as the input of the DMD. The same ablation was done on a Bi_2Te_3 film, keeping the same fluence and number of pulses as before. The results on the ablated Bi_2Te_3 film can be seen in Fig. 6.8a, along with the profile measurement of the ablated regions showing that the ablation was done through the whole film and therefore the features were ∼1 μm deep (Fig. 6.8b). This pattern was then used to create a PDMS mould which can be seen in Fig. 6.8c, along with its profile measurement that shows that the features have been clearly transferred on the mould and have the same height as in the master (Fig. 6.8d).

As the thickness of the Bi_2Te_3 film that was patterned through ablation via the DMD was of the order of ∼1 μm, the features formed in the PDMS mould also had heights of ∼1 μm, but features with greater heights can readily be formed from higher aspect ratio ablated master-moulds.

6.4.2 Laser-based photo-polymerisation

In this section, we demonstrate an additional approach that relies on DMD-based multiphoton-polymerisation for the creation of the master-mould. This approach allowed us to produce patterns with feature depths (in the master) and heights (in the

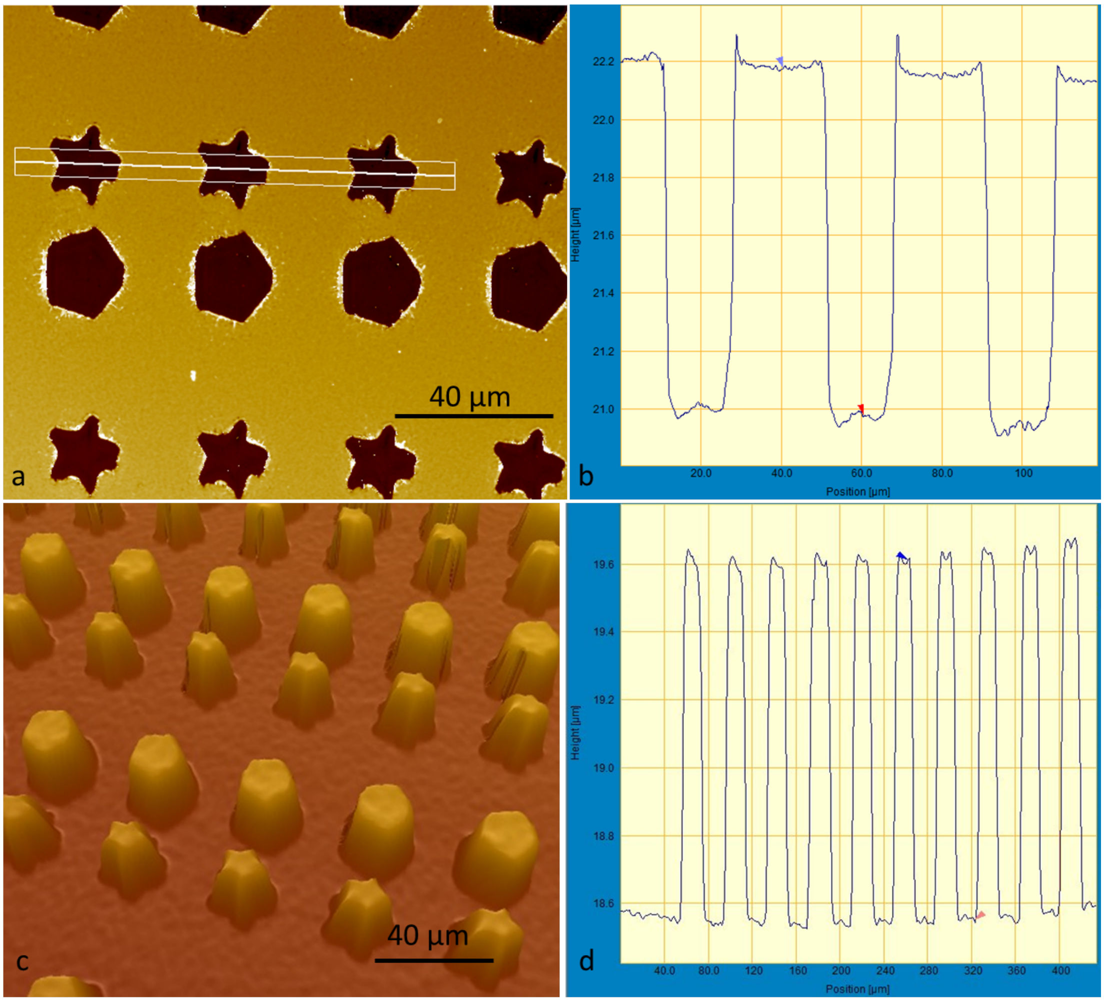

FIGURE 6.8: Image (a) shows a 2D array of shapes formed in a Bi_2Te_3 film via DMD-ablation, which acts as the master in this experiment, (b) shows the profile measurements of the master, showing ∼1 μm deep features, (c) shows the complementary 2D array formed in PDMS using the Bi_2Te_3 master in figure 6.8a, and (d) shows the profile measurements of the PDMS mould. Images have been taken using an interference-based surface profiler. The depths of the ablated features, and hence the corresponding heights of the upstanding PDMS structures was measured to be ∼1 μm. They however appear to be >1 μm because the images have been adapted through the profiler software for better visualisation.

PDMS mould) of ∼10 μm. To validate this route we first spin coated a ∼10 μm thick film of a photo-sensitive polymer (a silicon/zirconium hybrid negative resist) onto a glass substrate [166]. In order to produce a primary mould that had square holes, and hence a secondary PDMS mould that had upstanding square pillars, a DMD pattern that consisted of a square-ring/frame (as shown in the inset of Fig. 6.9c) was used, and stitched together to form an overlapping 2D array of structures. This is because unlike simple ablation wherein an imaged square would ablate and hence remove material to form a corresponding square hole, for the case of photo-polymerisation (with a negative resist), a square image pattern would result in the photo-polymerisation of the corresponding square-area which then remains insoluble during subsequent development of the photo-polymer. This would then result in the formation of upstanding square pillars in the master, contrary to what is desired. Instead, if a square frame is projected using the DMD, since light is present only in the outer square-frame, (the white area in Fig. 6.9c inset), it is only this exposed area that undergoes photo-polymerisation, and is rendered insoluble during subsequent development. This will hence result in the formation of an array of wells in the master. Fig. 6.9a shows a 2D array of wells created in the negative resist via DMD-photo-polymerisation using a square-frame pattern and Fig. 6.9b shows the 2D array of the complementary pattern formed in the secondary PDMS mould using this master. Fig. 6.9c shows the black/white bitmap image of the square frame that was projected via the DMD onto the resist for photo-polymerisation. Fig. 6.9c also shows the array of square frames that have been stitched together in the resist through a step-and-repeat illumination by the square frame pattern. The green square in the image is the fluorescence captured in real-time by the CCD camera used for the visualisation of the patterning procedure. As earlier, images shown in Fig. 6.9a and Fig. 6.9b have been acquired using an interference-based surface profiler.

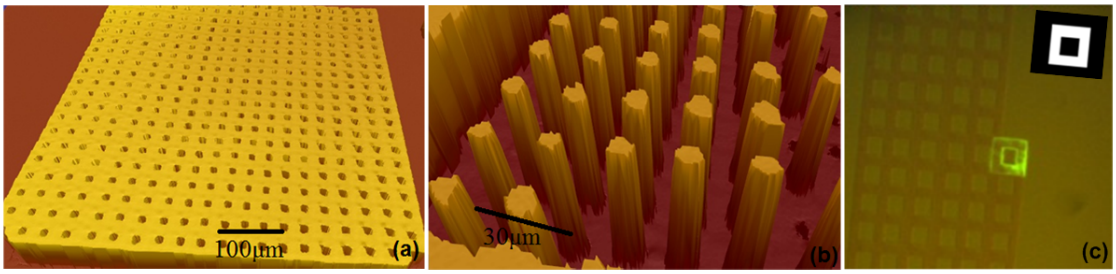

Figure 6.9: Images showing (a) a 2D array of wells formed via DMD-photo-polymerisation of a resist; (b) a 2D array of the complementary pattern formed in PDMS using the mould in (a), where both images have been taken using an interference-based surface profiler. Part (c) shows a CCD image of the step-and-repeat procedure in action, where the observed green fluorescence arises from illumination of a dye mixed in with the resist, for the purpose of alignment. The inset shows the DMD pattern that was used (white = laser light, black = no laser light). The heights of the upstanding PDMS structures in Fig. 6.9b were measured to be ~10 μm. As in Fig. 6.9b, they appear to be >10 μm because the images have been adapted through the profiler software for better visualisation.

6.5 Micro-contact printing of ink and proteins

Finally, to demonstrate the usefulness of this PDMS structuring approach for micro-contact printing, this PDMS-mould, which was composed of an array of surface-relief pillars was used to contact-print a pattern onto a glass substrate. Fig. 6.10a shows the secondary PDMS mould structured with an array of surface relief square patterns that were produced using the Bi_2Te_3 master mould formed via the DMD-based ablative route. The PDMS mask was first inked by dipping it for a few seconds in a black ink solution prepared by simple dilution in water. The inked PDMS mask was then contacted for a few tens of seconds with a glass slide by applying gentle pressure. The PDMS mask was detached and the ink pattern transferred onto the glass slide was imaged under an optical microscope. Fig. 6.10b shows the optical microscope image of the array of square ink patterns produced on the glass-slide.

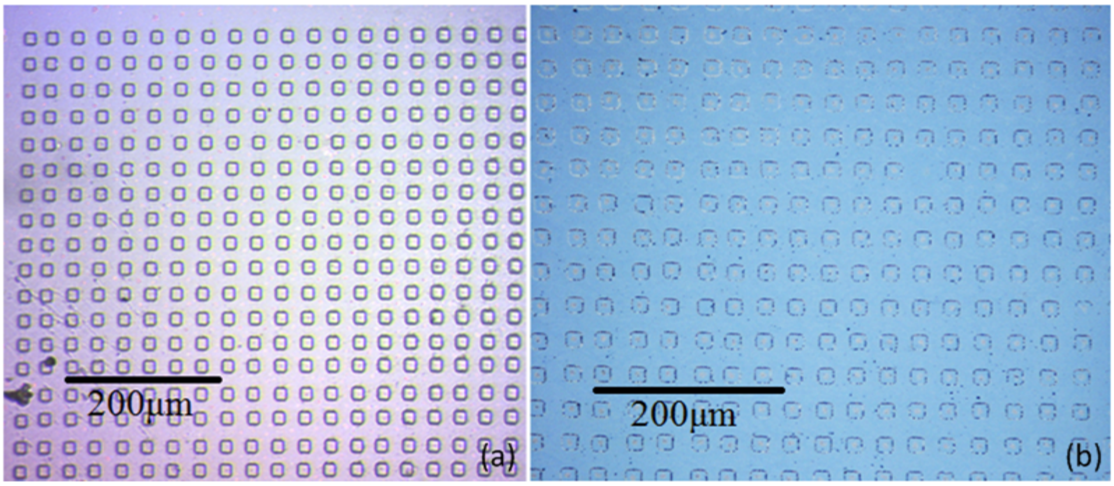

FIGURE 6.10: Images showing (a) PDMS-mask fabricated via DMD-ablation, (b) complementary ink-pattern.

Prior to the inking of the PDMS mould, to allow for adhesion of the water-based ink, it was necessary to render the PDMS surface hydrophilic, which required its treatment with oxygen (at 200 mTorr with a flow-rate of 90 sccm/min) in a plasma etcher for 20 s at 20 W. Figure 6.11 shows the contact angles of water droplets on PDMS that was treated with plasma and PDMS that was untreated. As shown here, the untreated hydrophobic PDMS had contact angles between 93° - 97°, whereas PDMS that had been treated with plasma was highly hydrophilic with contact angles between 20° - 22°, thus ensuring that the solution will diffuse faster and will cover the whole area of the stamp more easily.

In a further experiment a similar PDMS stamp was then used to contact-print an array of fluorescently-tagged biological molecules. Using a similar routine we were able to form an array of tetramethylrhodamine isothiocyanate (TRITC)-labelled Bovine Serum Albumin (BSA) on a pre-cleaned glass slide. 30 μl of a TRITC-labelled BSA solution (0.1 mg/ml) was pipetted onto the PDMS stamp. The stamp was then kept in the dark for 30 minutes for the BSA to be adsorbed onto the PDMS stamp, as the fluorescent proteins are photo-bleached after some time under normal light. Finally, the stamp was blow-dried with N_2 and pressed onto a clean glass slide for $\sim$30 s to transfer the biomaterial.

Plasma-treated PDMS	Untreated PDMS
21°	93°
20°	95°
22°	97°
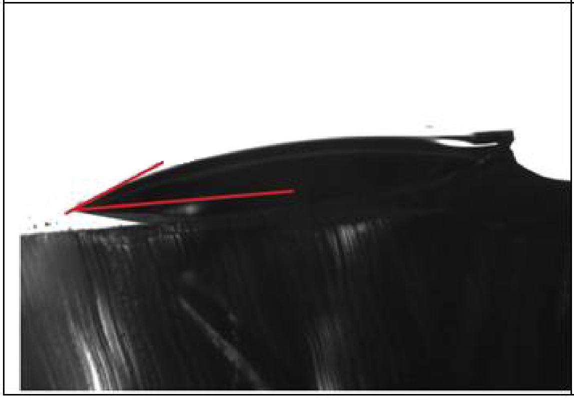	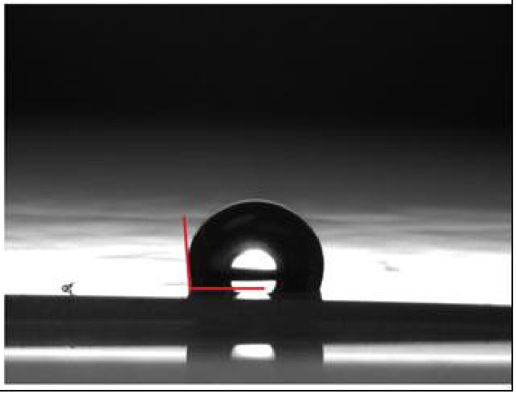

FIGURE 6.11: Contact angles of PDMS after plasma treatment and of untreated PDMS.

The contact-printed array was subsequently imaged using a fluorescent microscope. The tagged biomolecules were excited at a wavelength of 547 nm and the fluorescence at 572 nm was observed and imaged. Figure 6.12 shows an image captured using the fluorescence microscope. The white squares in Fig. 6.12 are the TRITC-labelled BSA molecules that fluoresce and hence appear white in this black and white image captured via the fluorescence microscope. This shows that it was indeed possible to successfully contact-print the fluorescently tagged biomolecules without damaging them using the PDMS-stamp (shown in Fig. 6.10a). Since the inked PDMS-stamp was pressed onto the glass slide using very slight finger-pressure, the pressure imparted through this manual procedure was non-uniform, which meant that some of the upstanding squares in the PDMS-stamp were unable to contact the glass slide and hence transfer the biomolecules. This is a common problem of μCP and there are several ways to overcome it, such as by applying pressure on the stamp using an automated actuator.

A different pattern that was prepared on a PDMS mould and looks similar to a square wave line can be seen in Fig. 6.13a. TRITC-labelled BSA proteins were added on the mould as previously described and then the mould was used as a stamp to produce the results seen in Fig. 6.13b. Again, non-uniformity was observed as the stamped pattern is brighter in certain areas, and this could be attributed partially to the stamping method. Nevertheless, the design that was patterned on the PDMS mould can be clearly seen on the glass slide.

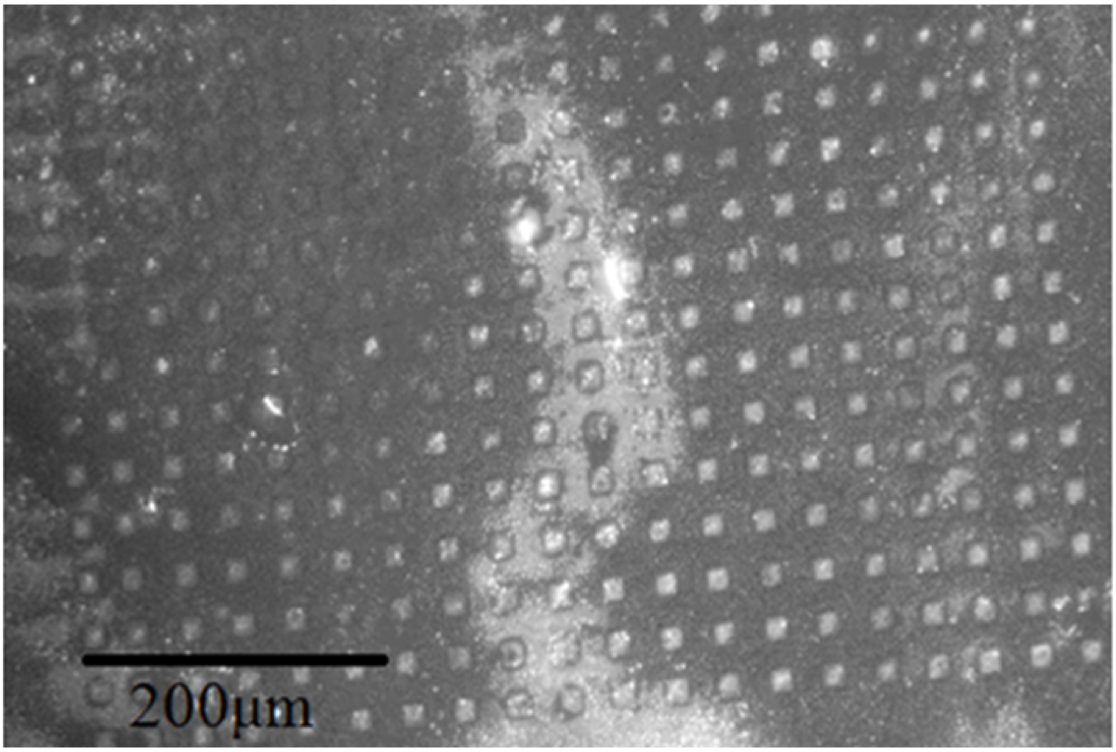

Figure 6.12: Image showing fluorescent TRITC-labelled BSA contact printed on a glass-slide using PDMS mould shown in Fig. 6.10a.

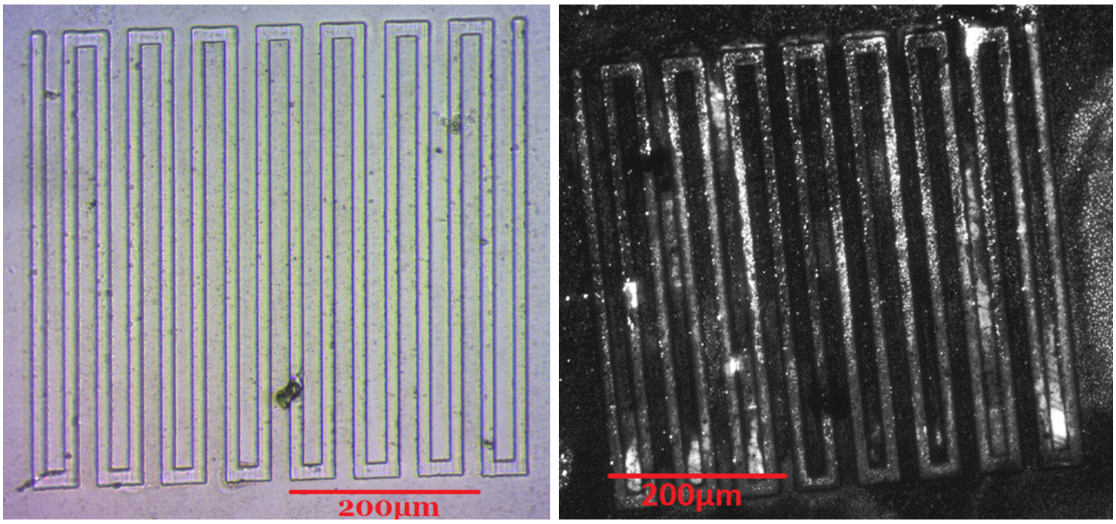

Figure 6.13: (a) Microscope image showing the surface of the PDMS mould, and (b) fluorescence microscope image showing the stamped pattern of TRITC-labelled BSA proteins on a glass slide.

6.6 Conclusions

In conclusion, in this chapter we have presented a rapid laser-based patterning procedure that employs a DMD in conjunction with a femtosecond laser. The laser-based patterning route was used for the fabrication of the master mould using two different processes. The first one was a laser-based ablative procedure and the second one was a laser-based photo-polymerisation procedure. The application for utilising these techniques was micro-contact printing for transferring biomolecules. The laser-structured master was used to cast a mould that had the inverse pattern of the features of the master. PDMS was used for the mould as it is the material of choice for μCP applications and has inherent properties that make it attractive for this type of application. The patterned PDMS mould was then used to contact print an array of a fluorescently tagged biomolecule, and microscope photos were obtained to confirm that the proteins have been correctly transferred.

We believe this laser-based approach can be extended to form complex micron-scale structures that are not only useful in contact printing applications but also in the fabrication of millimetre scale LOC fluidic devices. The flexibility that the use of the DMD provides, combined with the ease of changing the laser parameters for ablation or photopolymerisation, allow for rapid fabrication of different designs and patterns in a range of materials. It is therefore a technique that could compete with traditional photolithography processes for the fabrication of prototype devices.

Chapter 7

Conclusions and future work

7.1 Conclusions

In conclusion, the several objectives that were set have been achieved during the course of this work. Several laser-based techniques for the fabrication of POC paper-based diagnostic sensors have been researched, and the capability for the complete construction of such a device was reached.

The first target that was achieved was to show the feasibility of laser-transferring undamaged antibodies and other reagents on paper in order to manufacture paper-based medical diagnostic devices. This was demonstrated by the transfer of untagged and enzyme-linked antibodies on paper substrates that was performed using Laser Induced Forward Transfer with ns laser pulses. Several different materials were trialled as the donors that can contain and protect the antibodies during LIFT, and glycerol proved to be the most suitable option. In order to ensure the stability of the reagents that were LIFT-printed but also because the donor films used were transparent at the wavelength of the laser used, there was a need to use a thin gold Dynamic Release Layer. After the LIFT-printing process, the functionality and immunological reactivity of the LIFT-printed antibodies was confirmed by developing and demonstrating an ELISA protocol and establishing the standard calibration curves for the LIFT-printed pixels.

Additionally, it was shown that the localisation of the LIFT-printed pixels and immobilisation of the antibodies, which is a pre-requisite for paper-based diagnostic devices, was maintained throughout the wet-bench process which further justifies our use of the spatial patterning ability of LIFT. This immobilisation of the antibodies through the LIFT-printing process on the paper surface, also allowed the use of plain cellulose paper instead of the more expensive nitrocellulose membranes which should help reduce the final cost and more importantly allows for the fabrication of devices that do not need to be confined by hydrophobic barriers in fluidic channels, but can instead work in free-flow conditions. LIFT was proven to be equivalent to commercial dispensing machines (BioDot) in regards to the printed volumes of the reagents which is in the range of nl and the flexibility of the printed designs, although the current setup would not be able to compete in terms of speed. This work demonstrates that LIFT is a technique capable of transferring antibodies onto a paper substrate accurately and reproducibly, and that LIFT is a promising technology for manufacturing immunologic paper-based point-of-care diagnostic sensors.

Following the LIFT-printing experiments, we demonstrated laser-based patterning of cellulose paper for the creation of fluidic structures via photo-polymerisation. This LDW procedure is non-contact, thus it offers the advantage of minimizing cross-contamination that could arise during fabrication, it is non-lithographic and mask-less and we have shown its utility in the fabrication of diagnostic tests for protein and glucose detection. The width of the walls/barriers and the width of the channels are at the level of $\sim$100 μm, the smallest that have been reported so far in the literature, which will allow for miniaturisation of the diagnostic sensors, and therefore a corresponding minimal use of reagents. The process is ideal for rapid prototyping at preliminary trial-device fabrication stages and also for final device optimisation. Since the laser powers used are relatively low, the laser required for the process is relatively inexpensive. This means that the infrastructure required for this technique is not expensive and even several lasers could be used in parallel to speed up the process considerably and increase the production volumes. We believe that this technique is therefore ideal for use in mass-manufacturing of paper-based medical diagnostics.

Additionaly, we demonstrated that this laser-based direct-write technique based on the principle of light-induced polymerisation can be used for the rapid fabrication of fluidic structures in nitrocellulose membranes. Compared with other methods used in the production of microfluidic devices in nitrocellulose, the technique is also well-suited for up-scaling to mass-production. We have shown that using this method it is possible to create microfluidic channels and barrier-walls with dimensions of $\sim$100 μm and $\sim$60 μm respectively, the smallest values that have been reported so far in the literature. We believe that this technique could be an ideal choice for rapid fabrication and mass-production of nitrocellulose-based microfluidic devices that can be used for a variety of applications such as clinical diagnostics and analytical chemistry.

Furthermore, to strengthen the case that these devices can be actually used for medical diagnostics, we showed that they can be used for different detection tests, either single-step in the case of BSA, glucose and nitrite detection, or multi-step in the case of CRP detection. More importantly, we have demonstrated that these devices can be used for the detection of CRP in human bodily fluid samples, whether these were spiked, healthy or with elevated levels due to a condition of the subjects. There are also several advantages of using a laser-patterned paper-based device for these assays. Most important is the fact that the reagents and sample volumes used are only 2 μl per square well which is much lower than the usual 100-200 μl used in a standard ELISA test. This cuts down on the cost of the assay considerably, as reagents are typically very expensive. Another significant advantage is the reduction of the time required to perform this assay. After the incubation of the capture antibody on the paper device, the assays presented here require about 3 hours in total to complete, compared to 6 or more hours required for a standard ELISA test. Additionaly, the cost of the paper device is incremental compared to the cost of the plastic multi-well plate commonly used in ELISA tests. Finally, the whole footprint of the device is greatly reduced, allowing for easier and cheaper transportation.

As a continuation of the paper-patterning experiments, we reported on a new method based on our LDW technique that allows the fabrication of pre-programmed or timed fluid delivery in paper-based fluidic devices without any additional equipment or minimal actions from the user. Barriers, aligned perpendicular to the flow-path, and used to control the fluid flow in a channel were either solid barriers with differing depths, or barriers with differing porosity, and these could be fabricated by simple adjustments of the laser patterning parameters, such as the laser power and the writing speed. Both types of barriers yield similar results for control over the fluid flow. These programmable fluid delay techniques should help to further improve the functionalities of paper-based microfluidic devices as such control can be used to enable semi-automated multi-step fluidic protocols. In contrast to other methods reported for controlling fluidic transport, our approach eliminates the requirements for cleanroom-based steps, or custom-designed equipment, or the need for long flow paths, which can then translate into requirements for larger analyte volumes. Most importantly, since the delay-mechanism can be an integral part of the fabrication of the fluidic devices themselves, we believe this integrated process presents a considerable manufacturing and hence commercial advantage. Above all, we believe that this method could be an ideal choice for rapid fabrication of custom-designed paper-based microfluidic devices for realizing single or multistep analytical tests.

Finally, we have also presented a rapid laser-based patterning procedure that employs a DMD in conjunction with a femtosecond laser. The laser-based patterning route was used for the fabrication of the master mould using two different processes. The first one was a laser-based ablative procedure and the second one was a laser-based photopolymerisation procedure. The application for utilising these techniques was microcontact printing for transferring biomolecules. The laser-structured master was used to cast a mould that had the inverse pattern of the features of the master. PDMS was used for the mould as it is the material of choice for μCP applications and has inherent properties that make it attractive for this type of applications. The patterned PDMS mould was then used to contact print an array of fluorescently tagged biomolecules, and microscope photos were obtained to confirm that the proteins have been correctly transferred.

We believe this laser-based approach can be extended to form complex micron-scale structures that are not only useful in contact printing applications but also in the fabrication of millimetre scale LOC fluidic devices. The flexibility that the use of the DMD provides, combined with the ease of changing the laser parameters for ablation or photopolymerisation, allow for rapid fabrication of different designs and patterns in a wide range of materials. It is therefore a technique that could compete with the traditional photolithography processes for the fabrication of prototype devices.

Overall, it was demonstrated that laser direct-write techniques are excellent in the fabrication of medical diagnostic devices. They can be especially useful in creating novel POC paper-based diagnostics. It is believed that by employing these techniques, the field can benefit substantially. As a consequence, healthcare could be revolutionalised, both in developed and developing areas of the world. Affordable, robust and abundantly available, paper-based medical diagnostics have a huge impact on society, and the aim of this work had been to move the field a small step forward.

7.2 Future work

We believe the technology described in the previous chapters has great potential in the manufacturing of POC medical diagnostics. Although a great amount of work has been invested in optimising and testing the laser-based techniques, there is still room for improvements and innovations in this field. Therefore, we have already identified several key points that we believe could unlock the potential of our manufacturing techniques.

First of all, there is a huge range of materials and lasers that could be used with our technique. For example, several different polymers have already been tested, but we believe that by using specialised polymers would allow for easier, faster and more cost-effective manufacturing.

Second, we have shown that our devices have great capabilities in multiplexed diagnostics and that they could also improve the sensitivity of detection. So far we have targeted specific analytes to show the proof of principle, but our techniques could be implemented for the detection of real-world conditions and diseases, many of which require multi-analyte diagnosis. An example of such a device that can perform multiplexed diagnosis can be seen in Fig. 7.1. There are already collaborations in place for researching, manufacturing and trialling these paper-based devices for diagnosis of tuberculosis among other diseases. Another area that urgently requires rapid multi-analyte testing is bacteriology, especially since the growing resistance of bacteria to antibiotics is a major health problem. We believe that our laser-based techniques could produce devices that will help doctors quickly provide their patients with the correct treatment and reduce the unnecessary antimicrobial prescriptions.

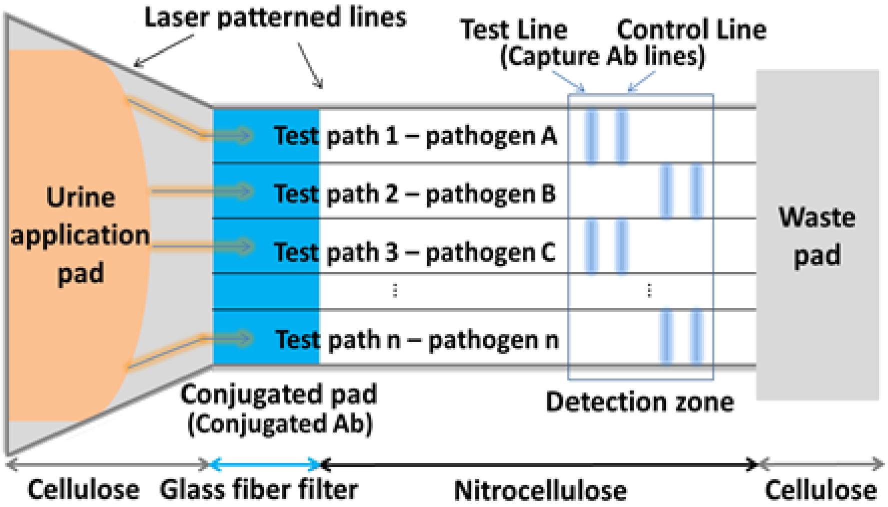

FIGURE 7.1: Schematic of a lateral flow device that can perform multi-analyte diagnosis.

Third, our technique's inherent versatility allows for the fabrication of advanced features on paper-based devices. So, another aspect of future work on this subject would be to further investigate channel multiplexing, controllable flow, time-gated mixing and forward-biased flow concepts. All of these advanced features would give greater functionalities to paper-based devices, enabling novel techniques to be introduced to POC diagnostics.

Finally, there are several innovative ideas that have been introduced during the course of this work, and further exploration is required. Laser structuring of fabrics could lead to 'smart plasters' or wearable continuous monitoring and diagnostics. Guiding or routing light through laser-polymerised tracks on paper or fabrics could open new ways of high-sensitivity diagnostics. 'Smart' polymers can be sensitive to a number of different stimuli, such as temperature, intensity of light, pH, electrical or magnetic fields, and they can respond in different ways. Introducing such materials to paper-based devices could allow for novel ways of analyte detection and manipulation of solutions in the device. One prime example is the ability of an azopolymer to act as a photoswitch, an ability that could be exploited to create light-sensitive switch-barriers that will allow or prevent the flow of fluids on demand.

Appendix A

Assay protocols

A.1 Assay for the detection of BSA

1. Add 250 mM citrate buffer at 1.8 pH and allow paper to dry for at least 1 hour.

2. Add 3.3 mM TBPB in 95% ethanol solution and allow paper to dry for at least 1 hour.

3. Add solutions of various BSA concentrations and incubate for 10 minutes.

4. Capture photographs of the test to determine the concentration of BSA.

A.2 Assay for glucose detection

1. Add the glucose oxidase / peroxidase solution (5:1 ratio and 15 units of protein per ml of solution) on the paper and allow to dry for at least 1 hour.

2. Add solutions of D-glucose in de-ionised water in various concentrations.

3. Capture photographs of the test to determine the concentration of glucose.

A.3 Assay for the detection of CRP

1. Add capture antibodies on paper. Leave overnight to dry in room temperature.

2. Block any areas of the paper that do not have bound capture antibodies by submerging the paper in a blocking solution. Blocking solution is 2%-5% BSA and 0.05% Tween20 in PBS. Incubate for at least 1 hour in room temperature.

3. Add the standard (9 ng/ml - 0.5 mg/ml) or sample on the paper at the required concentrations. Incubate for 0.5-2 hours.

4. Wash 3 times for 5 minutes each in a petri dish with wash buffer, 0.05% Tween20 in PBS.

5. Add biotinylated detection antibodies on the paper. Incubate for 0.5-1 hour.

6. Wash again as step 4.

7. Add streptavindin-HRP and incubate for 30 minutes in the dark.

8. Wash again as step 4.

9. Add TMB to induce colour change.

10. Capture photographs of the test to determine the concentration of CRP.

A.4 Assay for the detection of IL-6

1. Prepare dilutions of capture antibody (2 μg/ml). Add capture antibodies on paper. Leave overnight to dry in room temperature.

2. Block any areas of the paper that do not have bound capture antibodies by submerging the paper in a blocking solution. Blocking solution is 1%-5% BSA and 0.05% Tween20 in PBS. Incubate for at least 1 hour in room temperature.

3. Add the standard (75 pg/ml - 1.17 pg/ml) or sample on the paper at the required concentrations. Incubate for 0.5-2 hours.

4. Wash 3 times for 5 minutes each in a petri dish with wash buffer, 0.05% Tween20 in PBS.

5. Add biotinylated detection antibodies on the paper at their working concentration (0.1 - 0.4 μg/ml). Incubate for 0.5-1 hour.

6. Wash again as step 4.

7. Add streptavindin-HRP at working concentration and incubate for 30 minutes in the dark.

8. Wash again as step 4.

9. Add TMB to induce colour change.

10. Capture photographs of the test to determine the concentration of IL-6.

A.5 Assay for nitrite detection

1. Prepare Griess reagent by dissolving in DI water 50 mM sulfanilamide, 330 mM of citric acid and 10 mM of N-(l-naphthyl)-ethylenediamine dihydrochloride.

2. Add the Griess reagent on the paper and allow it to dry for at least 1 hour.

2. Prepare stock solution of 10 mM sodium nitrite and dilutions of it and add on the paper.

3. Capture photographs of the test to determine the concentration of nitrite.

A.6 Assay for the detection of hCG

1. Prepare dilutions of capture antibody (0.5 mg/ml, 2 mg/ml, 4 μg/ml). Add capture antibodies on paper. Leave overnight to dry in room temperature.

2. Block any areas of the paper that do not have bound capture antibodies by submerging the paper in a blocking solution. Blocking solution is 2%-5% BSA and 0.05% Tween20 in PBS. Incubate for at least 1 hour in room temperature.

3. Add the standard (100 ng/ml) or sample on the paper at the required concentrations. Incubate for 0.5-2 hours.

4. Wash 3 times for 5 minutes each in a petri dish with wash buffer, 0.05% Tween20 in PBS.

5. Add biotinylated detection antibodies on the paper at their working concentration. Incubate for 0.5-1 hour.

6. Wash again as step 4.

7. Add streptavindin-HRP at working concentration and incubate for 30 minutes in the dark.

8. Wash again as step 4.

9. Add TMB to induce colour change.

10. Capture photographs of the test to determine the concentration of hCG.

A.7 Assay for the detection of TNF-α

1. Prepare dilutions of capture antibody (4 μg/ml). Add capture antibodies on paper. Leave overnight to dry in room temperature.

2. Block any areas of the paper that do not have bound capture antibodies by submerging the paper in a blocking solution. Blocking solution is 2%-5% BSA and 0.05% Tween20 in PBS. Incubate for at least 1 hour in room temperature.

3. Add the standard (1000 pg/ml - 370 ng/ml) or sample on the paper at the required concentrations. Incubate for 0.5-2 hours.

4. Wash 3 times for 5 minutes each in a petri dish with wash buffer, 0.05% Tween20 in PBS.

5. Add biotinylated detection antibodies on the paper at their working concentration. Incubate for 0.5-1 hour.

6. Wash again as step 4.

7. Add streptavindin-HRP at working concentration and incubate for 30 minutes in the dark.

8. Wash again as step 4.

9. Add TMB to induce colour change.

10. Capture photographs of the test to determine the concentration of TNFα.

A.8 Assay for the detection of PIIINP

1. Prepare dilutions of capture antibody (100 μg/ml). Add capture antibodies on paper. Leave overnight to dry in room temperature.

2. Block any areas of the paper that do not have bound capture antibodies by submerging the paper in a blocking solution. Blocking solution is 2%-5% BSA and 0.05% Tween20 in PBS. Incubate for at least 1 hour in room temperature.

3. Add the standard (stock concentration: 50 μg/ml) or sample on the paper at the required concentrations. Incubate for 0.5-2 hours.

4. Wash 3 times for 5 minutes each in a petri dish with wash buffer, 0.05% Tween20 in PBS.

5. Add biotinylated detection antibodies on the paper at their working concentration (stock concentration: 630 μg/ml). Incubate for 0.5-1 hour.

6. Wash again as step 4.

7. Add streptavindin-HRP at working concentration and incubate for 30 minutes in the dark.

8. Wash again as step 4.

9. Add TMB to induce colour change.

10. Capture photographs of the test to determine the concentration of PIIINP.

A.9 Assay for the detection of IL-1β

1. Prepare dilutions of capture antibody (2 μg/ml). Add capture antibodies on paper. Leave overnight to dry in room temperature.

2. Block any areas of the paper that do not have bound capture antibodies by submerging the paper in a blocking solution. Blocking solution is 2%-5% BSA and 0.05% Tween20 in PBS. Incubate for at least 1 hour in room temperature.

3. Add the standard (3.9 pg/ml - 250 pg/ml) or sample on the paper at the required concentrations. Incubate for 0.5-2 hours.

4. Wash 3 times for 5 minutes each in a petri dish with wash buffer, 0.05% Tween20 in PBS.

5. Add IL-1β conjugate antibodies on the paper at their working concentration (stock concentration: 630 μg/ml). Incubate for 0.5-1 hour.

6. Wash again as step 4.

7. Add streptavindin-HRP at working concentration and incubate for 30 minutes in the dark.

8. Wash again as step 4.

9. Add TMB to induce colour change.

10. Capture photographs of the test to determine the concentration of PIIINP.

Appendix B

Calculations for biochemistry experiments

B.1 Preparation of solutions

1. Concentration by weight percentage (w/w)

$$\text{X\%} = \frac{\text{X g of solute}}{\text{100 g of solvent}} \times 100 \tag{B.1}$$

2. Concentration by volume percentage (v/v)

$$\text{X\%} = \frac{\text{X ml of solute}}{\text{100 ml of total solution}} \times 100 \tag{B.2}$$

3. Concentration by weight per volume percentage (w/v)

$$\text{X\%} = \frac{\text{X g of solute}}{\text{100 ml of total volume}} \times 100 \tag{B.3}$$

4. Concentration in molarity

$$\text{Molarity (M)} = \frac{\text{Moles}}{\text{liter of solution}} = \frac{\frac{\text{grams of solute}}{\text{molecular weight}}}{\text{liter of solution}} \tag{B.4}$$

B.2 Dilutions

1. Dilution calculation starting from a concentrated solution.

$$C_i \times V_i = C_f \times V_f \tag{B.5}$$

where C_i and C_f are the initial and final concentrations and V_i and V_f are the initial and final volumes respectively

2. Serial dilutions

Serial dilutions ivolve the systematic dilutions of an original solution in fixed steps, such as 1:2, 1:4, 1:8 and so on. An example would be to start with an original solution and carry out the following dilutions as seen in Fig. B.1.

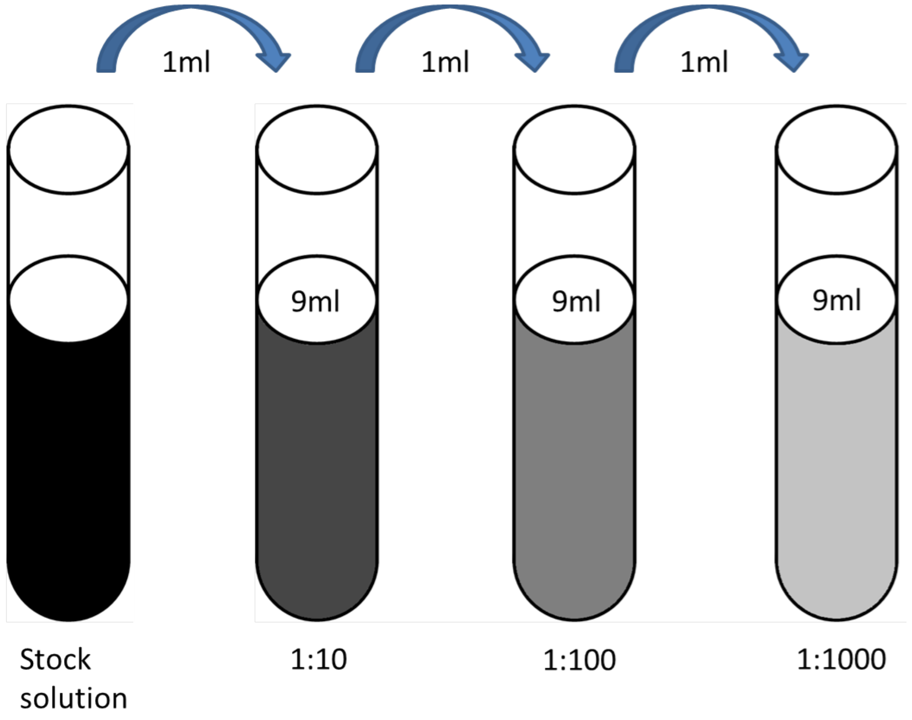

FIGURE B.1: Example diagram of the serial dilution procedure.

Appendix C

List of publications

C.1 Journal publications

- I. N. Katis, J. A. Holloway, J. Madsen, S. N. Faust, S. D. Garbis, P. J. S. Smith, D. Voegeli, D. L. Bader, R. W. Eason, and C. L. Sones. Paper-based colorimetric enzyme linked immunosorbent assay fabricated by laser induced forward transfer. Biomicrofluidics, 8(3), 2014. doi: 10.1063/1.4878696.
- C. L. Sones, I. N. Katis, P. J. W. He, B. Mills, M. F. Namiq, P. Shardlow, M. Ibsen, and R. W. Eason. Laser-induced photo-polymerisation for creation of paper-based fluidic devices. Lab Chip, 14:45674574, 2014. doi: 10.1039/C4LC00850B.
- P. J. W. He, I. N. Katis, R. W. Eason, and C. L. Sones. Laser-based patterning for fluidic devices in nitrocellulose. Biomicrofluidics, 9(2), 2015. doi: 10.1063/1.4919629.
- P. J. W. He, I. N. Katis, R. W. Eason, and C. L. Sones. Engineering fluidic delays in paper-based devices using laser direct-writing. Lab Chip, 15:40544061, 2015. doi: 10.1039/C5LC00590F.
- C. L. Sones, I. N. Katis, B. Mills, M. Feinaeugle, A. Mosayyebi, J. Butement, and R. W. Eason. Rapid and mask-less laser-processing technique for the fabrication of microstructures in polydimethylsiloxane. Applied Surface Science, 298:125 129, 2014. doi: 10.1016/j.apsusc.2014.01.138.

C.2 Conference and meeting contributions

- I. N. Katis, J. A. Holloway, J. Madsen, S. N. Faust, S. D. Garbis, P. J. S. Smith, D. Voegeli, D. L. Bader, R. W. Eason, and C. L. Sones. Towards paper-based point-of-care diagnostics fabricated by laser induced forward transfer. In E-MRS 2014 Materials Research Society Spring Meeting, 2014.

- I. N. Katis, P. J. W. He, R. W. Eason, and C. L. Sones. Laser manufacturing for multi-analyte paper-based diagnostic sensors. In European Conference on Lasers and Electro-Optics and the European Quantum Electronics Conference, June 2015.
- P. J. W. He, I. N. Katis, R. W. Eason, and C. L. Sones. Laser engineering of various porous materials for fabrication of paper-based microfluidic devices. In European Conference on Lasers and Electro-Optics and the European Quantum Electronics Conference, June 2015.
- I.N. Katis, P. J. W. He, R.W. Eason, and C.L. Sones. Direct-write laser techniques for the manufacture of multiplexed paper-based diagnostic sensors. In SPIE Photonics West - Microfluidics, BioMEMS, and Medical Microsystems XIII, February 2015.
- C. L. Sones, I. N. Katis, P. J. W. He, and R. W. Eason. Laser-direct-write methods for fabrication of paper-based medical diagnostic sensors. In Photonics 2014: 12th International Conference on Fiber Optics and Photonics, 2014.
- C. L. Sones, I. N. Katis, P. J. W. He, B. Mills, A. Mosayyebi, J. Butement, M. Feinaeugle, and R. W. Eason. Laser-based printing and patterning for biological applications. In International Workshop on the Fabrication and Application of Microstructured Optical Devices, 2014.
- C. L. Sones, I. N. Katis, B. Mills, M. Feinaeugle, A. Mosayyebi, J. Butement, and R. W. Eason. Rapid low-cost patterning of microstructures in polydimethylsiloxane via mask-less laser-machining. In CLEO/Europe-IQEC 2013, 2013.
- C. L. Sones, I. N. Katis, B. Mills, M. Feinaeugle, A. Mosayyebi, J. Butement, and R. W. Eason. Mask-less laser-machining for rapid low-cost patterning of microstructures in polydimethylsiloxane (pdms). In E-MRS 13 Materials Research Society Spring Meeting, 2013.
- R.W. Eason, B. Mills, M. Feinaeugle, D. Heath, J.A. Grant-Jacob, I.N. Katis, and C.L. Sones. Digital multimirror devices for precision laser micromachining. In ORC Industry Day, April 2014.
- R.W. Eason, B. Mills, M. Feinaeugle, D. Heath, D.P. Banks, C.L. Sones, J. Grant-Jacob, and I.N. Katis. Nanofabrication technologies: high-throughput for tomorrows metadevices. In Metamaterials retreat, 2014.

- R.W. Eason, D.P. Banks, K. Kaur, C.L. Sones, M. Feinaeugle, J. Grant-Jacob, B. Mills, I.N. Katis, and D. Heath. Lift: Laser-induced forward transfer printing of solid-phase materials for photonic and electronic applications. In Invited Seminar: Applied Optics Group Lunchtime Seminar, January 2014.
- M. Feinaeugle, R.W. Eason, C.L. Sones, B. Mills, J.A. Grant-Jacob, I.N. Katis, and D.J. Heath. Making additive manufacturing functional - the laser-assisted fabrication of electronic and photonic devices. In The Institution of Engineering and Technology (IET), May 2014.
- R. W. Eason, I. N. Katis, P. J. W. He, and C. L. Sones. Laser-polymerised fluidic channels for the manufacture of multiplexed paper-based diagnostic sensors. In PR15 conference, June 2015.
- C. L. Sones, I. N. Katis, B. Mills, M. Feinaeugle, M. Ibsen, and R. W. Eason. Laser patterning for paper-based fluidics. In SPIE Photonics West - Microfluidics, BioMEMS, and Medical Microsystems XII, February 2014.
- P. J. W. He, I. N. Katis, R. W. Eason, and C. L. Sones. Rapid prototyping of microfluidic channels in nitrocellulose using laser-direct-write patterning. In SPIE Photonics West - Microfluidics, BioMEMS, and Medical Microsystems XIII, February 2015.

Bibliography

[1] A. Pique. In *Direct-Write Technologies for Rapid Prototyping*. 2002. doi: 10.1016/B978-012174231-7/50052-X.

[2] J. A. Lewis and G. M. Gratson. Direct writing in three dimensions. *Materials Today*, 7(78):32 – 39, 2004. doi: 10.1016/S1369-7021(04)00344-X.

[3] K. K. B. Hon, L. Li, and I. M. Hutchings. Direct writing technologyadvances and developments. *CIRP Annals - Manufacturing Technology*, 57(2):601 – 620, 2008. doi: 10.1016/j.cirp.2008.09.006.

[4] P. P. Pronko, S. K. Dutta, J. Squier, J. V. Rudd, D. Du, and G. Mourou. Machining of sub-micron holes using a femtosecond laser at 800 nm. *Optics Communications*, 114(12):106 – 110, 1995. doi: 10.1016/0030-4018(94)00585-I.

[5] B. Mills, M. Feinaeugle, C. L. Sones, N. Rizvi, and R. W. Eason. Sub-micron-scale femtosecond laser ablation using a digital micromirror device. *Journal of Micromechanics and Microengineering*, 23(3):035005, 2013. doi: 10.1088/0960-1317/23/3/035005.

[6] J. Bohandy, B. F. Kim, and F. J. Adrian. Metal deposition from a supported metal film using an excimer laser. *Journal of Applied Physics*, 60(4):1538–1539, 1986. doi: 10.1063/1.337287.

[7] C. B. Arnold and A. Pique. Laser direct-write processing. *MRS Bulletin*, 32:9–15, 1 2007. doi: 10.1557/mrs2007.9.

[8] A. Palla-Papavlu, V. Dinca, C. Luculescu, J. Shaw-Stewart, M. Nagel, T. Lippert, and M. Dinescu. Laser induced forward transfer of soft materials. *Journal of Optics*, 12(12):124014, 2010. doi: 10.1088/2040-8978/12/12/124014.

[9] C. L. Sones, K. S. Kaur, P. Ganguly, D. P. Banks, Y. J. Ying, R. W. Eason, and S. Mailis. Laser-induced-forward-transfer: a rapid prototyping tool for fabrication of photonic devices. *Applied Physics A*, 101(2):333–338, 2010. doi: 10.1007/s00339-010-5827-5.

[10] E. Stratakis, A. Ranella, M. Farsari, and C. Fotakis. Laser-based micro/nanoengineering for biological applications. *Progress in Quantum Electronics*, 33(5):127 – 163, 2009. doi: 10.1016/j.pquantelec.2009.06.001.

[11] L. Koch, A. Deiwick, S. Schlie, S. Michael, M. Gruene, V. Coger, D. Zychlinski, A. Schambach, K. Reimers, P. M. Vogt, and B. Chichkov. Skin tissue generation by laser cell printing. *Biotechnology and Bioengineering*, 109(7):1855–1863, 2012. doi: 10.1002/bit.24455.

[12] F. Guillemot, A. Souquet, S. Catros, B. Guillotin, J. Lopez, M. Faucon, B. Pippenger, R. Bareille, M. Remy, S. Bellance, P. Chabassier, J.C. Fricain, and J. Amedee. High-throughput laser printing of cells and biomaterials for tissue engineering. *Acta Biomaterialia*, 6(7):2494 – 2500, 2010. doi: 10.1016/j.actbio.2009.09.029.

[13] B. Guillotin, A. Souquet, S. Catros, M. Duocastella, B. Pippenger, S. Bellance, R. Bareille, M. Remy, L. Bordenave, J. Amedee, and F. Guillemot. Laser assisted bioprinting of engineered tissue with high cell density and microscale organization. *Biomaterials*, 31(28):7250 – 7256, 2010. doi: 10.1016/j.biomaterials.2010.05.055.

[14] N. R. Schiele, D. T. Corr, Y. Huang, N. A. Raof, Y. Xie, and D. B. Chrisey. Laser-based direct-write techniques for cell printing. *Biofabrication*, 2(3):032001, 2010. doi: 10.1088/1758-5082/2/3/032001.

[15] A. Doraiswamy, R. J. Narayan, T. Lippert, L. Urech, A. Wokaun, M. Nagel, B. Hopp, M. Dinescu, R. Modi, R. C. Y. Auyeung, and D. B. Chrisey. Excimer laser forward transfer of mammalian cells using a novel triazene absorbing layer. *Applied Surface Science*, 252(13):4743 – 4747, 2006. doi: 10.1016/j.apsusc.2005.07.166.

[16] J. A. Barron, D. B. Krizman, and B. R. Ringeisen. Laser printing of single cells: statistical analysis, cell viability, and stress. *Annals of Biomedical Engineering*, 33 (2):121–130, 2005. doi: 10.1007/s10439-005-8971-x.

[17] B. Hopp, T. Smausz, G. Szabo, L. Kolozsvari, D. Kafetzopoulos, C. Fotakis, and A. Nogradi. Femtosecond laser printing of living cells using absorbing film-assisted laser-induced forward transfer. *Optical Engineering*, 51(1):014302–1–014302–6, 2012. doi: 10.1117/1.OE.51.1.014302.

[18] Y. Lin, Y. Huang, and D. B. Chrisey. Metallic foil-assisted laser cell printing. *Journal of Biomechanical Engineering*, 133(2):025001–025001–5, 2011. doi: 10.1115/1.4003132.

[19] B. R. Ringeisen, H. Kim, J. A. Barron, D. B. Krizman, D. B. Chrisey, S. Jackman, R. Y. C. Auyeung, and B. J. Spargo. Laser printing of pluripotent embryonal carcinoma cells. *Tissue Engineering*, 10:483–491, 2004. doi: 10.1089/107632704323061843.

[20] B. Hopp, T. Smausz, Z. Antal, N. Kresz, Z. Bor, and D. Chrisey. Absorbing film assisted laser induced forward transfer of fungi (trichoderma conidia). *Journal of Applied Physics*, 96(6):3478–3481, 2004. doi: 10.1063/1.1782275.

[21] J. A. Barron, H. D. Young, D. D. Dlott, M. M. Darfler, D. B. Krizman, and B. R. Ringeisen. Printing of protein microarrays via a capillary-free fluid jetting mechanism. *Proteomics*, 5(16):4138–4144, 2005. doi: 10.1002/pmic.200401294.

[22] C. Boutopoulos, P. Andreakou, D. Kafetzopoulos, S. Chatzandroulis, and I. Zergioti. Direct laser printing of biotin microarrays on low temperature oxide on si substrates. *physica status solidi (a)*, 205(11):2505–2508, 2008. doi: 10.1002/pssa.200780206.

[23] V. Dinca, A. Ranella, M. Farsari, D. Kafetzopoulos, M. Dinescu, A. Popescu, and C. Fotakis. Quantification of the activity of biomolecules in microarrays obtained by direct laser transfer. *Biomedical Microdevices*, 10(5):719–725, 2008. doi: 10.1007/s10544-008-9183-6.

[24] I. Zergioti, A. Karaiskou, D. G. Papazoglou, C. Fotakis, M. Kapsetaki, and D. Kafetzopoulos. Femtosecond laser microprinting of biomaterials. *Applied Physics Letters*, 86(16), 2005. doi: 10.1063/1.1906325.

[25] P. Serra, J. M. Fernandez-Pradas, F. X. Berthet, M. Colina, J. Elvira, and J. L. Morenza. Laser direct writing of biomolecule microarrays. *Applied Physics A*, 79 (4-6):949–952, 2004. doi: 10.1007/s00339-004-2577-2.

[26] J. A. Barron, R. Rosen, J. Jones-Meehan, B. J. Spargo, S. Belkin, and B. R. Ringeisen. Biological laser printing of genetically modified escherichia coli for biosensor applications. *Biosensors and Bioelectronics*, 20(2):246 – 252, 2004. doi: 10.1016/j.bios.2004.01.011.

[27] M. Colina, P. Serra, J. M. Fernandez-Pradas, L. Sevilla, and J. L. Morenza. Dna deposition through laser induced forward transfer. *Biosensors and Bioelectronics*, 20(8):1638 – 1642, 2005. doi: 10.1016/j.bios.2004.08.047.

[28] M. Chatzipetrou, G. Tsekenis, V. Tsouti, S. Chatzandroulis, D. Thanos, and I. Zergioti. Direct laser printing of oligonucleotides for the fabrication of a label-free biosensor. *Procedia Engineering*, 25(0):851 – 855, 2011. doi: 10.1016/j.proeng.2011.12.209.

[29] J. M. Fernandez-Pradas, M. Colina, P. Serra, J. Domnguez, and J. L. Morenza. Laser-induced forward transfer of biomolecules. *Thin Solid Films*, 453454(0):27 – 30, 2004. doi: 10.1016/j.tsf.2003.11.154.

[30] A. Karaiskou, I. Zergioti, C. Fotakis, M. Kapsetaki, and D. Kafetzopoulos. Microfabrication of biomaterials by the sub-ps laser-induced forward transfer process. *Applied Surface Science*, 208209:245 – 249, 2003. doi: 10.1016/S0169-4332(02)01396-X.

[31] F. J. Adrian, J. Bohandy, B. F. Kim, A. N. Jette, and P. Thompson. A study of the mechanism of metal deposition by the laser induced forward transfer process. *Journal of Vacuum Science & Technology B*, 5(5):1490–1494, 1987. doi: 10.1116/1.583661.

[32] W. A. Tolbert, I. Y. S. Lee, M. M. Doxtader, E. W. Ellis, and D. D. Dlott. High-speed color imaging by laser-ablation transfer with a dynamic release layer - fundamental mechanisms. *Journal of Imaging Science and Technology*, 37(4): 411–422, 1993.

[33] J. A. Barron, P. Wu, H. D. Ladouceur, and B. R. Ringeisen. Biological laser printing: A novel technique for creating heterogeneous 3-dimensional cell patterns. *Biomedical Microdevices*, 6(2):139–147, 2004. doi: 10.1023/B:BMMD.0000031751.67267.9f.

[34] P. Serra, M. Duocastella, J. M. Fernandez-Pradas, and J. L. Morenza. Liquids microprinting through laser-induced forward transfer. *Applied Surface Science*, 255(10):5342 – 5345, 2009. doi: 10.1016/j.apsusc.2008.07.200.

[35] N. T. Kattamis, P. E. Purnick, R. Weiss, and C. B. Arnold. Thick film laser induced forward transfer for deposition of thermally and mechanically sensitive materials. *Applied Physics Letters*, 91(17), 2007. doi: 10.1063/1.2799877.

[36] D. P. Banks, K. Kaur, R. Gazia, R. Fardel, M. Nagel, T. Lippert, and R. W. Eason. Triazene photopolymer dynamic release layer-assisted femtosecond laser-induced forward transfer with an active carrier substrate. *EPL (Europhysics Letters)*, 83 (3):38003, 2008.

[37] K. S. Kaur, R. Fardel, T. C. May-Smith, M. Nagel, D. P. Banks, C. Grivas, T. Lippert, and R. W. Eason. Shadowgraphic studies of triazene assisted laser-induced forward transfer of ceramic thin films. *Journal of Applied Physics*, 105 (11), 2009. doi: 10.1063/1.3132822.

[38] M. S. Brown, N. T. Kattamis, and C. B. Arnold. Time-resolved study of polyimide absorption layers for blister-actuated laser-induced forward transfer. *Journal of Applied Physics*, 107(8), 2010. doi: 10.1063/1.3327432.

[39] T. V. Kononenko, P. Alloncle, V. I. Konov, and M. Sentis. Shadowgraphic imaging of laser transfer driven by metal film blistering. *Applied Physics A*, 102(1):49–54, 2011. doi: 10.1007/s00339-010-6083-4.

[40] V. Menezes, K. Takayama, A. Gojani, and S.H.R. Hosseini. Shock wave driven microparticles for pharmaceutical applications. *Shock Waves*, 18(5):393–400, 2008. doi: 10.1007/s00193-008-0163-9.

[41] B. R. Ringeisen, D. B. Chrisey, A. Pique, H. D. Young, R. Modi, M. Bucaro, J. Jones-Meehan, and B. J. Spargo. Generation of mesoscopic patterns of viable escherichia coli by ambient laser transfer. *Biomaterials*, 23(1):161 – 166, 2002. doi: 10.1016/S0142-9612(01)00091-6.

[42] H. Kim, M. Duocastella, K. M. Charipar, R. C. Y. Auyeung, and A. Pique. Laser printing of conformal and multi-level 3d interconnects. *Applied Physics A*, 113(1): 5–8, 2013. doi: 10.1007/s00339-013-7909-7.

[43] A. Pique, D. W. Weir, P. K. Wu, B. Pratap, C. B. Arnold, B. R. Ringeisen, R. A. McGill, R. C. Y. Auyeung, R. A. Kant, and D. B. Chrisey. Direct-write of sensor devices by a laser forward transfer technique, 2002.

[44] R. C. Y. Auyeung, H. Kim, A. J. Birnbaum, M. Zalalutdinov, S. A. Mathews, and A. Pique. Laser decal transfer of freestanding microcantilevers and microbridges. *Applied Physics A*, 97(3):513–519, 2009. doi: 10.1007/s00339-009-5433-6.

[45] A. I. Kuznetsov, J. Koch, and B. N. Chichkov. Laser-induced backward transfer of gold nanodroplets. *Optics Express*, 17(21):18820–18825, Oct 2009. doi: 10.1364/OE.17.018820.

[46] A. Patrascioiu, M. Duocastella, J. M. Fernandez-Pradas, J. L. Morenza, and P. Serra. Liquids microprinting through a novel film-free femtosecond laser based technique. *Applied Surface Science*, 257(12):5190 – 5194, 2011. doi: 10.1016/j.apsusc.2010.11.093.

[47] C. Decker. Photoinitiated crosslinking polymerisation. *Progress in Polymer Science*, 21(4):593 – 650, 1996. doi: 10.1016/0079-6700(95)00027-5.

[48] C. Decker. *Laser-induced polymerization*, chapter 10, pages 207–223. 1985. doi: 10.1021/bk-1984-0266.ch009.

[49] G. M. Wallraff, R. D. Allen, W. D. Hinsberg, C. G. Willson, L. L. Simpson, S. F. Webber, and J. L. Sturtevant. *Chemically amplified photoresist for visible laser direct imaging*, volume 66, pages 49–51. 1992.

[50] S. Klein, A. Barsella, H. Leblond, H. Bulou, A. Fort, C. Andraud, G. Lemercier, J. C. Mulatier, and K. Dorkenoo. One-step waveguide and optical circuit writing in photopolymerizable materials processed by two-photon absorption. *Applied Physics Letters*, 86(21), 2005. doi: 10.1063/1.1915525.

[51] R. Guo, S. Xiao, X. Zhai, J. Li, A. Xia, and W. Huang. Micro lens fabrication by means of femtosecond two photon photopolymerization. *Optics Express*, 14(2): 810–816, Jan 2006. doi: 10.1364/OPEX.14.000810.

[52] A. Vitale, M. Quaglio, M. Cocuzza, C. F. Pirri, and R. Bongiovanni. Photopolymerization of a perfluoropolyether oligomer and photolithographic processes for the fabrication of microfluidic devices. *European Polymer Journal*, 48(6):1118 – 1126, 2012. doi: 10.1016/j.eurpolymj.2012.03.016.

[53] L. Li and J. T. Fourkas. Multiphoton polymerization. *Materials Today*, 10(6):30 – 37, 2007. doi: 10.1016/S1369-7021(07)70130-X.

[54] S. Kawata, H. B. Sun, T. Tanaka, and K. Takada. Finer features for functional microdevices. *Nature*, 412:697 – 698, 2001. doi: 10.1038/35089130.

[55] T. Baldacchini, C. N. LaFratta, R. A. Farrer, M. C. Teich, B. E. A. Saleh, M. J. Naughton, and J. T. Fourkas. Acrylic-based resin with favorable properties for three-dimensional two-photon polymerization. *Journal of Applied Physics*, 95(11): 6072–6076, 2004. doi: 10.1063/1.1728296.

[56] B. Mills, J. A. Grant-Jacob, M. Feinaeugle, and R. W. Eason. Single-pulse multiphoton polymerization of complex structures using a digital multimirror device. *Optics Express*, 21(12):14853–14858, Jun 2013. doi: 10.1364/OE.21.014853.

[57] B. Kaehr, N. Ertas, R. Nielson, R. Allen, R. T. Hill, M. Plenert, and J. B. Shear. Direct-write fabrication of functional protein matrixes using a low-cost q-switched laser. *Analytical Chemistry*, 78(9):3198–3202, 2006. doi: 10.1021/ac052267s.

[58] J. D. Pitts, P. J. Campagnola, G. A. Epling, and S. L. Goodman. Submicron multiphoton free-form fabrication of proteins and polymers: studies of reaction efficiencies and applications in sustained release. *Macromolecules*, 33(5):1514–1523, 2000. doi: 10.1021/ma9910437.

[59] R. M. Lequin. Enzyme immunoassay (eia)/enzyme-linked immunosorbent assay (elisa). *Clinical Chemistry*, 51(12):2415–2418, 2005. doi: 10.1373/clinchem.2005.051532.

[60] S.S. Deshpande. Antibodies: Biochemistry, structure, and function. In *Enzyme Immunoassays*, pages 24–51. 1996. doi: 10.1007/978-1-4613-1169-0_2.

[61] T. T. Ngo and H. M. Lenhoff. Enzymes as versatile labels and signal amplifiers for monitoring immunochemical reactions. *Molecular and Cellular Biochemistry*, 44(1):3–12, 1982. doi: 10.1007/BF00573840.

[62] A. Voller, A. Bartlett, and D. E. Bidwell. Enzyme immunoassays with special reference to elisa techniques. *Journal of Clinical Pathology*, 31(6):507 – 520, 1978. doi: 10.1016/j.snb.2008.07.020.

[63] C. D. Chin, V. Linder, and S. K. Sia. Lab-on-a-chip devices for global health: Past studies and future opportunities. *Lab Chip*, 7:41–57, 2007. doi: 10.1039/B611455E.

[64] X. Li, D. R. Ballerini, and W. Shen. A perspective on paper-based microfluidics: Current status and future trends. *Biomicrofluidics*, 6(1), 2012. doi: 10.1063/1.3687398.

[65] A. M. Foudeh, T. Fatanat Didar, T. Veres, and M. Tabrizian. Microfluidic designs and techniques using lab-on-a-chip devices for pathogen detection for point-of-care diagnostics. *Lab Chip*, 12:3249–3266, 2012. doi: 10.1039/C2LC40630F.

[66] A. W. Martinez, S. T. Phillips, G. M. Whitesides, and E. Carrilho. Diagnostics for the developing world: Microfluidic paper-based analytical devices. *Analytical Chemistry*, 82(1):3–10, 2010. doi: 10.1021/ac9013989.

[67] P. Yager, G. J. Domingo, and J. Gerdes. Point-of-care diagnostics for global health. *Annual Review of Biomedical Engineering*, 10(1):107–144, 2008. doi: 10.1146/annurev.bioeng.10.061807.160524.

[68] A.W. Martinez, S.T. Phillips, M.J. Butte, and G.M. Whitesides. Patterned paper as a platform for inexpensive, low-volume, portable bioassays. *Angewandte Chemie International Edition*, 46(8):1318–1320, 2007. doi: 10.1002/anie.200603817.

[69] S. J. Vella, P. Beattie, R. Cademartiri, A. Laromaine, A. W. Martinez, S. T. Phillips, K. A. Mirica, and G. M. Whitesides. Measuring markers of liver function using a micropatterned paper device designed for blood from a fingerstick. *Analytical Chemistry*, 84(6):2883–2891, 2012. doi: 10.1021/ac203434x.

[70] V. Gubala, L. F. Harris, A. J. Ricco, M. X. Tan, and D. E. Williams. Point of care diagnostics: Status and future. *Analytical Chemistry*, 84(2):487–515, 2012. doi: 10.1021/ac2030199.

[71] G. A. Posthuma-Trumpie, J. Korf, and A. van Amerongen. Lateral flow (immuno)assay: its strengths, weaknesses, opportunities and threats. a literature survey. *Analytical and Bioanalytical Chemistry*, 393(2):569–582, 2009. doi: 10.1007/s00216-008-2287-2.

[72] J. Hu, S. Q. Wang, L. Wang, F. Li, B. Pingguan-Murphy, T. J. Lu, and F. Xu. Advances in paper-based point-of-care diagnostics. *Biosensors and Bioelectronics*, 54:585 – 597, 2014. doi: 10.1016/j.bios.2013.10.075.

[73] A. K. Yetisen, M. S. Akram, and C. R. Lowe. Paper-based microfluidic point-of-care diagnostic devices. *Lab Chip*, 13:2210–2251, 2013. doi: 10.1039/C3LC50169H.

[74] A. Yu, J. Shang, F. Cheng, B. A. Paik, J. M. Kaplan, R. B. Andrade, and D. M. Ratner. Biofunctional paper via the covalent modification of cellulose. *Langmuir*, 28(30):11265–11273, 2012. doi: 10.1021/la301661x.

[75] U. Bora, P. Sharma, K. Kannan, and P. Nahar. Photoreactive cellulose membranea novel matrix for covalent immobilization of biomolecules. *Journal of Biotechnology*, 126(2):220–229, 2006. doi: 10.1016/j.jbiotec.2006.04.013.

[76] V. Dinca, A. Palla Papavlu, A. Matei, C. Luculescu, M. Dinescu, T. Lippert, F. Di Pietrantonio, D. Cannata, M. Benetti, and E. Verona. A comparative study of drl-lift and lift on integrated polyisobutylene polymer matrices. *Applied Physics A*, 101(2):429–434, 2010. doi: 10.1007/s00339-010-5826-6.

[77] C-M. Cheng, A.W. Martinez, J. Gong, C.R. Mace, S.T. Phillips, E. Carrilho, K.A. Mirica, and G.M. Whitesides. Paper-based elisa. *Angewandte Chemie International Edition*, 49(28):4771–4774, 2010. doi: 10.1002/anie.201001005.

[78] I. N. Katis, J. A. Holloway, J. Madsen, S. N. Faust, S. D. Garbis, P. J. S. Smith, D. Voegeli, D. L. Bader, R. W. Eason, and C. L. Sones. Paper-based colorimetric enzyme linked immunosorbent assay fabricated by laser induced forward transfer. *Biomicrofluidics*, 8(3), 2014. doi: 10.1063/1.4878696.

[79] I. N. Katis, J. A. Holloway, J. Madsen, S. N. Faust, S. D. Garbis, P. J. S. Smith, D. Voegeli, D. L. Bader, R. W. Eason, and C. L. Sones. Towards paper-based point-of-care diagnostics fabricated by laser induced forward transfer. In *E-MRS 2014 Materials Research Society Spring Meeting*, 2014.

[80] P. Serra, M. Colina, J. M. Fernandez-Pradas, L. Sevilla, and J. L. Morenza. Preparation of functional dna microarrays through laser-induced forward transfer. *Applied Physics Letters*, 85(9):1639–1641, 2004. doi: 10.1063/1.1787614.

[81] Y. Lin, Y. Huang, and D. B. Chrisey. Droplet formation in matrix-assisted pulsed-laser evaporation direct writing of glycerol-water solution. *Journal of Applied Physics*, 105(9), 2009. doi: 10.1063/1.3116724.

[82] L. J. Yang, W. Z. Lin, T. J. Yao, and Y. C. Tai. Photo-patternable gelatin as protection layers in surface micromachinings. In *The Fifteenth IEEE International Conference on Micro Electro Mechanical Systems*, pages 471–474, Jan 2002. doi: 10.1109/MEMSYS.2002.984304.

[83] A. W. P. Vermeer and W. Norde. The thermal stability of immunoglobulin: Unfolding and aggregation of a multi-domain protein. *Biophysical Journal*, 78(1):394 – 404, 2000. doi: 10.1016/S0006-3495(00)76602-1.

[84] J. Wang, B. Yiu, J. Obermeyer, C. D. M. Filipe, J. D. Brennan, and R. Pelton. Effects of temperature and relative humidity on the stability of paper-immobilized antibodies. *Biomacromolecules*, 13(2):559–564, 2012. doi: 10.1021/bm2017405.

[85] E. Carrilho, A. W. Martinez, and G. M. Whitesides. Understanding wax printing: A simple micropatterning process for paper-based microfluidics. *Analytical Chemistry*, 81(16):7091–7095, 2009. doi: 10.1021/ac901071p.

[86] Y. Lu, W. Shi, L. Jiang, J. Qin, and B. Lin. Rapid prototyping of paper-based microfluidics with wax for low-cost, portable bioassay. *Electrophoresis*, 30(9):1497–1500, 2009. doi: 10.1002/elps.200800563.

[87] E. Carrilho, S. T. Phillips, S. J. Vella, A. W. Martinez, and G. M. Whitesides. Paper microzone plates. *Analytical Chemistry*, 81(15):5990–5998, 2009. doi: 10.1021/ac900847g.

[88] S. Wang, L. Ge, X. Song, J. Yu, S. Ge, J. Huang, and F. Zeng. Paper-based chemiluminescence elisa: Lab-on-paper based on chitosan modified paper device and wax-screen-printing. *Biosensors and Bioelectronics*, 31(1):212 – 218, 2012. doi: 10.1016/j.bios.2011.10.019.

[89] P. Yager, T. Edwards, E. Fu, K. Helton, K. Nelson, M. R. Tam, and B. H. Weigl. Microfluidic diagnostic technologies for global public health. *Nature*, 442(7101): 412 – 418, 2006. doi: 10.1038/nature05064.

[90] D. R. Ballerini, X. Li, and W. Shen. Patterned paper and alternative materials as substrates for low-cost microfluidic diagnostics. *Microfluidics and Nanofluidics*, 13(5):769–787, 2012. doi: 10.1007/s10404-012-0999-2.

[91] R. Pelton. Bioactive paper provides a low-cost platform for diagnostics. *TrAC Trends in Analytical Chemistry*, 28(8):925 – 942, 2009. doi: 10.1016/j.trac.2009.05.005.

[92] C. L. Sones, I. N. Katis, P. J. W. He, B. Mills, M. F. Namiq, P. Shardlow, M. Ibsen, and R. W. Eason. Laser-induced photo-polymerisation for creation of paper-based fluidic devices. *Lab Chip*, 14:4567–4574, 2014. doi: 10.1039/C4LC00850B.

[93] P. J. W. He, I. N. Katis, R. W. Eason, and C. L. Sones. Laser-based patterning for fluidic devices in nitrocellulose. *Biomicrofluidics*, 9(2), 2015. doi: 10.1063/1.4919629.

[94] I. N. Katis, P. J. W. He, R. W. Eason, and C. L. Sones. Laser manufacturing for multi-analyte paper-based diagnostic sensors. In *European Conference on Lasers and Electro-Optics and the European Quantum Electronics Conference*, June 2015.

[95] P. J. W. He, I. N. Katis, R. W. Eason, and C. L. Sones. Laser engineering of various porous materials for fabrication of paper-based microfluidic devices. In *European Conference on Lasers and Electro-Optics and the European Quantum Electronics Conference*, June 2015.

[96] I.N. Katis, P. J. W. He, R.W. Eason, and C.L. Sones. Direct-write laser techniques for the manufacture of multiplexed paper-based diagnostic sensors. In *SPIE Photonics West - Microfluidics, BioMEMS, and Medical Microsystems XIII*, February 2015.

[97] C. L. Sones, I. N. Katis, P. J. W. He, and R. W. Eason. Laser-direct-write methods for fabrication of paper-based medical diagnostic sensors. In *Photonics 2014: 12th International Conference on Fiber Optics and Photonics*, 2014.

[98] C. L. Sones, I. N. Katis, P. J. W. He, B. Mills, A. Mosayyebi, J. Butement, M. Feinaeugle, and R. W. Eason. Laser-based printing and patterning for biological applications. In *International Workshop on the Fabrication and Application of Microstructured Optical Devices*, 2014.

[99] P. J. W. He, I. N. Katis, R. W. Eason, and C. L. Sones. Rapid prototyping of microfluidic channels in nitrocellulose using laser-direct-write patterning. In *SPIE Photonics West - Microfluidics, BioMEMS, and Medical Microsystems XIII*, February 2015.

[100] C. L. Sones, I. N. Katis, B. Mills, M. Feinaeugle, M. Ibsen, and R. W. Eason. Laser patterning for paper-based fluidics. In *SPIE Photonics West - Microfluidics, BioMEMS, and Medical Microsystems XII*, February 2014.

[101] R. W. Eason, I. N. Katis, P. J. W. He, and C. L. Sones. Laser-polymerised fluidic channels for the manufacture of multiplexed paper-based diagnostic sensors. In *PR15 conference*, June 2015.

[102] D. A. Bruzewicz, M. Reches, and G. M. Whitesides. Low-cost printing of poly(dimethylsiloxane) barriers to define microchannels in paper. *Analytical Chemistry*, 80(9):3387–3392, 2008. doi: 10.1021/ac702605a.

[103] K. Abe, K. Suzuki, and D. Citterio. Inkjet-printed microfluidic multianalyte chemical sensing paper. *Analytical Chemistry*, 80(18):6928–6934, 2008. doi: 10.1021/ac800604v.

[104] X. Li, J. Tian, T. Nguyen, and W. Shen. Paper-based microfluidic devices by plasma treatment. *Analytical Chemistry*, 80(23):9131–9134, 2008. doi: 10.1021/ac801729t.

[105] X. Li, J. Tian, and W. Shen. Progress in patterned paper sizing for fabrication of paper-based microfluidic sensors. *Cellulose*, 17(3):649–659, 2010. doi: 10.1007/s10570-010-9401-2.

[106] E. M. Fenton, M. R. Mascarenas, G. P. Lopez, and S. S. Sibbett. Multiplex lateral-flow test strips fabricated by two-dimensional shaping. *ACS Applied Materials & Interfaces*, 1(1):124–129, 2009. doi: 10.1021/am800043z.

[107] W. Wang, W-Y. Wu, W. Wang, and J-J. Zhu. Tree-shaped paper strip for semi-quantitative colorimetric detection of protein with self-calibration. *Journal of Chromatography A*, 1217(24):3896 – 3899, 2010. doi: 10.1016/j.chroma.2010.04.017.

[108] X. Fang, S. Wei, and J. Kong. Paper-based microfluidics with high resolution, cut on a glass fiber membrane for bioassays. *Lab Chip*, 14:911–915, 2014. doi: 10.1039/C3LC51246K.

[109] X. Li, J. Tian, G. Garnier, and W. Shen. Fabrication of paper-based microfluidic sensors by printing. *Colloids and Surfaces B: Biointerfaces*, 76(2):564 – 570, 2010. doi: 10.1016/j.colsurfb.2009.12.023.

[110] J. L. Delaney, C. F. Hogan, J. Tian, and W. Shen. Electrogenerated chemiluminescence detection in paper-based microfluidic sensors. *Analytical Chemistry*, 83(4):1300–1306, 2011. doi: 10.1021/ac102392t.

[111] K. Abe, K. Kotera, K. Suzuki, and D. Citterio. Inkjet-printed paperfluidic immuno-chemical sensing device. *Analytical and Bioanalytical Chemistry*, 398(2):885–893, 2010. doi: 10.1007/s00216-010-4011-2.

[112] S. M. Z. Hossain, R. E. Luckham, M. J. McFadden, and J. D. Brennan. Reagentless bidirectional lateral flow bioactive paper sensors for detection of pesticides in

beverage and food samples. *Analytical Chemistry*, 81(21):9055–9064, 2009. doi: 10.1021/ac901714h.

[113] J. Olkkonen, K. Lehtinen, and T. Erho. Flexographically printed fluidic structures in paper. *Analytical Chemistry*, 82(24):10246–10250, 2010. doi: 10.1021/ac1027066.

[114] W. Dungchai, O. Chailapakul, and C. S. Henry. A low-cost, simple, and rapid fabrication method for paper-based microfluidics using wax screen-printing. *Analyst*, 136:77–82, 2011. doi: 10.1039/C0AN00406E.

[115] G. Chitnis, Z. Ding, C. L. Chang, C. A. Savran, and B. Ziaie. Laser-treated hydrophobic paper: an inexpensive microfluidic platform. *Lab Chip*, 11:1161–1165, 2011. doi: 10.1039/C0LC00512F.

[116] X. Fang, S. Wei, and J. Kong. Paper-based microfluidics with high resolution, cut on a glass fiber membrane for bioassays. *Lab Chip*, 14:911–915, 2014. doi: 10.1039/C3LC51246K.

[117] A. W. Martinez, S. T. Phillips, B. J. Wiley, M. Gupta, and G. M. Whitesides. Flash: A rapid method for prototyping paper-based microfluidic devices. *Lab Chip*, 8:2146–2150, 2008. doi: 10.1039/B811135A.

[118] V. Leung, A. A. M. Shehata, C. D. M. Filipe, and R. Pelton. Streaming potential sensing in paper-based microfluidic channels. *Colloids and Surfaces A: Physicochemical and Engineering Aspects*, 364(13):16 – 18, 2010. doi: 10.1016/j.colsurfa.2010.04.008.

[119] C. D. Souza, O. C. Braga, I. C. Vieira, and A. Spinelli. Electroanalytical determination of sulfadiazine and sulfamethoxazole in pharmaceuticals using a boron-doped diamond electrode. *Sensors and Actuators B: Chemical*, 135(1):66 – 73, 2008. doi: 10.1016/j.snb.2008.07.020.

[120] E. Fu, P. Kauffman, B. Lutz, and P. Yager. Chemical signal amplification in two-dimensional paper networks. *Sensors and actuators B, Chemical*, 149(1):325 – 328, 2010. doi: 10.1016/j.snb.2010.06.024.

[121] B. M. Jayawardane, S. Wei, I. D. McKelvie, and S. D. Kolev. Microfluidic paper-based analytical device for the determination of nitrite and nitrate. *Analytical Chemistry*, 86(15):7274–7279, 2014. doi: 10.1021/ac5013249.

[122] N. Lopez-Ruiz, V. F. Curto, M. M. Erenas, F. Benito-Lopez, D. Diamond, A. J. Palma, and L. F. Capitan-Vallvey. Smartphone-based simultaneous ph and nitrite

colorimetric determination for paper microfluidic devices. *Analytical Chemistry*, 86(19):9554–9562, 2014. doi: 10.1021/ac5019205.

[123] J. Scheller, A. Chalaris, D. Schmidt-Arras, and S. Rose-John. The pro- and anti-inflammatory properties of the cytokine interleukin-6. *Biochimica et Biophysica Acta (BBA) - Molecular Cell Research*, 1813(5):878 – 888, 2011. doi: 10.1016/j.bbamcr.2011.01.034.

[124] A. W. Martinez, S. T. Phillips, and G. M. Whitesides. Three-dimensional microfluidic devices fabricated in layered paper and tape. *Proceedings of the National Academy of Sciences*, 105(50):19606–19611, 2008. doi: 10.1073/pnas.0810903105.

[125] A. Apilux, Y. Ukita, M. Chikae, O. Chailapakul, and Y. Takamura. Development of automated paper-based devices for sequential multistep sandwich enzyme-linked immunosorbent assays using inkjet printing. *Lab Chip*, 13:126–135, 2013. doi: 10.1039/C2LC40690J.

[126] B. Lutz, T. Liang, E. Fu, S. Ramachandran, P. Kauffman, and P. Yager. Dissolvable fluidic time delays for programming multi-step assays in instrument-free paper diagnostics. *Lab Chip*, 13:2840–2847, 2013. doi: 10.1039/C3LC50178G.

[127] H. Chen, J. Cogswell, C. Anagnostopoulos, and M. Faghri. A fluidic diode, valves, and a sequential-loading circuit fabricated on layered paper. *Lab Chip*, 12:2909–2913, 2012. doi: 10.1039/C2LC20970E.

[128] A. W. Martinez, S. T. Phillips, Z. Nie, C. M. Cheng, E. Carrilho, B. J. Wiley, and G. M. Whitesides. Programmable diagnostic devices made from paper and tape. *Lab Chip*, 10:2499–2504, 2010. doi: 10.1039/C0LC00021C.

[129] H. Noh and S. T. Phillips. Fluidic timers for time-dependent, point-of-care assays on paper. *Analytical Chemistry*, 82(19):8071–8078, 2010. doi: 10.1021/ac1005537.

[130] H. Noh and S. T. Phillips. Metering the capillary-driven flow of fluids in paper-based microfluidic devices. *Analytical Chemistry*, 82(10):4181–4187, 2010. doi: 10.1021/ac100431y.

[131] N. K. Thom, K. Yeung, M. B. Pillion, and S. T. Phillips. "fluidic batteries" as low-cost sources of power in paper-based microfluidic devices. *Lab Chip*, 12:1768–1770, 2012. doi: 10.1039/C2LC40126F.

[132] H. Lee and S. Choi. An origami paper-based bacteria-powered battery. *Nano Energy*, 15:549 – 557, 2015. doi: 10.1016/j.nanoen.2015.05.019.

[133] J. L. Osborn, B. Lutz, E. Fu, P. Kauffman, D. Y. Stevens, and P. Yager. Microfluidics without pumps: reinventing the t-sensor and h-filter in paper networks. *Lab Chip*, 10:2659–2665, 2010. doi: 10.1039/C004821F.

[134] E. Fu, S. A. Ramsey, P. Kauffman, B. Lutz, and P. Yager. Transport in two-dimensional paper networks. *Microfluidics and Nanofluidics*, 10:29–35, 2011. doi: 10.1007/s10404-010-0643-y.

[135] E. Fu, B. Lutz, P. Kauffman, and P. Yager. Controlled reagent transport in disposable 2d paper networks. *Lab Chip*, 10:918–920, 2010. doi: 10.1039/B919614E.

[136] D. L. Giokas, G. Z. Tsogas, and A. G. Vlessidis. Programming fluid transport in paper-based microfluidic devices using razor-crafted open channels. *Analytical Chemistry*, 86(13):6202–6207, 2014. doi: 10.1021/ac501273v.

[137] P. J. W. He, I. N. Katis, R. W. Eason, and C. L. Sones. Engineering fluidic delays in paper-based devices using laser direct-writing. *Lab Chip*, 15:4054–4061, 2015. doi: 10.1039/C5LC00590F.

[138] J. Garra, T. Long, J. Currie, T. Schneider, R. White, and M. Paranjape. Dry etching of polydimethylsiloxane for microfluidic systems. *Journal of Vacuum Science & Technology A*, 20(3):975–982, 2002. doi: http://dx.doi.org/10.1116/1.1460896.

[139] B.-H. Jo, L.M. Van Lerberghe, K.M. Motsegood, and D.J. Beebe. Three-dimensional micro-channel fabrication in polydimethylsiloxane (pdms) elastomer. *Journal of Microelectromechanical Systems*, 9(1):76–81, March 2000. doi: 10.1109/84.825780.

[140] L. Miccio, M. Paturzo, A. Finizio, and P. Ferraro. Light induced patterning of poly(dimethylsiloxane) microstructures. *Optics Express*, 18(11):10947–10955, May 2010. doi: 10.1364/OE.18.010947.

[141] W. R. Childs and R. G. Nuzzo. Decal transfer microlithography: a new soft-lithographic patterning method. *Journal of the American Chemical Society*, 124 (45):13583–13596, 2002. doi: 10.1021/ja020942z.

[142] A.L. Thangawng, M.A. Swartz, M.R. Glucksberg, and R. S. Ruoff. Bonddetach lithography: A method for micro/nanolithography by precision pdms patterning. *Small*, 3(1):132–138, 2007. doi: 10.1002/smll.200500418.

[143] M. S. Thomas, B. Millare, J. M. Clift, D. Bao, C. Hong, and V. I. Vullev. Print-and-peel fabrication for microfluidics: Whats in it for biomedical applications? *Annals of Biomedical Engineering*, 38(1):21–32, 2010. doi: 10.1007/s10439-009-9831-x.

[144] J. C. McDonald, M. L. Chabinyc, S. J. Metallo, J. R. Anderson, A. D. Stroock, and G. M. Whitesides. Prototyping of microfluidic devices in poly(dimethylsiloxane) using solid-object printing. *Analytical Chemistry*, 74(7):1537–1545, 2002. doi: 10.1021/ac010938q.

[145] J. C. McDonald and G. M. Whitesides. Poly(dimethylsiloxane) as a material for fabricating microfluidic devices. *Accounts of Chemical Research*, 35(7):491–499, 2002. doi: 10.1021/ar010110q.

[146] J. C. McDonald, D. C. Duffy, J. R. Anderson, D. T. Chiu, H. Wu, O. J. A. Schueller, and G. M. Whitesides. Fabrication of microfluidic systems in poly(dimethylsiloxane). *Electrophoresis*, 21(1):27–40, 2000. doi: 10.1002/(SICI)1522-2683(20000101)21:1⟨27::AID-ELPS27⟩3.0.CO;2-C.

[147] Y. Xia and G. M. Whitesides. Soft lithography. *Angewandte Chemie International Edition*, 37(5):550–575, 1998. doi: 10.1002/(SICI)1521-3773(19980316)37:5⟨550::AID-ANIE550⟩3.0.CO;2-G.

[148] R. R. Gattass and E. Mazur. Femtosecond laser micromachining in transparent materials. *Nature Photonics*, 2(4):219–225, 2008. doi: 10.1038/nphoton.2008.47.

[149] M. D. Shirk and P. A. Molian. A review of ultrashort pulsed laser ablation of materials. *Journal of Laser Applications*, 10(1):18–28, 1998. doi: 10.2351/1.521827.

[150] S. Maruo and J. T. Fourkas. Recent progress in multiphoton microfabrication. *Laser & Photonics Reviews*, 2(1-2):100–111, 2008. doi: 10.1002/lpor.200710039.

[151] S. Maruo, O. Nakamura, and S. Kawata. Three-dimensional microfabrication with two-photon-absorbed photopolymerization. *Optics Letters*, 22(2):132–134, Jan 1997. doi: 10.1364/OL.22.000132.

[152] C. L. Sones, I. N. Katis, B. Mills, M. Feinaeugle, A. Mosayyebi, J. Butement, and R. W. Eason. Rapid and mask-less laser-processing technique for the fabrication of microstructures in polydimethylsiloxane. *Applied Surface Science*, 298:125 – 129, 2014. doi: 10.1016/j.apsusc.2014.01.138.

[153] C. L. Sones, I. N. Katis, B. Mills, M. Feinaeugle, A. Mosayyebi, J. Butement, and R. W. Eason. Rapid low-cost patterning of microstructures in polydimethylsiloxane via mask-less laser-machining. In *CLEO/Europe-IQEC 2013*, 2013.

[154] C. L. Sones, I. N. Katis, B. Mills, M. Feinaeugle, A. Mosayyebi, J. Butement, and R. W. Eason. Mask-less laser-machining for rapid low-cost patterning of microstructures in polydimethylsiloxane (pdms). In *E-MRS '13 Materials Research Society Spring Meeting*, 2013.

[155] D. B. Weibel, W. R. DiLuzio, and G. M. Whitesides. Microfabrication meets microbiology. *Nature Reviews Microbiology*, 5(3):209–218, Mar 2007.

[156] S. K. Sia and G. M. Whitesides. Microfluidic devices fabricated in poly(dimethylsiloxane) for biological studies. *Electrophoresis*, 24(21):3563–3576, 2003. doi: 10.1002/elps.200305584.

[157] A. Kumar and G. M. Whitesides. Features of gold having micrometer to centimeter dimensions can be formed through a combination of stamping with an elastomeric stamp and an alkanethiol ink followed by chemical etching. *Applied Physics Letters*, 63(14):2002–2004, 1993. doi: 10.1063/1.110628.

[158] D.C. Trimbach, H. Stapert, J. vanOrselen, K.D. Jandt, C.W.M. Bastiaansen, and D.J. Broer. Improved microcontact printing of proteins using hydrophilic thermoplastic elastomers as stamp materials. *Advanced Engineering Materials*, 9(12): 1123–1128, 2007. doi: 10.1002/adem.200700282.

[159] A. Perl, D. N. Reinhoudt, and J. Huskens. Microcontact printing: Limitations and achievements. *Advanced Materials*, 21(22):2257–2268, 2009. doi: 10.1002/adma.200801864.

[160] S. Alom Ruiz and C. S. Chen. Microcontact printing: A tool to pattern. *Soft Matter*, 3:168–177, 2007. doi: 10.1039/B613349E.

[161] J. L. Wilbur, A. Kumar, H. A. Biebuyck, E. Kim, and G. M. Whitesides. Microcontact printing of self-assembled monolayers: applications in microfabrication. *Nanotechnology*, 7(4):452, 1996. doi: 10.1088/0957-4484/7/4/028.

[162] A. S. Blawas and W. M. Reichert. Protein patterning. *Biomaterials*, 19(79):595 – 609, 1998. doi: 10.1016/S0142-9612(97)00218-4.

[163] C. S. Chen, M. Mrksich, S. Huang, G. M. Whitesides, and D. E. Ingber. Geometric control of cell life and death. *Science*, 276(5317):1425–1428, 1997. doi: 10.1126/science.276.5317.1425.

[164] S. N. Bhatia, U. J. Balis, M. L. Yarmush, and M. Toner. Effect of cellcell interactions in preservation of cellular phenotype: cocultivation of hepatocytes and nonparenchymal cells. *The FASEB Journal*, 13(14):1883–1900, 1999.

[165] S. A. Lange, V. Benes, D. P. Kern, J. K. H. Hrber, and A. Bernard. Microcontact printing of dna molecules. *Analytical Chemistry*, 76(6):1641–1647, 2004. doi: 10.1021/ac035127w.

[166] A. Ovsianikov, J. Viertl, B. Chichkov, M. Oubaha, B. MacCraith, I. Sakellari, A. Giakoumaki, D. Gray, M. Vamvakaki, M. Farsari, and C. Fotakis. Ultra-low shrinkage hybrid photosensitive material for two-photon polymerization microfabrication. *ACS Nano*, 2(11):2257–2262, 2008. doi: 10.1021/nn800451w.

Reprints of published journal papers